Republic of Iraq

Ministry of Higher Education and Scientific Research

University of Kerbala

Civil Engineering Department

Laboratory Performance of Shallow Buried Plastic Pipes below Geocell Reinforced Subbase Layer Under Repeated Load

A Thesis

Submitted to the Civil Engineering Department in the University of Kerbala in Partial Fulfillment of the Requirements for the Degree of Master of Science in Infrastructure Engineering

By

Sajjad Emad Rasheed

B.Sc. in Civil Engineering of University of Kerbala , (2014)

Supervised by

Prof. Dr. Mohammad Y. Fattah

Assist. Prof. Dr. Waqed H. Hassan

September 2017   Thu Al-Hujja 1438

بِسْمِ اللَّهِ الرَّحْمٰنِ الرَّحِيمِ

يَرْفَعِ اللَّهُ الَّذِينَ آمَنُوا مِنكُمْ وَالَّذِينَ أُوتُوا الْعِلْمَ دَرَجَاتٍ

صدق الله العلي العظيم

(المجادلة: من الآية 11)

LINGUISTIC CERTIFICATE

I certify that the thesis entitled **"Laboratory Performance of Shallow Buried Plastic Pipes below Geocell Reinforced Subbase Layer under Repeated Load"** which has been submitted by (**Sajjad Emad Rasheed**) has prepared under my linguistic supervision. Its language has been amended to meet the English style.

Signature:

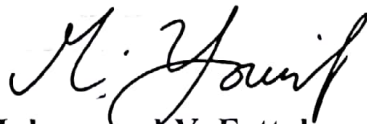Name: Dr. Alaa M. Shaban

Linguistic advisor

Collage of Engineering / Civil Engineering
Department University of Kerbala

Date: 16 / 8 / 2017

SUPERVISOR CERTIFICATE

We certify that the thesis entitled " **Laboratory Performance of Shallow Buried Plastic Pipes Below Geocell Reinforced Subbase Layer Under Repeated Load**" prepared by "**Sajjad Emad Rasheed**", has been carried out completely under our supervision at Collage of Engineering, University of Kerbala, in partial fulfillment of the requirements for the Degree of Master of Science in Infrastructure Engineering.

Signature:

Prof. Dr. Mohammad Y. Fattah

Date:14/8 / 2017

Signature:

Asist.Prof.Dr. Waqed H. Hassan

Date:14/8/ 2017

In view of the available recommendations, we forward this thesis for debate by the examining committee.

Signature:

Asist.Prof.Dr. Waqed H. Hassan

Chairman of Civil Engineering Department, University of Kerbala

Date: 14/ 8/ 2017

Certificate of Examination Committee

As members of the Final Examination Committee, we certify that we have read the Thesis prepared by "Sajjad Emad Rasheed", entitled "Laboratory Performance of Shallow Buried Plastic Pipes below Geocell Reinforced Subbase Layer under Repeated Load" and recommend that it be accepted as fulfilling the Thesis requirement for the Degree of Master of Science in Infrastructure Engineering.

Supervisor
Signature:
Prof. Dr. Mohammad Y. Fattah
Date: 14 / 2 /2018

Supervisor
Signature: Waqed H. H.
Assist. Prof. Dr. Waqed H. Hassan
Date: 8 / 2 /2018

Member
Signature:
Assist. Prof. Dr. Karim H. Ibrahim
Date: 14 / 2 /2018

Member
Signature:
Dr. Raid R. A. Almuhanna
Date: 8/ 2 /2018

Chairman
Signature:
Assist. Prof. Dr. Rasul Mejbel Khalaf
Date: 14/ 2 /2018

Approved by the dean of the college of engineering, University of Kerbala

Signature:
Assist. Prof. Dr. Basim Khlail Nile
Date: 14/ 2 /2018

Dedication

To my mother, a strong and gentle woman who raised my two sisters and me by herself, and provided us with everything we have ever needed. I pray to God every day that you will get better soon.

To the memory of my aunt, you will forever be remembered, rest in peace.

ACKNOWLEDGEMENT

Abstract

Developing a physical model is a common method to obtain the information involving soil-pipe interaction, which can provide different testing conditions. The present study deals with the experimental investigations of the behavior of buried PVC pipes. A number of laboratory experiments were conducted using PVC pipes which were buried in medium sand layer and below a subbase layer reinforced with geocells and subjected to two dynamic repeated loading amplitudes (0.5 ton and 1 ton) and three different loading frequencies (0.5 Hz, 1 Hz, 2 Hz) to study the effects of the geocell reinforcement layer inclusion on the stress reaching the pipe crown, vibration of the pipe and the soil surface settlement. The results of the experimental work showed that the reduction of surface settlement due to the geocell reinforcement ranges from 29 to 43 % when the amplitude of load is (0.5) ton, whereas, the reduction varies from 32 to 41% when the load amplitude is up to (1) ton. When using geocell reinforcement, the amplitude of crown displacement is reduced by about 25 to 35% and 13 to 18% when the load amplitude is 0.5 and 1 ton, respectively. When using geocell reinforcement, the value of vertical pressure is decreased by about 13 to 41 % when the load amplitude is 0.5 ton and by about 25 to32 % when the load amplitude is 1 ton.

The results of experimental work were verified using the finite element software PLAXIS 3D. The geocell reinforcement was modeled using the geogrid element, which is defined as a slender structure element that has the ability to withstand axial stresses but no bending stiffness. Geogrids cannot sustain compression; however, they provide a high tensile resistance. The results of the numerical simulation of the experimental work showed that the maximum percentage of error between the

experimental and the numerical results in terms of surface settlement is about 10%. The maximum percentage of error between the experimental and the numerical results in terms of crown displacement is about 6%. The maximum percentage of error between the experimental and the numerical results in terms of vertical stress reaching the crown is about 11%. This modeling was found successful through good convergence with experimental results. Study results showed that the numerical modeling compares well with the experimental work results, and showed that geocell reinforcement has a significant positive change of reduction of the surface settlement, vertical stress above the pipe crown and the vertical displacement of the pipe crown. A parametric study was also developed based on the literature review, the experimental results, and the calibrated numerical models to study the effect of multiple parameters on a full-scale model.

Contents

V

List of Figures

IX

List of Plates

List of Tables

List of Symbols

a_0	Amplitude of load
α_R	Mass proportional Rayleigh damping coefficient
βR	Stiffness proportional Rayleigh damping coefficient
b	Width of geocell reinforcement
B	Width of footing model
c	Cohesion of soil
C_c	Coefficient of curvature
C_u	Coefficient of uniformity
d	Equivalent diameter of cells
D	Diameter of the pipe
D_{10}	Diameter corresponding to percent passing of 10 %
D_{30}	Diameter corresponding to percent passing of 30 %
D_{60}	Diameter corresponding to percent passing of 60 %
E	Young's modulus
fn	n^{th} natural frequency of the soil deposit
F	Applied force
Gs	Specific gravity
Hz	Hertz (cycle/sec).
k_o	Coefficient of lateral earth pressure.

RD	Relative density
R_{inter}	Reduced Interface Strength
S	Vehicle speed
t	Time
vs	Shear wave velocity
γ	Unit weight of the soil
$\gamma_{d\,(max)}$	Maximum unit weight
$\gamma_{d\,(min)}$	Minimum unit weight
ν	Poisson's ratio
φ	Angle of soil internal friction.
ψ	Dilatancy angle
σdy	Dynamic Stress Response
ω	Frequency of load
ωr	Operating frequency of the machine

List of Abbreviations

AASHTO	American Association of State Highway and Transportation Officials
ASTM	American Society for Testing and Materials
BSM	Bidirectional Shifting Function Method
BSI	British Standard Institute
CANDE	Culvert Design and Analysis
DEM	Discrete Element Method
FEM	Finite Element Method
FHWA	Federal Highway Administration
HDPE	High Density Polyethylene
HL-93	Truck loads

LVDT	Linear Variable Differential Transformers
PLC	Programmable Logic Controller
PVC	Poly Vinyl Chloride
SIDD	Standard Installation Design and Analysis
UKWIR	United Kingdom Water Industry Research
UPVC	Un Plasticized Poly Vinyl Chloride
USCS	Unified Soil Classification System

Chapter One

Introduction

1.1 General

Buried pipes and/or conduits have improved the living standards for people since the civilization beginning. The structures remaining from those civilizations were discovered in different parts of the world where many of those civilizations utilized functional sewer and water systems (Moser, 2001). Buried pipes serve many purposes, including drain lines, sewer lines, gas lines, water mains, electrical and telephone conduits, coal slurry lines, oil lines, culverts, heat distribution lines and subway tunnels. In comparing the design used in the 1800's to the design applications we have today, it is apparent that the degree of technology has increased significantly.

Engineers and planners take subsurface infrastructure into account before developing buildings and houses for a community. The underground pipe systems function as arteries for towns, and the sewer systems that convey the waste are considered as the veins of these towns (Moser, 2001). High-quality drinking water is taken for granted by humans in today's society. To confirm acceptable quality, pipes should be designed and assembled to prevent the introduction of contaminants. The same standards apply to sewer pipes to prevent seepage of contaminants into the ground, which may reach the water table and aquifers.

Soil reinforcing in the form of geosynthetic reinforcement is gaining popularity in infrastructure engineering. These types of reinforcements increase the foundation bed overall performance by reducing the settlement and improving the capacity of load carrying.

1.2 Types of Buried Pipes

Buried pipes are mainly categorized into two classes, rigid and flexible. The pipe is classified as flexible when it can deflect minimally by 2 percent of its diameter without reaching structural distress, otherwise it is considered as rigid pipe; in other words, pipes that cannot deflect safely, without failing, by 2 percent of their diameter are classified as rigid pipes. Today's market, the most available/used rigid pipes are clay, cast iron, reinforced/unreinforced concrete pipes, and most of the obtainable flexible pipes are PVC (Polyvinyl Chloride), steel, ductile iron (Tan and Moore, 2007).

The useful properties of the PVC pipe attain its position as one of the most versatile of all pipe's materials, a fact which is proved by the variety of applications that PVC pipes served.

1.3 Effects of Loads on Buried Pipes

Buried pipes have an important role in the city infrastructure; they must support the weight of the surrounding soil, so they must be protected and properly installed to avoid serious ramifications to the pipe system, the above pavement and buildings.

1.4 Problem Statement

Flexible pipes such as PVC are installed at a shallow depth. Thus, enhancing the period of expected serviceability, preventing premature cracking, and protecting of the buried pipe system from dynamic traffic loading is required.

1.5 Objectives of the Study

This study aims to determine the mitigation effects of using geocell reinforcement on a buried pipe and evaluating this concept by laboratory

scale modeling and validating the experimental work using the well-known finite element program PLAXIS 3D, 2013.

To accomplish the above objective, the following steps are taken into account:

1. Investigation of the role of reinforced subbase layer in the protection of buried pipes.
2. Investigation of the surface settlement with and without the geocell reinforcement.
3. Investigation of the vertical stress reaching the pipe and the displacement amplitude that occurs above the pipe due to dynamic traffic loading.
4. Developing a finite element model that can validate the experimental work to a certain extent.

1.6 Limitations

The most obvious limitations of this study are:

1. Load amplitude and frequency.
2. Relative density of soil.
3. Type of soil.
4. Material of pipe.
5. Depth of pipe and reinforcement

1.7 Thesis Layout

This study is presented in seven chapters, which are outlined as follows:

Chapter One: presented a brief introduction to the topic.

Chapter Two: shows a review of published literature to describe the current understanding of the soil-pipeline interaction aspect. The chapter describes previous studies that are related with the main topic. Numerical and analytical methods, field-testing of soil and pipe conditions are included.

Chapter Three: presents the experimental work details, which include the complete setup design for the model tests, testing program, and testing procedures.

Chapter Four: presents the numerical simulation of experiments using the finite element method.

Chapter Five: presents the results and discussion of the experimental work tests and the verification problem.

Chapter Six: presents a parametric study on the buried pipe problem.

Chapter Seven: presents conclusions obtained from the experimental and numerical study and recommendations for future studies.

Chapter Two

Review of Literature

2.1 Introduction

The underground structures behavior is complicated in comparison with superstructures. The main reason is the soil-structure interaction, which is hard to predict in many cases. Since subsurface structures are quite spread in the urban areas and serve the vital needs of the societies, there is a great sensitivity and importance to lifelines. Although numerous codes and provisions are suggested for the lifelines safe design, the designed and constructed lifelines are unsafe to damage when exposed to heavy dynamic loadings mainly strong blasts or earthquakes.

Most of the theoretical studies presented shortcomings in considering the real soil response against the pipe and vice versa despite the large number of studies, which have been done to model the soil-pipe interaction, which resulted in many mathematical relations and empirical equations.

Developing a physical model is a common way to obtain actual information relating to soil pipe interaction, which is capable of providing different conditions. The main parameters associated with the field behavior of the pipe can then be measured and studied somewhat accurately.

The literature that is connected to the core objectives of this study is briefly reviewed in this chapter. Other literature related to some topics is mentioned when these topics will be discussed. This chapter also discusses soil arching associated with buried pipes.

5

2.2 Soil Response under Dynamic Loadings.

The nature of load producing source determines the dynamic loading type in soil or the structure foundation. Dynamic loadings may fluctuate in their position, direction or magnitude with time. Several types of forces variation may co-exist (Das and Ramana, 2011).

There are several types of dynamic conditions that fall into a number of categories: (1) machinery vibrations, (2) earthquakes, and (3) many human made disturbances; like soil compaction, water hammer in pipes, rail or wheel loadings, pile driving, etc. (Handy and Spangler, 1973).

2.3 Buried Pipes

Utility installations and highway drainage necessitate the placement, design and backfilling of conduits to support the facilities and ensure adequate performance of the roadway system. A well-designed pipe may fail due to inappropriate or inadequate installation techniques. Therefore, the importance of the pipe behavior during the backfilling operations and placement is stressed throughout this chapter.

2.3.1 Effects of loads on underground pipes

Low-pressure pipes, especially sewers, gravity mains or even large diameter pumping mains should be designed for external loads as well as internal loads. The vertical soil load acting in combination with vacuum pressure inside the pipe could cause the pipe to collapse unless the pipe is adequately supported or stiffened.

2.3.2 External loads from soil

The soil-structure interaction subject was the interest of engineers for over a century. The horseless carriage production started in the year 1902, so there was an apparent need for improved roads. A number of road drainage projects started

using concrete drain tile and clay tile, but there was no sensible method for calculating the imposed earth load on these drains, and this resulted in many pipelines failure.

The imposed loads on buried pipes depend on the stiffness of the soil and the pipe, which results in a statically indeterminate problem in which the pressure of the soil on the pipe causes a deflection that, in turn, determine the pressure of the soil.

When designing rigid pipes (for example, clay or concrete pipes), the vertical pressure caused by traffic and soil is the key factor affecting the pipe; a horizontally reacting pressure is either negligible or nonexistent. As for flexible pipes, the deflection of the pipe is caused by vertical load, which in turn results in a horizontal supporting soil pressure. If the vertical pressure and horizontal soil pressure are close to being equal, the load around the pipe approximates a hydrostatic load. For deep burial pipes, there is a high probability of buckling for flexible pipes. (Moser, 2001).

2.3.3 Longitudinal loading

Specific types of failures in pipes which have been perceived over the years are suggestive that the pipeline is subjected to the vertical pressure only under ideal conditions. There are other types of forces that yield axially acting bending stresses in the pipe in some way. These types of forces may vary and thus, cannot lend themselves with any degree of confidence to quantitative analysis. Some of the main reasons of beam action or pipeline axial bending are (Moser, 2001):

1. Differential settlement.

2. Ground movement caused by external forces like frost heave or earthquakes.

3. Non-uniform bedding support.

2.3.4 Live load

This type of load is imposed on a small area of the surface above the underground pipe (e.g., through the contact area of a tire or crawler track). As the effect of this load progresses downward into the soil, the area over which it is effective grows larger and since the total load is fixed, the pressure or load intensity is diminished Thus a deeply buried pipe is usually subjected to a lower intensity of loading from a surface load than a shallow-covered pipe. Design tables for maximum allowable soil cover regularly take into account the surcharge load to represent construction loadings or traffic (Moser, 2001).

2.3.5 Types of pipes

Almost all pipes can be categorized as either rigid or flexible, depending on the pipe performance after installation. Rigid pipe such as non-reinforced concrete pipe, reinforced and clay pipe is defined as the pipe that cannot deflect more than 2% without substantial structural distress. Flexible pipe benefits of its ability to deflect, move under loads without structural damage. Common types of flexible pipe are manufactured from polyethylene, polyvinyl chloride (PVC), aluminum and steel. Figure (2.1) shows variance responses of flexible and rigid pipe to loads. Both flexible and rigid pipe necessitate adequate backfill, although the interaction between the backfill and the pipe may vary.
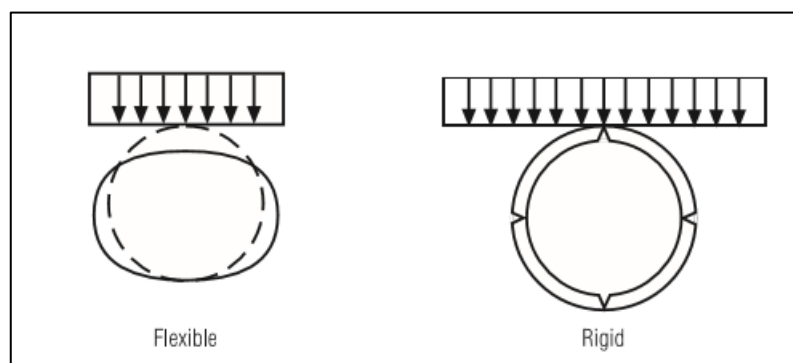
Figure 2.1 Pipe response to loading.

When loads are applied to rigid pipe, the load is transferred through the pipe wall into the bedding, when flexible pipe deflects against the backfill, the

load is transferred to and carried by the backfill. Adequate backfilling is very important for both types of materials in allowing this load transfer to occur (Suleiman, 2002). Figure (2.2) shows the interaction between the pipe and the backfill and the corresponding load transfer.
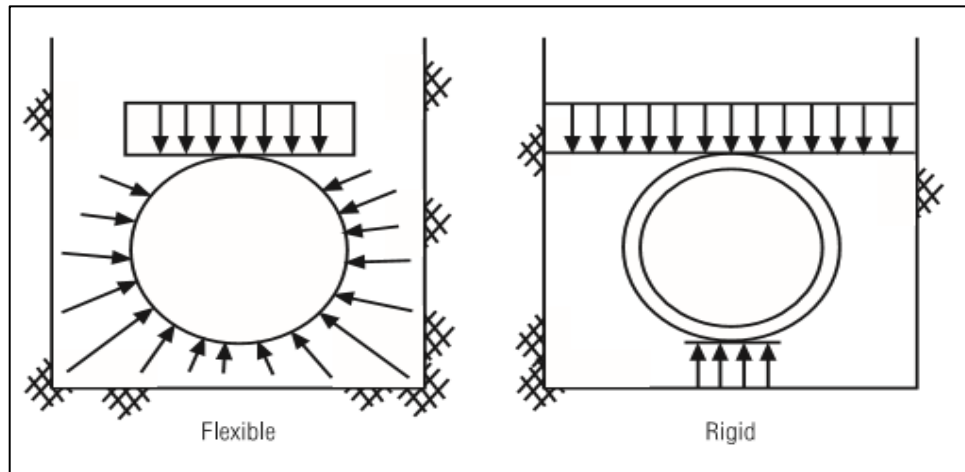
Figure 2.2 Pipe-backfill interaction.

Flexible pipes have great advantages over rigid pipes in that the flexible pipe can be buried much deeper than a similar rigid pipe because the rigid pipe is usually stronger than the adjacent backfill material, thus it must support the prism load above the pipe as well as the earth loads. On the other hand, a flexible has less strength than the surrounding backfill so the envelope of the backfill is mobilized to support the earth loads. The interaction between the pipe and the backfill is significantly effective at increasing the pipe structural properties that it allows the pipe to be installed deeper than a rigid pipe when properly installed (Andreasen, 1991)

2.4 Load distribution through soil

Predicting the settlements of embankments, buildings, bridges and other types of structures depends highly on the vertical pressure estimation at any point in the soil mass due to the vertical external loadings. A number of equations have been established to calculate the stresses at any point in the soil mass, and these equations are based on the elasticity theory. A constant number of ratios between

stresses and strains exist according to elastic theory. The material is not necessarily required be elastic in order for the theory to be applicable, but constant ratios must exist between stresses and related strains. Consequently, in the non-elastic soil masses, the elasticity theory can be assumed to hold as long as the induced stresses in the soil mass are relatively small. Since the stresses in the structure subsoil having an adequate factor of safety to resist shear failure are relatively small when compared to the ultimate strength of the material, the soil may be assumed to have an elastic behavior under such stresses. When the soil is subjected to a surface loading, the loading increases the vertical stresses within the soil mass. The greatest value of the increased stress is directly under the loaded area, but extend indefinitely in all directions. Based on the elastic theory, many formulas have been used to compute stresses in soils. (Murthy, 2002)

2.5 Geosynthetics

ASTM defines a geosynthetic as a planer product made of a polymeric material used with soil, rock, earth, or other geotechnical-related material, as an integral part of a civil engineering project, structure, or system.

There are many types of geosynthetics: (Berg and Anderson, 2009)

1. **Geomembranes**: are low-permeability geosynthetics used as fluid barriers.
2. **Geotextile**: is a permeable geosynthetic made of textile materials and have the ability to filter, reinforce, separate, drain, or protect.
3. **Geogrids**: are mainly used for reinforcement; they are formed by a regular network of tensile elements with apertures of sufficient size to interlock with surrounding fill material.

Geotextiles and related products such as nets and grids can be combined with geomembranes and other synthetics to get the benefit of the best attributes of each component. These are called geocomposites, and they may be composites of geotextile-geonets, geotextile-geogrids, geotextile-geomembranes,

geomembrane-geonets, geotextile-polymeric cores, and even three-dimensional polymeric cell structures. There is almost no limit to the variety of geocomposites that are possible and useful. The general generic term encompassing all these materials is geosynthetic (Berg and Anderson, 2009). Figure (2.3) shows different types of geosynthetics.
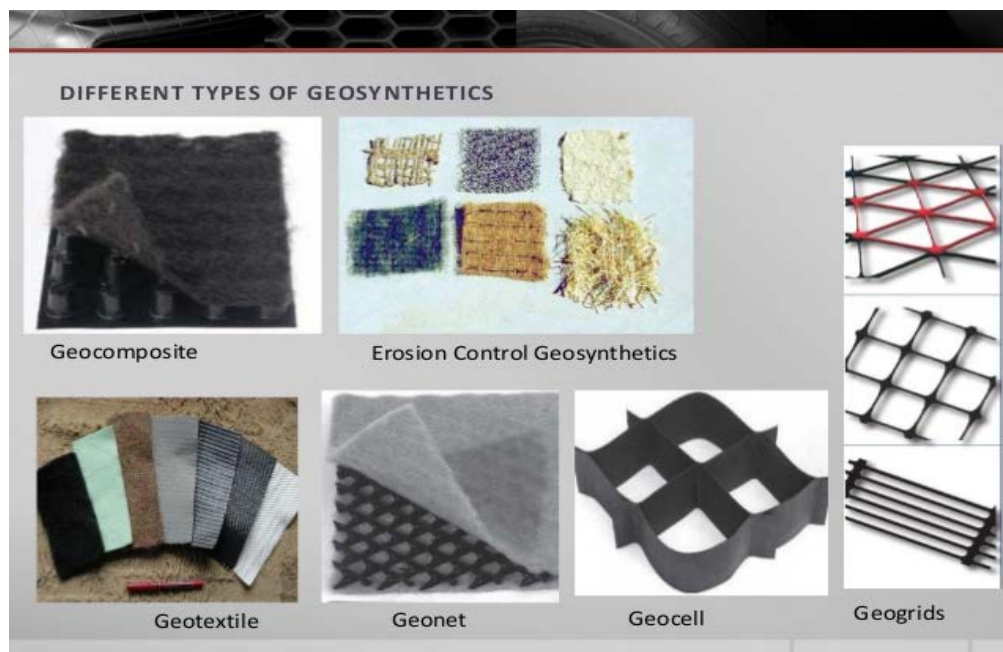
Figure 2.3 Different types of geosynthetics.

4. **Geocells**: are three-dimensional, honeycomb-shaped soil-reinforcing geosynthetics composed of polymeric materials and are primarily used for the confinement of granular material, (Figure 2.4). Geocells are placed at grade, in-filled with granular material, and compacted. The cellular structures of the geocells provide lateral and vertical confinement and tensioned membrane effect, thereby increasing the bearing capacity and providing a wider stress distribution (Rea and James, 1978). As a result, rutting or permanent deformations under traffic loading can be reduced. Typically, the geocell-base/subbase system is underlain by a geotextile to separate the in-filled base/subbase material from the subgrade, (Figure 2.5).

Figure 2.4 Geocells reinforcement.

Figure 2.5 Use of geocells in pavement layers.

2.5.1 Use of geosynthetics in protection of buried pipes

The protection of buried pipes and underground utilities by using the geosynthetic reinforcement is relatively a new concept. (Tafreshi and Khalaj, 2008) conducted laboratory experiments on HDPE (High-density polyethylene) pipes buried in sand with a small diameter and reinforced by geogrids and subjected to repeated loads. Significant reduction in the deformation of the pipe was observed by the researchers in the presence of geogrids. (Palmeira and Andrade, 2010) used a combination of geogrid and geotextile for the protection of the buried pipes in their model experiments. They observed that the

12

reinforcement produced major resistance to penetrating, sharp object and protects the buried pipes from the accidental damage. Recently, geocells are showing their efficacy in soil engineering applications.

2.6 Subbase Layer

It is a layer (or layers) located under the base layer. A proper layer of subbase consists of various sizes of crushed stone aggregate. Depending on the sub soils, 8-12 inches (200-300 mm) of various sizes of subbase may be needed. Added subbase materials may be sufficient with well-drained sub soils, without movement, and a proper pitch and grade. If the subbase layer is knowingly sufficient enough, grading and compaction with plate compactor or vibratory roller in small areas, may be all that is necessary.

2.6.1 Functions of subbase layer in flexible pavement system

The subbase layer primarily works as a structural support; it can also help in: (FHWA, 2001)

- Drainage improvement.
- Minimize the intrusion of fines from the subgrade into the pavement structure.
- Provide a working platform for construction.
- Minimize damage due to frost action.

The subbase is generally made up of materials with lower quality than the base course but better than the subgrade soils (Figure 2.6).
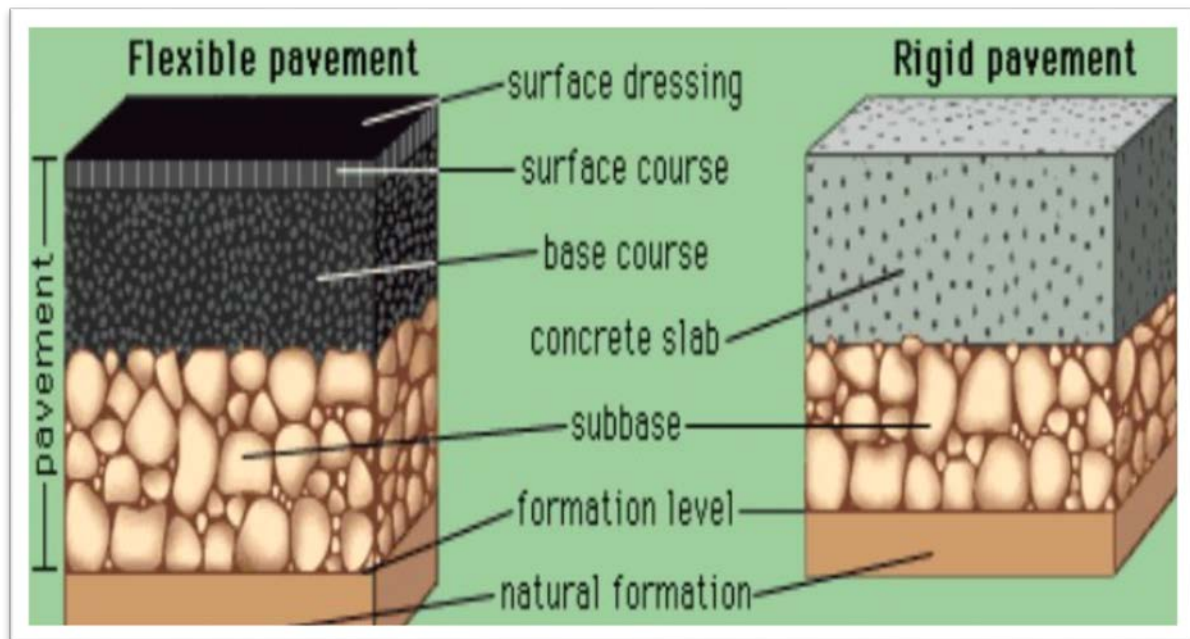
Figure 2.6 Subbase layer in flexible and rigid pavement.

2.7 Previous studies

2.7.1 Experimental studies

In spite of the availability of some instructions and standards e.g. (ASTM, 2008); (BSI, 1980) installing and maintaining underground pipes, backfill material optimization must be investigated, specifically in the case of backfill material reinforcement. There are common topics related with buried pipes regardless of their materials. Haque (1998) monitored and reported field performance of reinforced concrete pipe specimens of 1520 mm diameter during installation and subsequent highway embankment constructions. The pipes were instrumented in two sections, primary section at the crown, invert, right spring line and left spring line and secondary section at the right and left shoulder and haunch. At each location, gauges were placed on outside and inside of concrete wall and on inner and outer steel cages for monitoring the strains. Also, the changes in diameter in horizontal and vertical directions were measured by LVDTs (linear variable differential transformers), the pressure was measured by pressure cells and change in temperature inside the pipes was measured by

thermometers. The objectives were the comparisons between the experimental measurements and the results of both SIDD (standard installation design and analysis) and CANDE (Culvert Analysis and Design) finite elements programs.

Reddy and AtaoĞLu (2002), aimed primarily in their study to measure bending moments and the deflections of high density buried polyethylene pipes. The experiment on the buried HDPE pipe performance was conducted in soil chambers and the buried pipe was subjected to three different service loading levels. Diametric changes and strains were measured for a duration of 10,000 hours. The experimental findings discussion was fixated on specific recent concerns, related to the deflection of HDPE pipes, bending moments and longitudinal and transverse stresses. The failure criterion which was 7.5 % change in vertical diameter, was detected at 3200 hours for the specimens at 50° C, and subjected to maximum service loading. H-20 truck loading was used to determine the maximum allowable loading of the specimens. Most of the imposed loads from vehicles are less than the ones from the H-20 trucks. The models were also exposed to high temperature levels to accelerate the mechanisms of failure for the viscoelastic HDPE pipes. A 7.5% vertical change in diameter (the failure criterion) bending was measured. A 7.5% vertical change in diameter was measured for the specimens heated to 50° C, with the maximum loading. Life prediction was determined from the Arrhenius equation and the Bidirectional Shifting Function method (BSM). The two methods resulted in similar life predictions, but the BSM was more conservative (Reddy et al., 2001). A deflection of 7.5% was measured at 3200 hours when the model was subjected to maximum loading and heated to 40° C. Therefore, extrapolation had to be performed for this temperature environment to determine the maximum service life before failure (vertical deflection of 7.5 %). Based on the vertical deflection, life prediction at surrounding temperatures was performed from these values. The maximum measured service life for the models subjected to maximum loadings

and at surroundings temperatures was approximately 30 years for notched specimens and 80 years for unnotched specimens with the assumption of 90 % compaction and proper installation.

Davis et al. (2007) used fracture mechanics to predict the crack growth from inherent defects in the UPVC (Unplasticized Polyvinyl Chloride) pipe wall. A Monte Carlo simulation model was established in order to capture uncertainty in the process of pipe fracture, which generates a theoretical pipeline, consists of a series of independent pipe segments. The maximum value of inherent deflection in each pipe segment was considered as a stochastic variable, which is represented by the probability distribution function of Weibull. Based on the Weibull distribution and for each segment in the theoretical pipeline, the Monte Carlo simulation randomly assigns a maximum inherent defect size. The Monte Carlo (Mooney, 1997) simulation output provides the number of new segment of pipe installed for each simulation year, and the years of failure for each pipe segment. These data combination allows for the estimation of the rate of average failure (length/ failures /year). The rate of average failure versus age curves were extracted from the UKWIR (United Kingdom Water Industry Research) database for comparison with actual failure rates recorded by water utilities. Only longitudinal pipes failures were included to ensure a fair comparison. The predicted curves agreed within the 95% limits of confidence for actual rates of failure although the shape of the UKWIR failure rate curve was not fully captured.

Tafreshi and Khalaj (2008) evaluated the behavior of small-diameter high density polyethylene HDPE pipes (110 mm diameter and 4.03 mm wall thickness) buried in reinforced sand and subjected to repeated loading (550 kPa load amplitude). The influence of between 1 and 5 layers of reinforcement in soil with relative densities of 42%, 57%, and 72% was examined. The depth of the pipes was set as 1.5- 3 times their diameter. The test was implemented in a trench of 550 mm width. It was stated, that the proportion of soil surface settlement and

vertical pipe diameter change can be reduced by up to 51% and 40%, respectively, when using the five reinforcement layers in backfill of the highest relative density (72%) when the pipe is at its deepest embedment.

Based on the results of their tests, (Tafreshi and Mehrjardi, 2008) linked a neural network with a genetic algorithm and found out that to obtain a 2% vertical diametric strain and a soil surface settlement of 10 mm, a 2.5 ratio for embedment depth of the pipe to pipe diameter, one geogrid layer and a soil relative density of 75% would be required.

Recently, environmental concerns and a rising desire to take uncommon solutions into consideration means that the lightweight materials, for example: geofoam, wood fiber, tire rubbers, fly ash and reinforcement materials like geotextile, geogrids and geocells are now taken into account. (Zhang et al., 2008) and (Consoli et al., 2009) presented a modern soil reinforcing concept, by using vertical-horizontal (V-H) orthogonal reinforcing elements instead of the orthodox horizontal reinforcement. They conducted an inclusive set of tri-axial tests on sand reinforced with multi V-H orthogonal elements layers to investigate the behavior of the reinforced sand in terms of stress-strain relationship and shear strength. The results indicated that the inclusion of V-H orthogonal reinforcing elements inclusion increased the internal angle of friction as well as a small cohesion increase.

Kim and Santamarina (2008) studied the zero-lateral strain and small strain responses of largest of rubber particles and small rigid sand particle mixtures. The results showed that the mixture response was controlled by the sand skeleton when the volume fraction of rubber particles was less than 0.3, and vice versa when the volume fraction of rubber particles was more than 0.6. For this reason, proportions of rubber particles ranging from 0 to 20% representing a maximum

of 54% by volume were investigated, thus covering the range of fullness use identified by (Kim and Santamarina, 2008).

Recently, increasing the bearing capacity of soil by using three-dimensional reinforcement has been clearly proved by numerous researchers (Zhang et al., 2010); (Huang et al., 2011); (Lambert et al., 2011);(Boushehrian et al., 2011); (Tavakoli et al., 2012). (Emersleben and Meyer, 2010) conducted radial load tests to estimate the influence of multiple parameters such as interconnected cells number, the stiffness of geocell, the height of geocell and the height of soil cover on the mechanism of interaction between earth resistance and hoop stresses. The test results have revealed that the most important parameters in the behavior of the system are the number of adjacent cells and the geocell material stiffness.

Tafreshi and Dawson (2012) investigated the strip footing performance, which was supported on sand beds reinforced with a planer and three-dimensional geotextile under a repeated and static loads combination. The results showed that the three-dimensional reinforcement was more effective than the planer reinforcement under the effect of dynamic loading. In spite of this research on the ground improvement by using geocell reinforcement, there is a lack of information regarding the behavior of pipelines buried under soil supported by geocell reinforcement.

The experiments of (Tavakoli et al., 2012), with the concern of using rubber as a bedding material and cover (lightweight fill) for the pipe trench, cannot disregard the debates of whether it is suitable to put rubber particles in the ground with the chance of these particles causing deterioration to ground water quality.

Fang et al. (2013) established methods to estimate the structural reliability by using probability ideas. When the remaining ultimate strength of an

underground pipeline exceeded the limit, breakage occurs and the pipe distribution network overall reliability is reduced. Their study was concerned with estimating structural failure of underground flexible pipes due to excessive deflection caused by induced corrosion, bending stress, buckling, wall thrust subject to externally applied loading. The cross-sectional area and the moment of inertia of pipe wall were directly changed with time with the change of thickness of the pipe wall due to corrosion. Therefore, the survival or the reliability chance of the pipe material is decreased over time. One numerical example was presented for a buried steel pipe to predict the probability of failure using (Madsen, 1977) algorithm and Monte Carlo simulation. Then the sensitivity analysis and parametric study have been conducted on the pipeline reliability with different influencing factors, e.g., diameter, backfill height, pipe thickness, etc.

Srivastava and Goyal (2012) investigated the load-displacement relationships by conducting model plate load tests on buried flexible pipes under the surface footing. The tests were conducted in a rectangular box after the model footing was placed on the surface of sand placed at two different relative densities, see Figure (2.7). Different combinations of tests were performed, such as, (1) model footing placed over sand compacted at low relative density (RD =50%) and model buried flexible pipe (PVC pipe) placed at 0.5B and 1.0B depth; where B = diameter of the model footing, and (2) model footing placed over sand compacted at high relative density (RD = 88%) and model buried flexible pipe (PVC pipe) placed at 0.5B and 1.0B depth (Figure 2.8). The results provided a useful explanation about the behavior of soil-pipe combination system in terms of load-displacement relationship. The presence of a buried flexible pipe below the footing and the effect of the sand bearing capacity in different relative densities were also discussed. The two-dimensional finite element software PLAXIS was used to verify the experimental results, and in light of the experimental findings, the results obtained numerically were discussed.
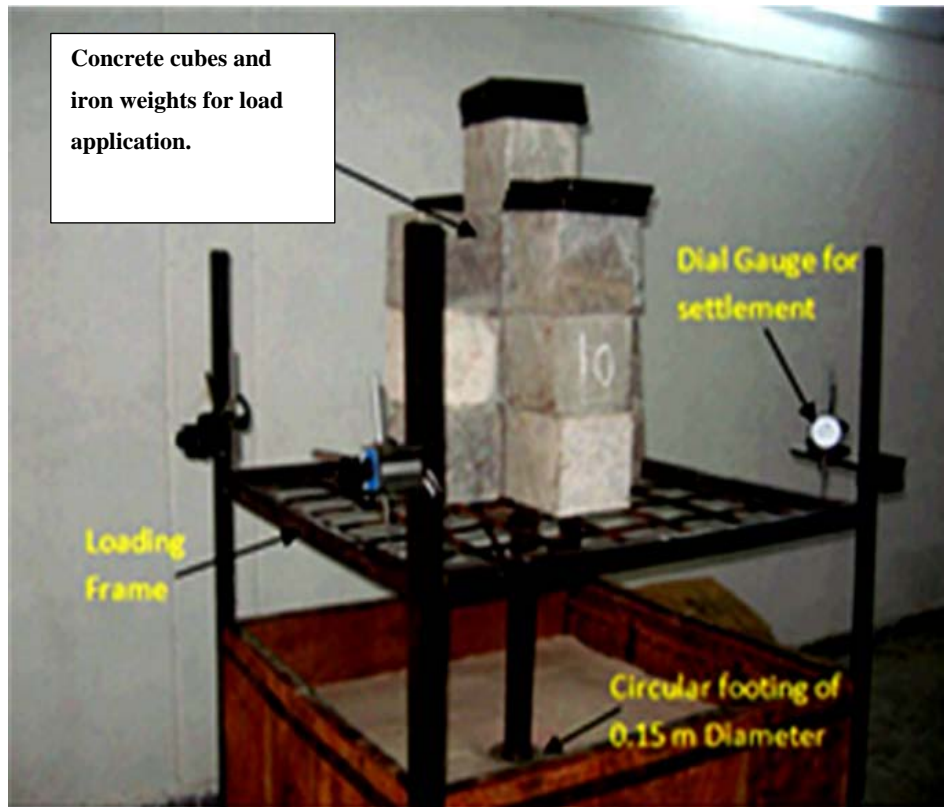
Figure 2.7 Experimental setup for studying load settlement response of model footing. after Srivastava and Goyal (2012).
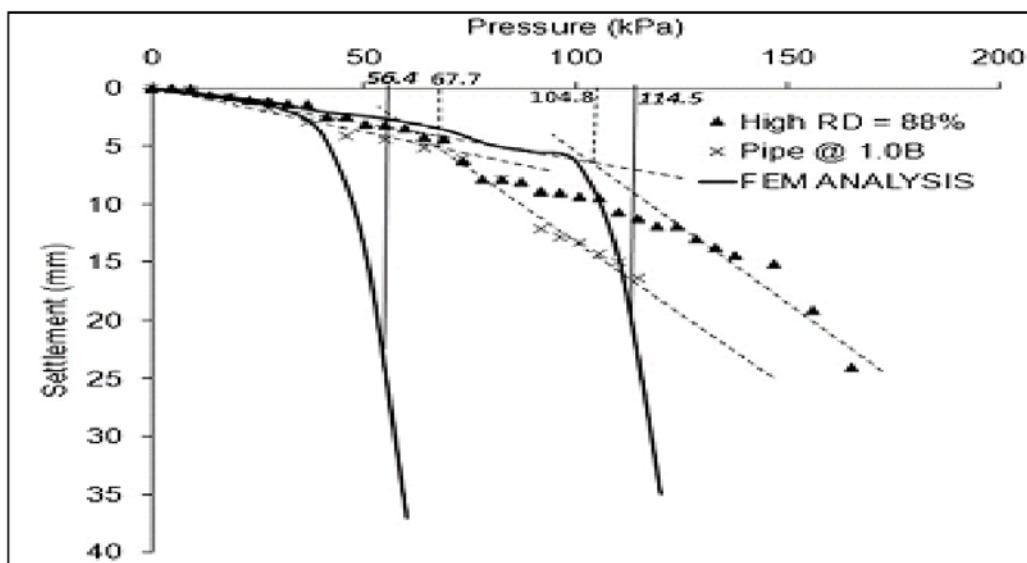
a. Dense sand
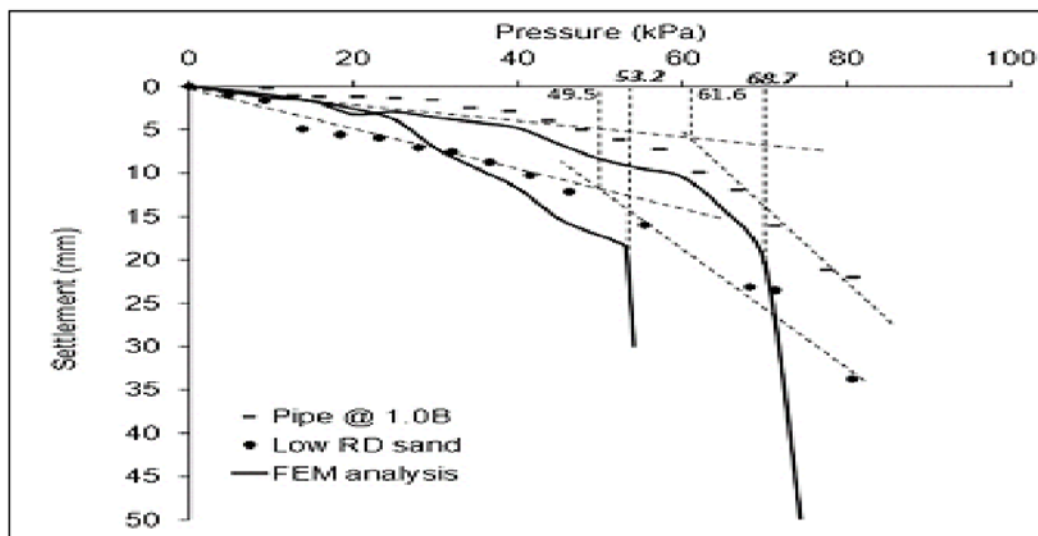
b. Loose sand

Figure 2.8 Load settlement of model footing over buried
flexible pipe embedded in sand after Srivastava and Goyal (2012).

Marto et al. (2013) showed that the addition of planar reinforcement in the
sand decreased much both the monotonic and cumulative settlements leading to
an economic design of the footings. Generally, soil has a low tensile strength. The
main objective of strengthening the soil mass is to improve stability, increase
bearing capacity and decrease total and differential settlements and lateral
deformations. A known technique in soil reinforcement is the use of polymeric
materials. Using this technique can significantly reduce costs and improve the
soil performance in comparison with conventional designs. A review of
experimental and numerical tests conducted by different previous researchers on
reinforced soil with synthetic materials especially geogrid under static loading
had been done and could be summarized as stated by (Marto et al., 2013):

- The presence of geogrid in the soil makes the relationship between the
  settlement and applied pressure of the reinforced soil almost linear until
  reaching the failure stage.

- The bearing capacity increases according to number of reinforcement layers.

- Improvement of bearing capacity prorates counter to the vertical space between geogrid layers.

- The reinforcement efficiency related conversely to geogrid width.

Hegde et al. (2014) described laboratory tests on PVC pipes with small diameter buried in geosynthetic reinforced and unreinforced sand subjected to static loading. The study focus was to assess the quality of combining geogrid and geocell reinforcement system in protecting the underground utilities and buried pipelines. A pipe with a 1.4 mm thickness and a 75 mm outer diameter was founded below the footing at different depths ranging from 1B to 2B (B is the width of the footing). Biaxial geogrid (SS-20) and commercially available Neoweb geocell reinforcement were used in the study. The results showed that combining geogrid and geocell reinforcement system considerably decreases the pipe deformation as compared to unreinforced soil bed. More than 40% reduction in the strain and more than 50% reduction in the pressure values were observed in the reinforced bed as compared to the unreinforced bed at different depths. On the other hand, the foundation bed performance was also found to be highly influenced by the depth of the pipe, even in the presence of the relatively stiff reinforcement system.

2.7.2 Numerical studies

The finite element analysis has proved to be very useful in the analyses of buried structures. Many finite element programs are available in the market and each of which has several advantages and disadvantages depending on the case study. Some of these programs are PLAXIS, which is used in this thesis, PIPE 5, a version of SAP (Wilson, 1971) modified by Utah State University

22

researchers for the analysis of the flexible pipe, CANDE (Culvert Analysis and Design) (Katona et al., 1976), which is mostly used in the U.S., SPIDA (Heger et al., 1985) which is used for the analysis of rigid concrete pipes and some others such as ABAQUS (1998), ADINA and SIGMA/W. Some of the numerical studies carried out by the researchers are reviewed in this section.

(Crofts et al., 1977) suggested a method for calculating the horizontal movement of a long shallow buried pipeline due to nearby excavation and backfilling of a long deep trench parallel to the pipeline. The problem model consisted of a beam embedded in an elastic foundation which is locally displaced laterally was analyzed and an approach was suggested for estimating the risk of pipe fracture.

A soil pipe system was modeled by (Suleiman, 2002) using ANSYS, a general finite element software. Many case studies were analyzed by using both large and small deflection theories of ANSYS and the results were compared to the results of the software CANDE, a common software for analyzing underground pipe systems. A code was also written within ANSYS to include the following soil parameters: the power bulk modulus, the hyperbolic tangent modulus and the hyperbolic bulk modulus. All of the acquired results were in good agreement when using the modified soil models with ANSYS, less than 10% except in one case with the results obtained using CANDE for 6.1 m soil cover above the spring line for the case of 610 mm pipe diameter with ML soil. The large deflection theory resulted in an insignificant effect, a little less than 5% when compared with ANSYS small deflection theory results for soil heights that are less than 6.1 m above the spring line, and that proves the adequacy of the small deflection theory for these cases.

Sivakumar Babu et al. (2006) re-examined underground flexible pipes behavior with the influence of several uncertainties in external load; the stiffness

of soil, soil and pipe properties were considered as random variables. The point estimate method was conducted to assess the reliability of deflection of a typical pipe section with typical soil properties with respect to two measures of reliability, safety margin and factor of safety. The results indicated thatthe conventional tolerable deflection limit of 5% of the diameter of a flexible pipe with a factor of safety of 4 is conservative.

Trickey and Moore (2007) used ANSYS finite element software to investigate the behavior of three dimensional underground pipes subjected to circular surface loading code. The previous work by (Poulos and Davis, 1974) has been reviewed with the consideration of the longitudinal behavior under surface loading. Several analyses were performed on pipes with varying burial depths and pipe stiffness and the following conclusions were founded:

- Peak moment decreases as the pipes become more remote from the ground surface and increases with pipe stiffness.
- Flexible pipe deflections considerably decrease as the embedment depth increases.
- The burial depth that is close to the ground surface has a small impact on the peak deflection.

2.8 Soil Arching

Soil arching is one of the most occurring phenomena in soils,(Terzaghi, 1943). This effect is more recognized in underground structures. Underground openings can be built utilizing the arching action to account for the reduction in the overburden pressure. The soil medium adjacent to the underground opening can increase the structure's load-carrying ability compared to an identical unburied structure.

Researchers have tried to understand the soil arching mechanism for decades. Much research has been done in this area, including theoretical derivations, analytical methods, numerical analyses, and experimental investigations. Researchers also applied the arching theory to practical engineering problems, for example, the soil plug problem (Paikowsky, 1989) and the sheet pile design (Rowe, 1952).

In the 1920's and 1930's, the importance of the arching around tunnels was recognized. Designers found that the support loads were far less than the overburden and that considerable savings could be achieved if accurate predictions of load were possible. This gave rise to empirical relations for tunnel support loading. Some of these relations are still in use today (Széchy, 1973), including Terzaghi's design values for underground structure support loads under various ground conditions. Terzaghi (1943) and Proctor and White (1946) stated that the interest in tunnel support loads also led to experimental and theoretical treatment of the problem (most notable Terzaghi's research in 1936 and 1943).

In the 1950's, the decision to build an interstate highway system in America created new interest in the loads on underground conduits. Larger culverts, with fill heights and culvert loadings greater than ever before, were required. Researchers reviewed and updated Marston's recommendations in light of experience obtained in the several decades since his investigations. Particular attention was given to the positive effects of load redistribution around flexible culverts, and techniques for reducing the load on a culvert through specific backfilling procedures (Spangler et al., 1947) ; (Handy and Spangler, 1973).

The direction of arching-related research shifted once again in the 1960's when the Defense Department of the United States sponsored considerable research in the area of soil-structure interaction. Techniques were needed for the

design of massive defense facilities and it was recognized that the arching phenomenon would allow facilities placed below ground to withstand nuclear attacks during the war, which would destroy any surface facilities, (Whitman et al., 1962).

Most of the research was presented at the "Symposium on Soil- Structure Interaction" in 1964. Starting in the 1970's, computer-based techniques have been broadly utilized in the studies of arching problems.

Getzler et al. (1970) used the finite difference method to analyze the arching pressures in an ideal elastic soil model. The principal compressive stress trajectories produced by differential settlement showed that an arch is formed in the overlying soil, abutting on both sides of the structure and transferring part of the load to those zones. Both magnitude and mode of the arching vary with depth of cover, beginning with two small separate local arches over the edges, through single arch with a saddle-shaped crown and ending with fully-developed arch which increases up to a fixed limiting size corresponding to geometric and elastic conditions.

Rude (1983) utilized a linear elastic finite element program to calculate the behavior of a culvert installed in a laboratory testing tank. Rude's predictions based on the program had shown good agreement with experimental results. More recently, individual particle's properties and interparticle relationships were taken into account in the numerical analysis.

Sakaguchi et al. (1993) used the "Discrete Element Method" (DEM) for computer simulations on the formation of arches plugging flow. They considered the rolling friction effect between particles and got a good agreement between the simulation outcomes and experimental measurements. (Terzaghi, 1936) have been duplicated by several researchers, e.g. (McNulty, 1965), (Harris, 1974), (Vardoulakis et al., 1981), and (Evans, 1983).

No real advances have been obtained in these research projects compared to Terzaghi's approach. Lately, some new technologies were applied in the arching studies. Iglesia et al. (1991) used centrifuge modeling to study scaling issues and arching in geomaterials. However, the stress distribution across the yielding surface and the correct shape of the sliding surfaces are still not known well techniques to measure the distribution of stresses within a soil body are required. The "Photogrammetric Method and the "Tactile Sensing Method" (Paikowsky and Hajduk, 1997) are the new techniques being investigated recently for measuring the stress distribution in granular soil. Materials like photo-elastic particles can also be utilized to study the shape of the sliding surfaces related to the arching effect (Paikowsky et al., 1995).

2.9 Summary

Throughout the reviewing of the literature, it appears that there is slight literature in studying the behavior of underground pipes that are buried under the geocell reinforced soil. Furthermore, this problem is not studied enough experimentally under static and dynamic load application. Scarce literature was found on simulating such problem by 3D finite element program for both static and dynamic analysis especially when the soil above the buried pipe is reinforced by geocell. Therefore, necessity has been appeared to fill the lack of knowledge in this problem.

As a result, an extensive experimental program was planned to study the problem of buried pipe under geocell reinforced subbase course subjected to dynamic traffic load. In addition, a numerical simulation for the problem by using PLAXIS 3D, 2013 finite element program is planned too.

Chapter Three

Experimental Work

3.1 Introduction

The focus of this chapter is on the experimental work, the testing procedure and the used materials and equipment. The testing program includes a number of tests on a laboratory model to study the behavior of geocell reinforced subbase layer in the protection of buried flexible PVC pipe subjected to dynamic traffic loading. The effect of a number of variables was taken into consideration such as: frequency of the load (ω), load amplitude (a_o) and the width of the geocell opening.

3.2 Testing program

A total of 12 models were tested in which, the geocells were used in 6 models and the other 6 models were un-reinforced. The models were subjected to two load amplitudes: 0.5 ton and 1 ton, and the frequencies used were: 0.5 Hz, 1 Hz and 2 Hz. The bedding material is sand prepared at 60% relative density and the subbase compaction ratio was 80%.

The conducted testing program in this study is summerized and shown in Figure (3.1).
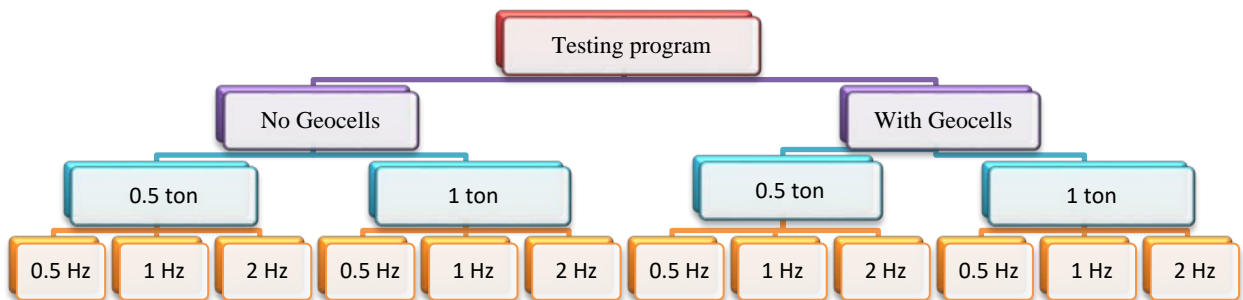
Figure 3.1 Flow chart of the testing program.

3.3 Soils and the other used Materials

3.3.1 Sand

The properties of the used sand include specific gravity, grain size distribution, and maximum and minimum dry unit weights. A summary of the test results with standard specification that followed in each test is presented in Table (3.1). According to the grain size distribution curve results presented in Figure (3.2), it can be seen that the sand is of medium to coarse size. According to the Unified Soil Classification System (USCS), the sand is classified as poorly graded sand with symbol SP.

Table 3.1 Sand physical properties.

Properties	Values	Standards
Specific gravity (Gs)	2.65	ASTM D 854
Soil classification	SP	ASTM D 422
γ_{dry} max. (kN/m^3)	18.81	ASTM D 4253
γ_{dry} min. (kN/m^3)	15.33	ASTM D 4254
Internal friction angle	38˚	ASTM D 3080

$D_{10}=0.16$ mm
$D_{30}=0.23$ mm
$D_{60}=0.38$ mm
$C_u= 2.38$
$C_c=0.87$
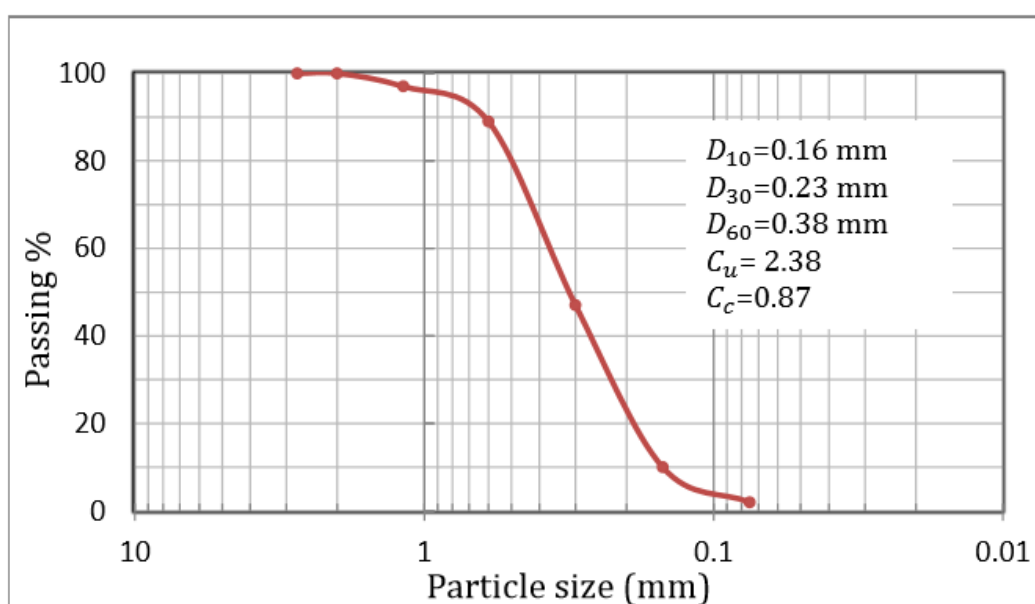
Figure 3.2 Grain size distribution curve.

3.3.2 Subbase layer

The subbase course is the layer of material under the base course. The use of two different granular materials is more economic instead of using the more expensive base course material for the entire layer.

Mechanical sieve analysis was carried out to determine the grading of subbase material. Table (3-2) shows the percentage of passing for used materials and allowable limits of the Iraqi specification requirements for gradation of subbase (R6).

The physical properties of the subbase material are shown in Table (3.3).

Table 3.2 Iraqi standards for subbase gradation (SORB, 1983 - R6).

Sieve size (mm)	Iraqi standards for passing Type B %	Subbase passing %
75	100	100
50	100	100
25	75-95	81
9.5	40-75	48
4.75	30-60	35
2.36	21-47	28
0.3	14-28	25
0.075	5-15	10

Table 3.3 Physical properties of the subbase material.

Type of test	ASTM standards	Results
California bearing ratio (CBR) at maximum dry density	D1883-05	42%
Optimum moisture content (O.M.C)	D1557 – 12	5.6
Maximum dry density (g/cm^3)	-	2.24
Specific gravity	D-854-14	2.56

3.3.3 Plastic PVC pipe

Even though the diameters of pipes may vary over an extensive range, a rational dimension representing the small pipe used for different services (sewer, gas mains, and drainage, etc.) is selected. The type of pipe that was selected for this study is a PVC (Poly Vinyl Chloride) pipe since it is widely used in urban facilities.

A one to ten scale factor was used in this study, so that the selected pipe has a 1.4 mm wall thickness and an outer diameter of 110 mm (Plate 3.1). The length of the selected pipe was chosen to be 700 mm which is less than the length of the tank by 100 mm in order to fit the pipe inside the tank. Two caps were used to close both ends of the pipe to prevent the soil particles from entering the pipe.
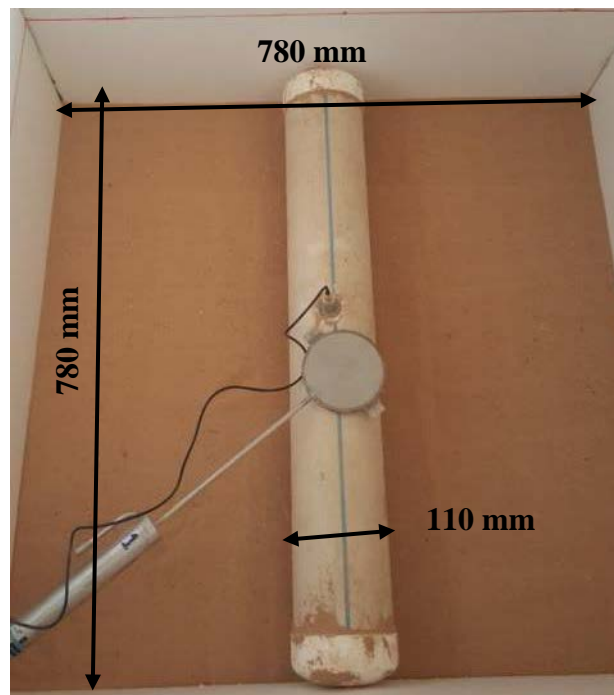
Plate 3.1 PVC pipe.

3.3.4 Geocell Reinforcement

The geocell reinforcement that was used in the experimental work was made locally from polymeric tabs that were sewn together in order to create a "honeycomb" shape, the pocket size of the geocell was taken as the equivalent diameter of circular shape ($A_{geocell}$) and the diameter was set to 70 mm so the ratio of geocell opening diameter to the footing width is about 0.7 which was found to give the best performance as reported by Dash et al. (2003) and Fattah and Redha (2016). The geocell height was selected to be (25 mm)

Additionally, in order to determine the tensile modulus and the strength of the geocell reinforcement, a tensile test was conducted by Ridha (2016) in the University of Technology. Plate (3.3) presents the setup of the tensile test. It can be shown from Figures (3.3) and (3.4) that the tensile modulus M which is the secant slope of the stress-strain curve is (40 kN/m) and the yield strength was calculated as (0.47 kN/m) at 5% strain.

Plate 3.2 Geocell reinforcement.

Plate 3.3 Geocell tensile test.
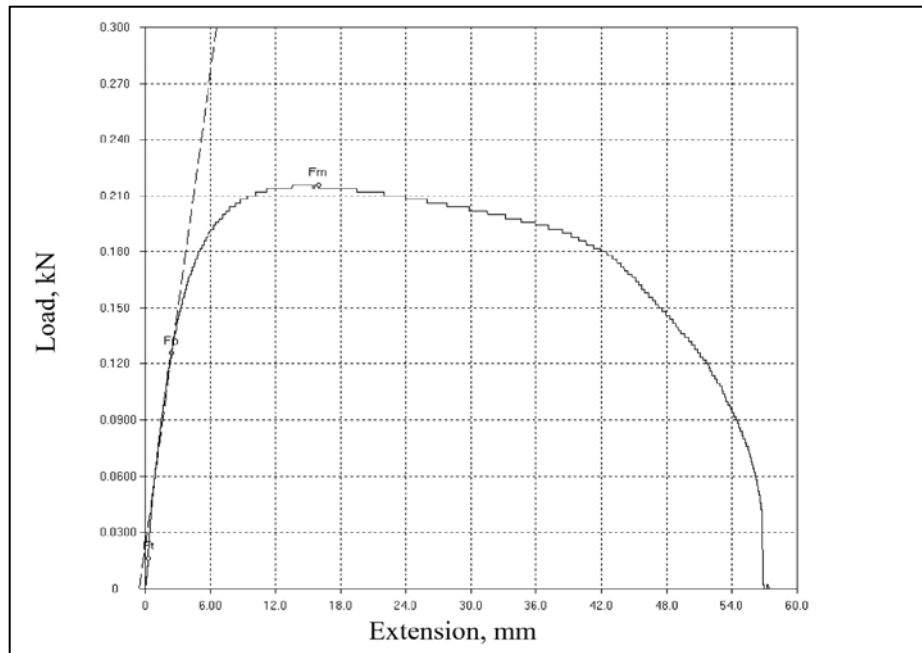
Figure 3.3 Load-displacement relationship of the geocell reinforcement
(after Ridha, 2016).
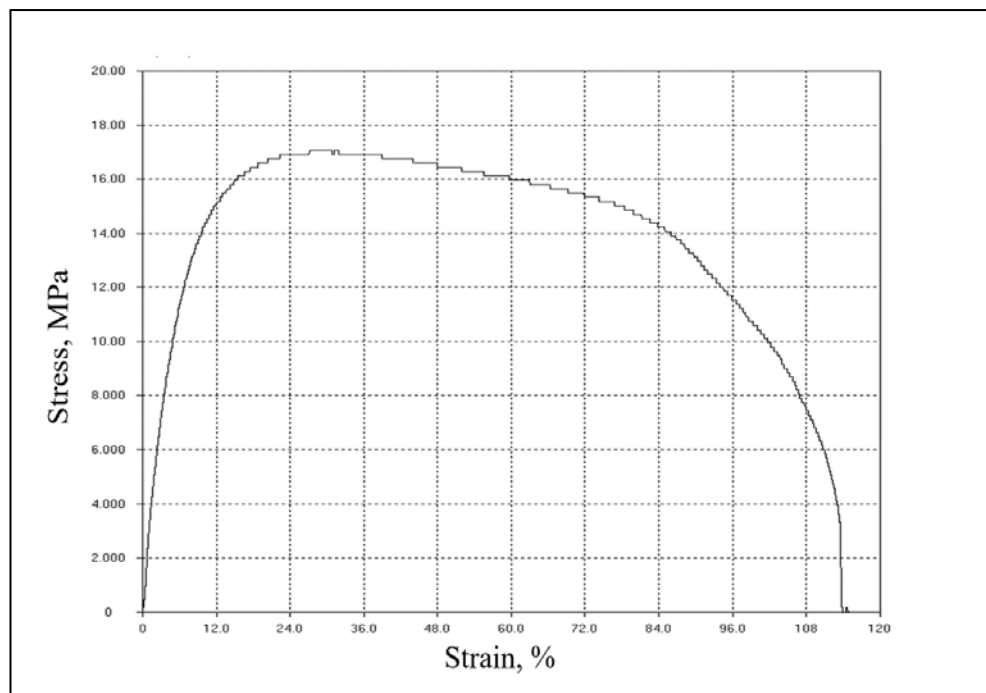
Figure 3.4 The stress-strain relationship of geocell
reinforcement (after Ridha, 2016).

3.4 Test Setup

It is essential to simulate the conditions of the experimental work in order to investigate the effect of the geocell reinforcement in traffic load transferring over buried pipes. Special devices and testing setup were designed in previous experiments conducted by (Abd Al-Kaream, 2013) in order to achieve this goal. A number of modifications were applied to support high load amplitudes. The setup is capable of applying different dynamic load amplitudes at different frequencies. Plate (3.4) shows the general view of the setup which was set at University of Technology-Baghdad. The test setup includes the following parts:

1. Steel box
2. Data acquisition system,
3. Shaft encoder,
4. Axial system of loading,
5. Model steel footing, and
6. Loading steel frame.
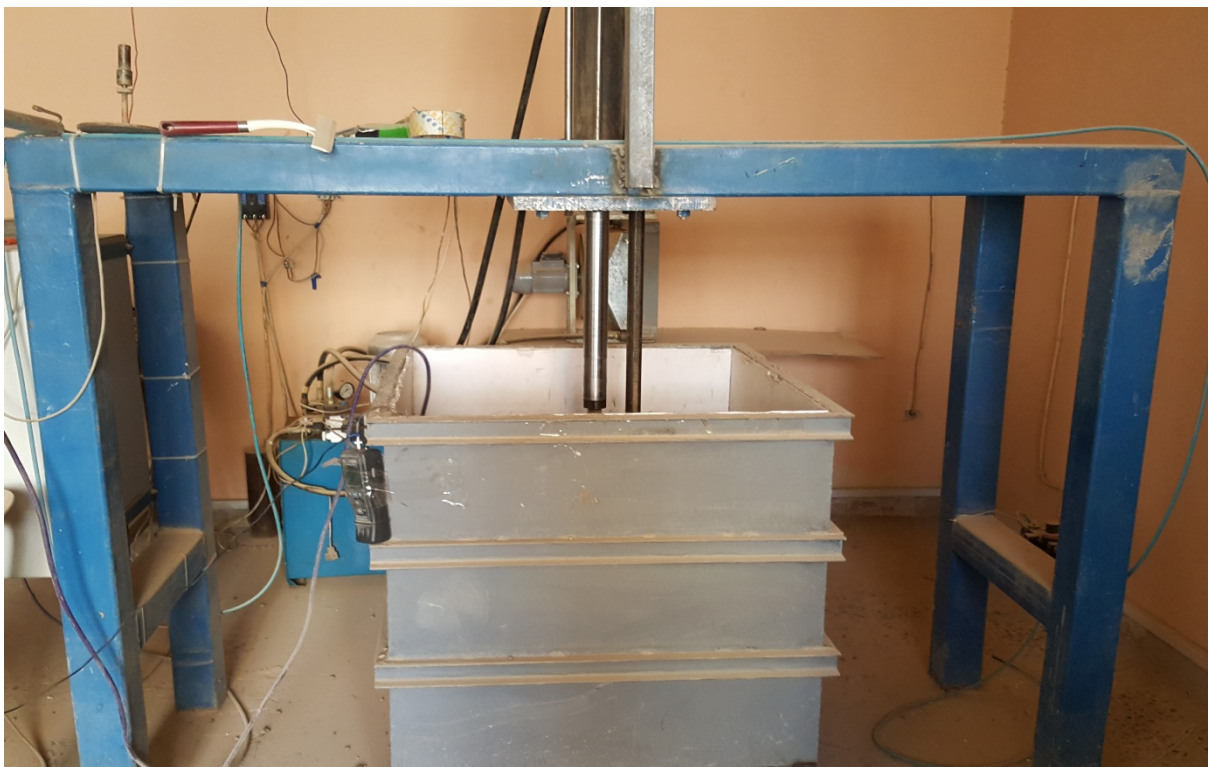
Plate 3.4 Testing setup.

3.4.1 Steel box

The experimental work was conducted in a cubic steel box. The box has a 800 mm width which agrees with the recommendations of (ASTM, D 2321-08) and (BSI, 1980). The width of the trench should have a minimum value to be equal or more than 1.25 times the outside diameter of the pipe with a 300 mm addition according to (ASTM, D 2321-08). BSI (1980) also recommends width of the trench should be equal or more than the pipe outside diameter (110 mm) with an addition of 300 mm. The other two dimensions of the steel box were also made to be 800 mm, made up of 6 mm thick steel plates. Three steel U-sections stiffeners were added around the tank to ensure its rigidity, as presented in Plate (3.5). The steel test box consisted of four flat faces, with a sufficient rigidity in order to impose a plane-strain state on the soil for the simulation of a straight long buried pipe section. A 10 mm thick cork was used to cover the inside faces of the tank to damp and absorb the waves of the dynamic loading transmitted to the box walls during the experiment.
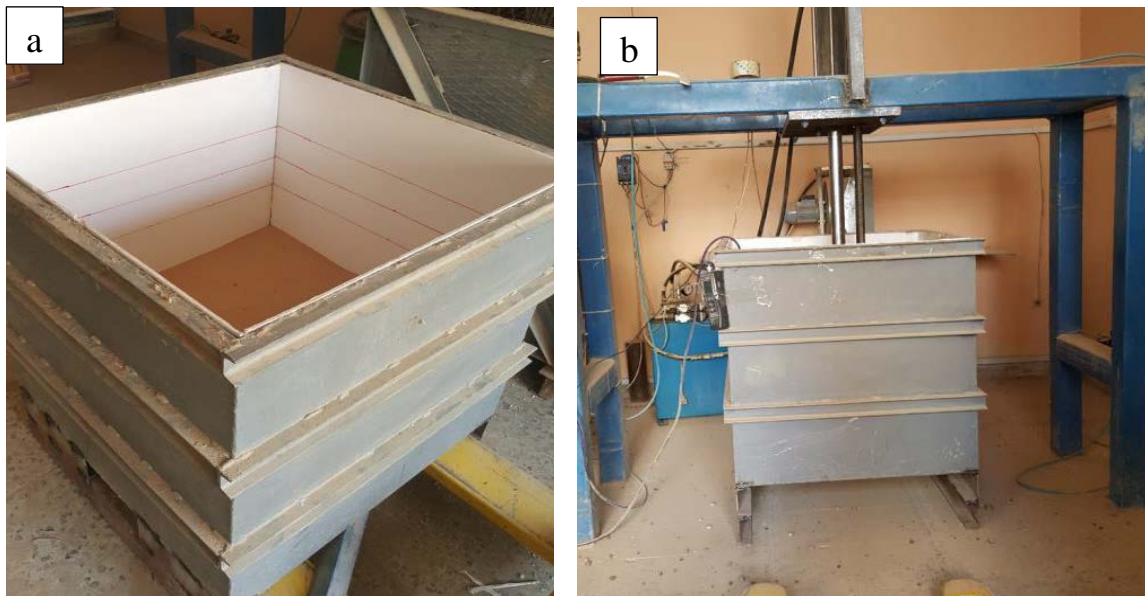
Plate 3.5 Steel tank.

3.4.2 Data acquiring system

It is essential to find a procedure for measuring the surface settlement due to the application of dynamic load during the test in order to study the real performance of the tested models. Data acquisition system was used in order to find total accurate information that involves a large number of readings in a short period.

The Programmable Logic Controller (PLC) is a digital computer that programs electro mechanical processes that are considered as a high technical processing unit. According to the research requirement, this system analyzes the data digitally, PLC, has an advantage over other computers in that it can be immune to electrical noise. The device contains LCD touch screen that has three touch-buttons and can view a simplified ladder of data.

In general, PLC program is repeatedly executed and saves data in its built-in memory if the electrical current was turned off. The PLC system is shown in Plate (3.6).
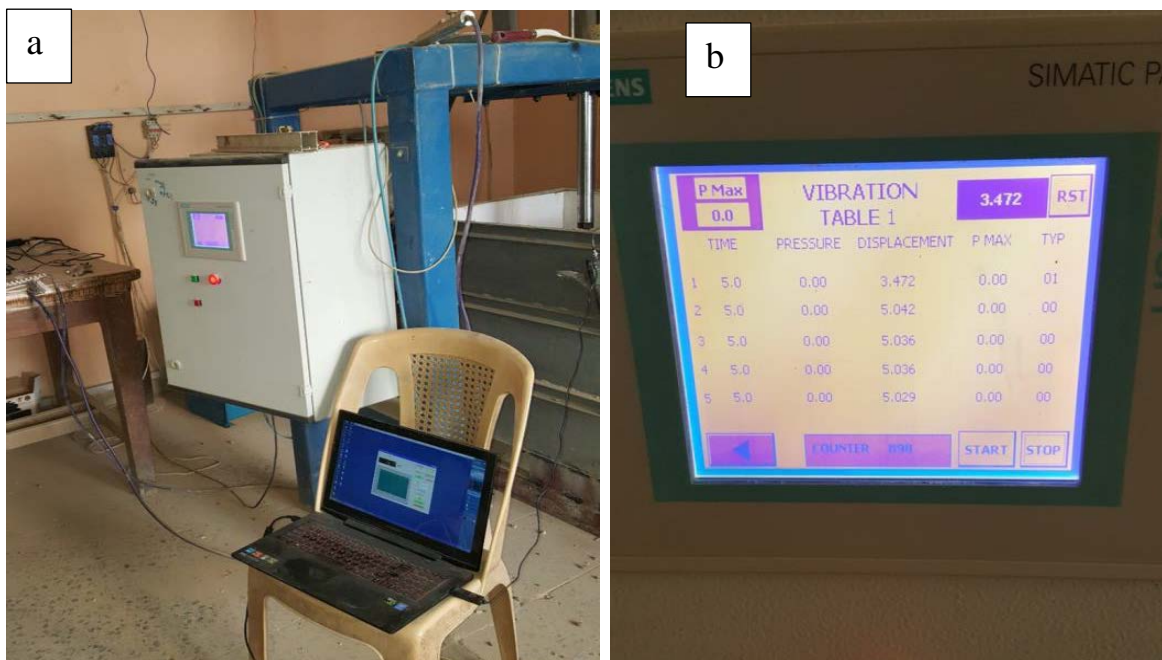
Plate 3.6 PLC system.

3.4.3 The shaft encoder

The shaft encoder is an electromechanical device used for sensing in myriad applications on motors paired with drives and automated machinery for everything from consumer electronics, elevators, and conveyor speed monitoring to position control on automated industrial machines and robotics. They track the turning of motor shafts to generate digital position and motion information. Whether incremental or absolute, magnetic or optical, rotary encoders track motor shaft rotation to generate digital position and motion information. The absolute output refers to the shaft current position. The electrical signal recorded by the shaft encoder can be translated into displacement reading by the PLC. The shaft encoder is shown in as Plate (3.7).
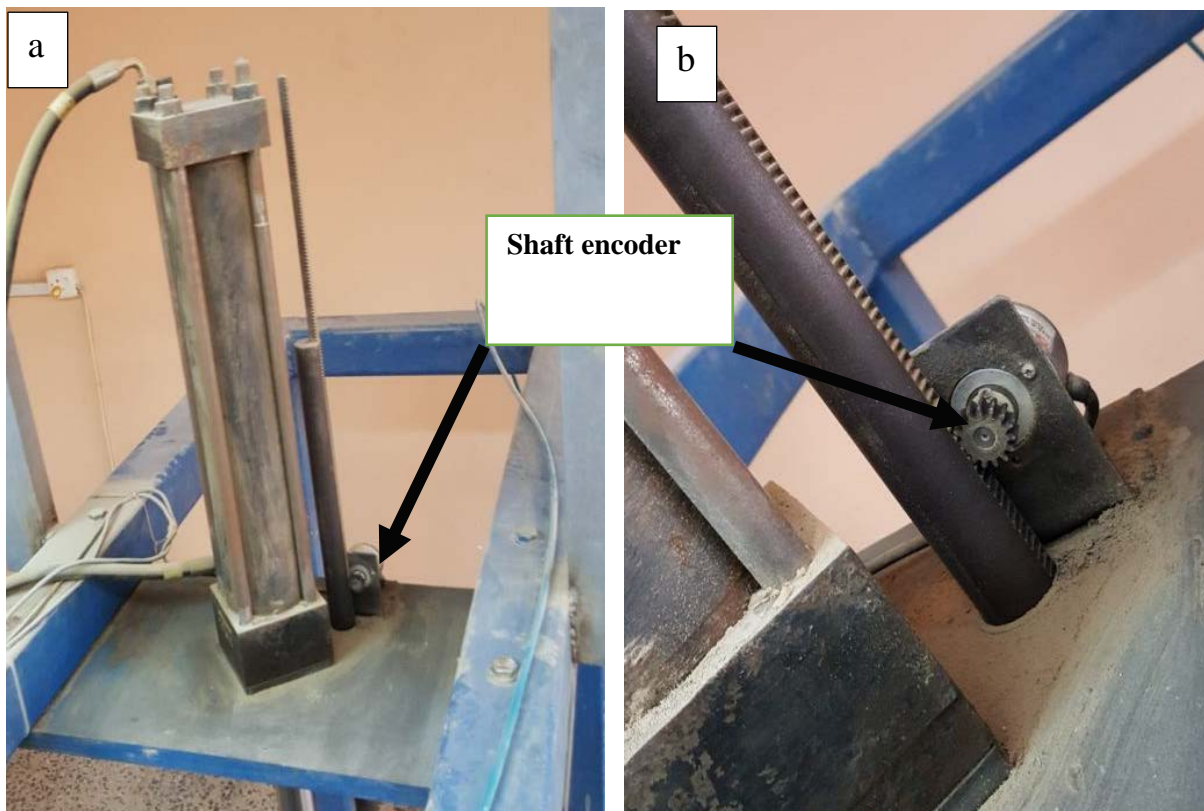
Plate 3.7 Shaft encoder.

3.4.4 The axial loading system

The axial loading system has two main units:

- **The Hydraulic control system**: The hydraulic control system applies the dynamic loading and moves of the piston. The movement of the hydraulic cylinder is electrically controlled by the PLC system and the value of dynamic load amplitude is controlled by a valve shown in Plate (3.8)
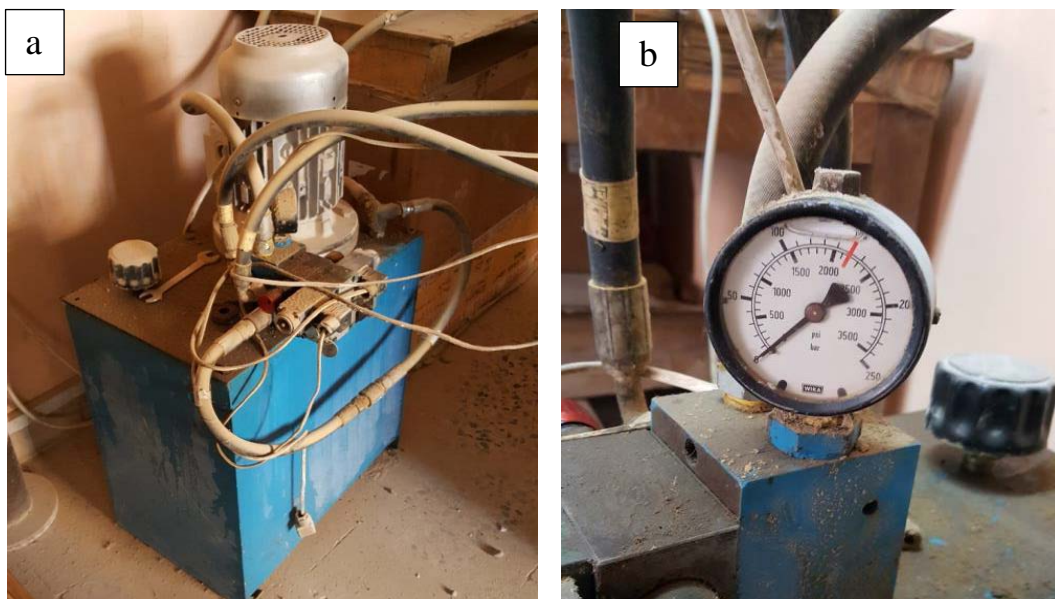
Plate 3.8 Hydraulic control system.

- **The Hydraulic jack system**: This system is made up of a hydraulic steel tank with a capacity of 70 liters. The system contains two holes; the upper hole is used for oil filling and the lower hole is for discharge. The tank discharge is about 12 litter/min and maximum pressure of 150 bars. These values are regulated by a gear type pump that has a fixed geometrical volume as shown in Plate (3.9).
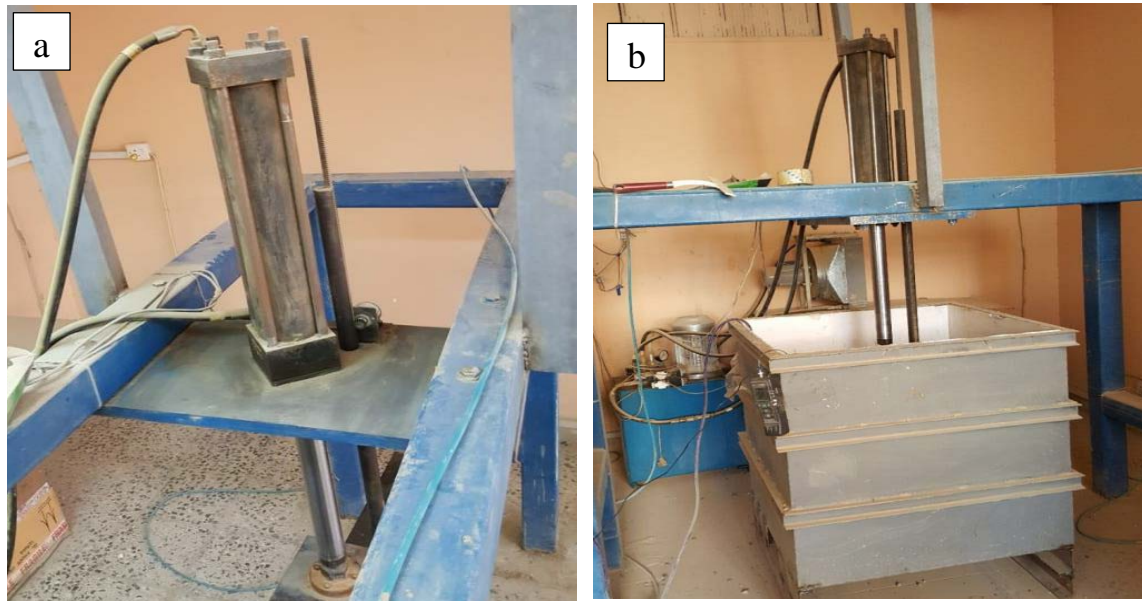
Plate 3.9 Hydraulic jack system.

3.4.5 Model steel footing

In order to simulate the vehicle path above the buried flexible pipe, a steel strip footing which was made of steel of dimensions 760 mm length, 100 mm width, and a thickness of 30 mm was manufactured as shown in Plate (3.10).
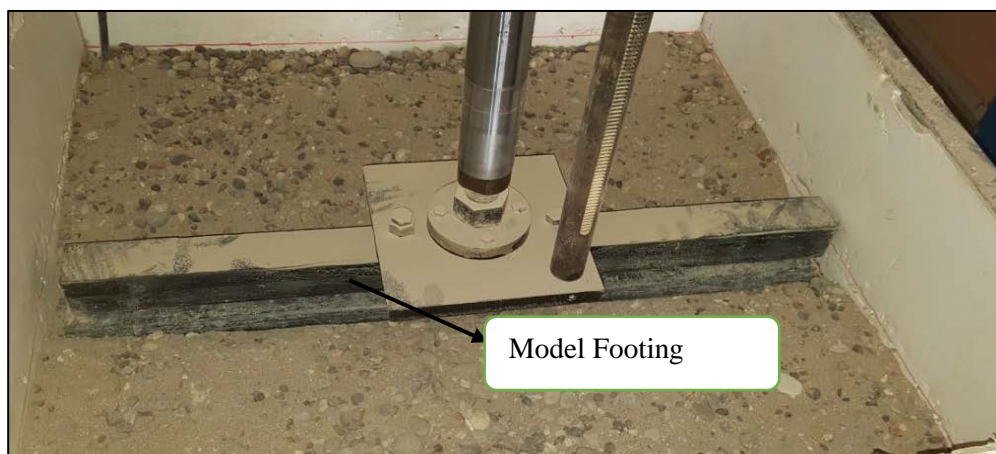
Plate 3.10 Model steel Footing.

3.4.6 Loading steel frame

A steel frame was designed and constructed to ensure that the hydraulic jack is being kept vertical which is used to apply the concentrated loading as shown in Plate (3.11).

The steel frame was made up of four beams and four columns. The beams and columns were made of steel that has a square cross-sectional area of (100 mm×100 mm) and a 40 mm wall thickness. Dimensions of the steel frame (height× width× length) are (700 mm × 1700 mm ×1700 mm). Two beams were added in order to strengthen and support the loading frame to bear the applied dynamic loading, as shown in Figure (3.5), part No. 4.

In order to carry the hydraulic jack system and the surface settlement-measuring device (the shaft encoder), a steel plate was welded in the frame center, as shown in Figure (3.5). Four base plates with the dimensions (200 mm×200 mm×20 mm) were used to fix the steel frame to the floor base using four 16 mm bolts (Abd Al-Kaream, 2013).

Plate 3.11 Loading steel frame.
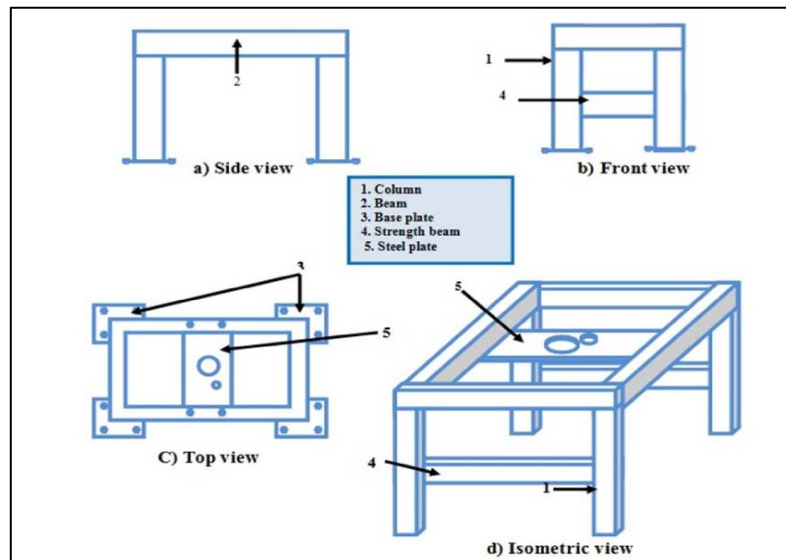
Figure 3.5 Loading steel frame (after Abed Al-Kareem, 2013).

3.5 Devices

3.5.1 Vibration meter

One channel vibration meter was used in the experiment in order to measure the crown vertical displacement. The capacity of this device ranges from 0.001 to 2.217 mm. The vibration meter can measure the velocity, displacement, and acceleration of motion. In addition, the collected data can be easily transferred to any computer by using specific software. The VT- 8204 vibration meter is shown in Plate (3.12).

Plate 3.12 Vibration meter (VT-8204).

3.5.2 Pressure Cell

The pressure cell that was used during the experiment is a Geokon pressure cell. The cell, which is a 100 mm in diameter, is appropriate for traffic stress measurement with an ultimate capacity of 250 kPa. The placement of the pressure cell was set above the pipe crown. The Geokon model 3515 pressure cell is shown in Plate (3.13).

Plate 3.13 Pressure cell.

3.6 Subbase and Sand Deposits Preparation

The subbase and sand deposits were prepared with a tamping steel hammer that was made for this purpose. The relative densities of the subbase and the sand layers were set to 80% and 60%, respectively, which means that the required weights for achieving the relative densities are already determined since the volume of the container layers and the densities of the subbase and sand are also pre-calculated (the steel tank was divided into 10 cm layers).

Each layer of soil was tamped to a pre-calculated depth. The PVC pipe was installed on 200 mm soil bedding. Then the probe of the vibration meter and the pressure cell were fixed above the crown of the pipe, after that, the geocell reinforcement was positioned in the chosen width and depth. After the final layer completion, a sharp edge ruler was used to level the top surface to obtain a flat surface as near as possible. Then the steel footing was placed on top of the model

surface. The steps of the sand and the subbase deposit preparation are presented in Plate (3.14).
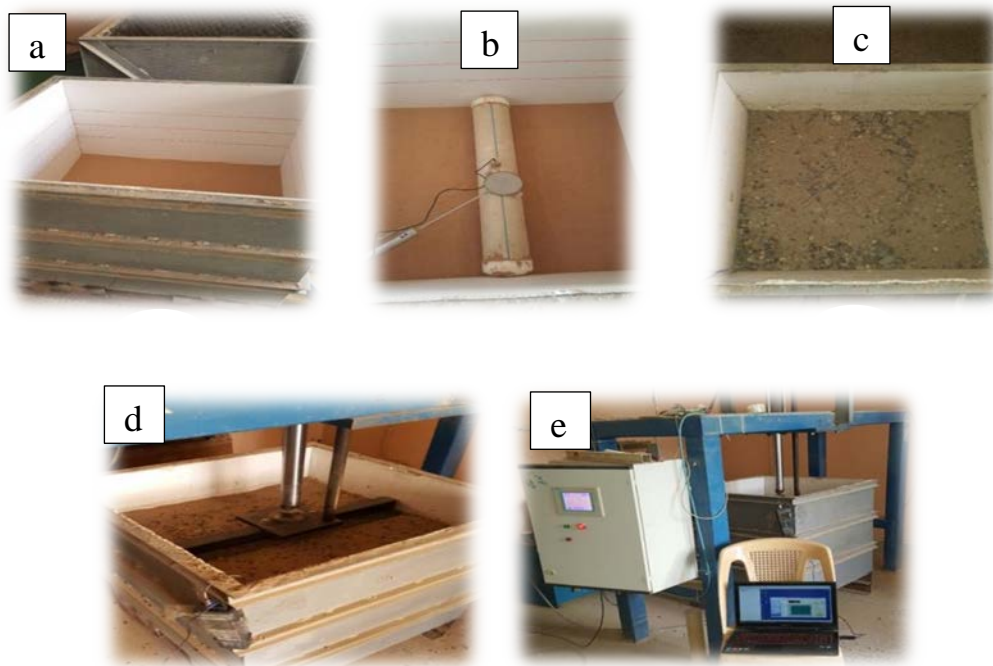
Plate 3.14 Model preparation steps.

3.7 The Dynamic Loading Test

The dynamic load was applied for 1000 seconds for each test. The half-sine wave dynamic function was utilized in this study. The shape of the function is displayed in (Figure 3.6); so, the equation of the applied dynamic load (F) at any time (t) is:

$$(F) = a_0 * \sin \omega * t \tag{3.1}$$

where:

F = applied force,

t = time,

a_0 = the amplitude of load, and

ω = the load frequency.

The positive part (half of the sine wave) is the only part that was applied to the test models.
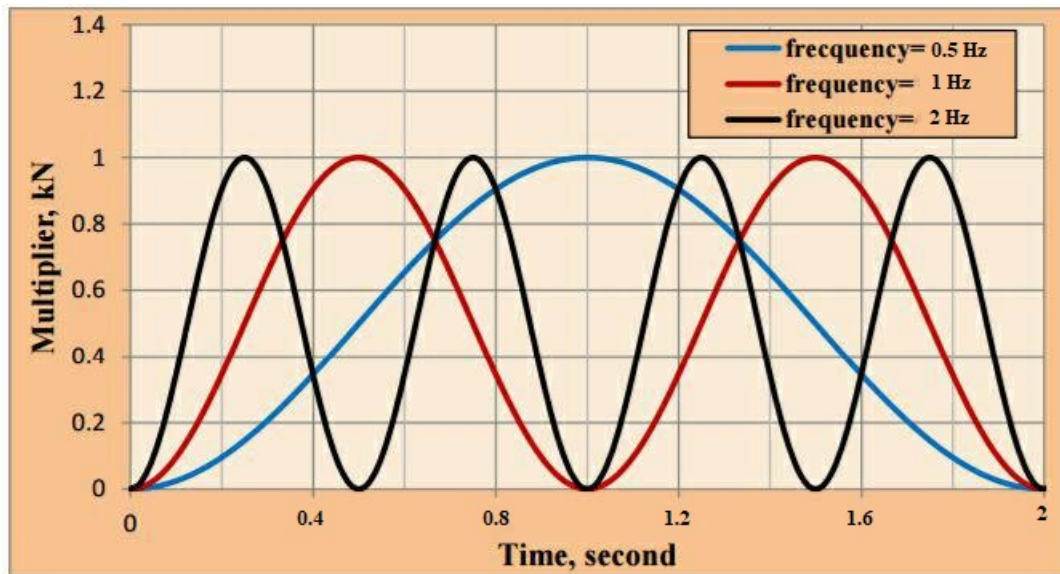
Figure 3.6 Shape of the applied traffic-loading wave.

Chapter Four

Numerical Simulation of Experiments by the Finite Element Method

4.1 Overview

The emphasis of this chapter is the calibration of numerical analysis to effectively model the laboratory model tests. As discussed in the literature review, a few items are critical to achieve this goal. It is critical to model both the unique physical properties of the pipe and the non-linear stress-strain properties of the soil materials. It is also important to consider the construction steps to capture the movements and stresses in the pipe and backfill. PLAXIS 3D 2013 was selected to simulate the laboratory model tests. As with any numerical model, there are limitations of how precisely a system can be modeled and each model presents its own unique set of problems. The PLAXIS 3D model lends itself well to modeling the macro or large-scale properties of the system.

The equations of the finite element method required for simulation of the buried pipe problem are described in the next section. This is followed by numerical simulation of the model experiments described in Chapter Three.

4.2 Finite Element Equations

The static formulation of the employed finite element method in PLAXIS 3D is briefly presented here, the equation of time-dependent movement of a volume influenced by dynamic loading is: (Brinkgreve et al., 2015)

$$[M]\{ü\} + [C]\{u̇\} + [K]\{u\} = \{F\} \qquad\qquad (4.1)$$

where: $[M]$ is the mass matrix

$[C]$ is the damping matrix

$[K]$ is the stiffness matrix

$\{ü\}$ is the acceleration vector

$\{u̇\}$ is the velocity vector

$\{u\}$ is the displacement vector

$\{F\}$ is the force vector

In the matrix $[M]$, the mass of materials (water, soil and any constructions) is considered. In PLAXIS 3D, the mass matrix is executed as a lumped matrix. The damping of the materials is presented by the matrix C. In reality, irreversible deformations (plasticity or viscosity) or friction are causing material damping. More vibration energy can be dissipated with more plasticity or more viscosity. The phenomena of damping can still be considered using the matrix C if elasticity is assumed.

In the formulations of finite element, C is usually expressed as a function of the stiffness and mass matrices (Rayleigh damping) (Zienkiewicz and Taylor, 1991) as:

$$C = \alpha_R\, M + \beta_R\, K \qquad\qquad (4.2)$$

Where α_R is the mass proportional Rayleigh damping coefficient, and

β_R is the stiffness proportional Rayleigh damping coefficient.

4.3 Soil Deposit Natural Frequency

The soil deposit natural frequency can be calculated using the following equation (Kramer, 1996):

$$f_n = \frac{v_s}{4H}(1 + 2n) \tag{4.3}$$

where, f_n is the nth natural frequency of the soil deposit in Hz, v_s is the shear wave velocity of the surrounding soil medium and n = 0, 1, 2...

For n = 0, the first natural frequency, f_1 (i.e. the fundamental frequency) of vibration of the soil deposit of thickness H is given by:

$$f_1 = \frac{v_s}{4H} \tag{4.4}$$

4.4 Modeling the Soil and Interface Behavior

Soil elements in 3D finite element mesh are modeled as tetrahedral elements with 10 nodes as shown in Figure (4.1). The soil tends to behave in a non-linear way under load. This non-linear stress-strain conduct may be modeled at a few levels of modernity. Obviously, a number of model parameters expands with the level of refinement. PLAXIS 3D can support various models to simulate the soil behavior. Due to the lack of knowledge and available testing equipment, the Mohr-Coulomb model (MC) is used to simulate the sand and subbase layers. The Mohr-Coulomb model (linear elastic-perfectly plastic) failure contour requires five input parameters which are familiar to most civil engineers and can be calculated from basic soil tests.

The five parameters of the Mohr-Coulomb model (in case of the drain behavior) are:

E': Effective Young's modulus (kN/m^2), and

ν': Poisson's ratio.

The other Mohr-Coulomb parameters are:

ϕ'': Effective friction angle,

c'_{ref}: Effective cohesion, (kN/m^2) and

ψ: Dilatancy angle.
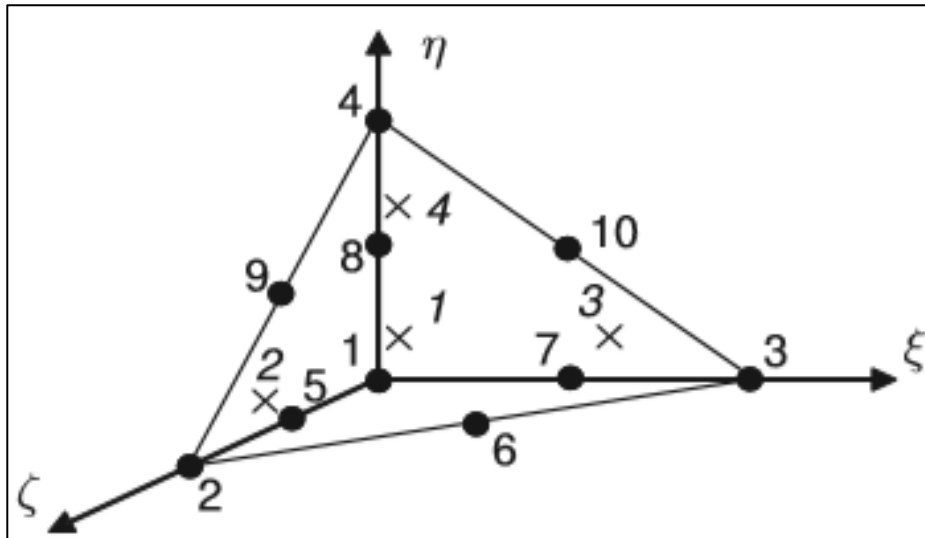
Figure 4.1 3D soil elements (10-node tetrahedrons).

4.4.1 Elements of interface

Interface elements allow the soil element to slip or separate from the pipe surface when the shear stresses and the normal stresses in the interface reach a threshold. The absence of interface elements leads to the direct connection between the soil elements and the structural elements thereby leading to higher values.

Elements of interface differ from other elements in that other elements have a single node while the interface elements have couples of nodes. The distance between the two nodes of a pair is zero. The elements of the interface are integrated numerically by using 3-point Gauss integration. The numbering and position of the integration points and nodes are shown in Figure (4.2). Each node has three translational degrees of freedom (u_x, u_y, u_z). Interface elements, as a result can allow for differential displacements between the node pairs (gapping and slipping) (Goodman et al., 1968) and (Van Langen and Vermeer, 1991).
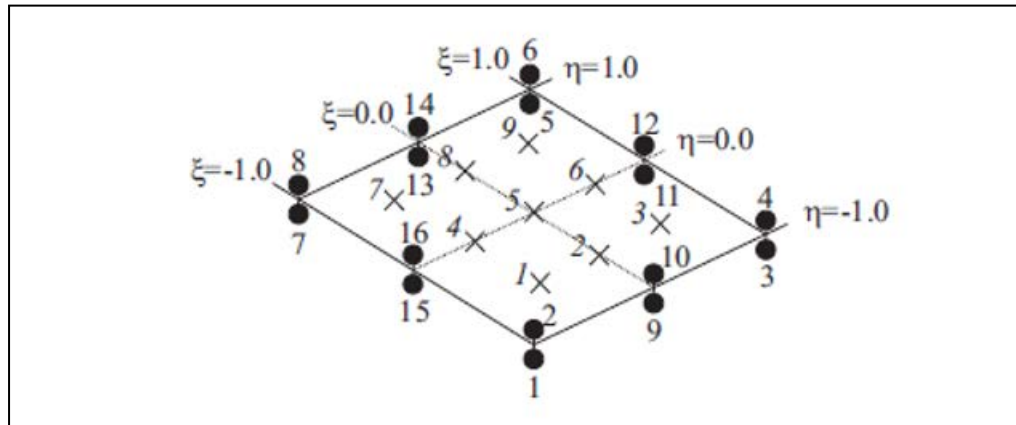
Figure 4.2 Local numbering and positioning of nodes (•) and integration points (x) of a 16-node interface element (PLAXIS 3D Reference Manual, 2013).

4.4.2 Interface strength

When using the Mohr-Coulomb model, the main interface parameter is the interface strength ($R_{inter.}$). This parameter can be set using the following options:

Rigid: In case of the interface having no reduced strength with regard to the surrounding soil strength, this option should be used. This option means that there is no slipping between the soil and the structure.

Manual: The value of R_{inter} depends on the soil-structure interaction. In general, for real soil-structure interaction, the interface is weaker and more flexible than the surrounding soil, which means that the value of R_{inter} should be less than 1. Suitable values for R_{inter} for the case of the interaction between various types of soil and structures in the soil can be found in the literature. In the absence of detailed information, it may be assumed that R_{inter} is of the order of 2/3. A value of R_{inter} greater than 1 would not normally be used.

4.5 Selection of Material Parameters

4.5.1 Soil parameters

The parameters of sand and subbase are listed in Table (4.1). They are selected either from laboratory tests or assumed using conventional relationships.

Table 4.1 Soil properties for the verification problem.

Soil	Sand	Subbase
Model	Mohr-Coulomb	Mohr-Coulomb
Unit weight γ (KN/m^3)	17.2	17.6
Modulus of elasticity E' (kN/m^2)	30000*	90000*
Angle of internal friction ϕ (°)	38	40*
Dilatancy angle ψ (°)	8*	10*
Poisson's ratio	0.3*	0.35*

*: assumed.

4.6 PVC pipe modeling

The PVC pipe was modeled using plate element. Plates are structural objects used to model thin two-dimensional structures in the ground with a significant flexural rigidity (bending stiffness). After meshing, plates are composed of 6-node triangular plate elements with six degrees of freedom per node: three translational degrees of freedom (u_x, u_y and u_z) and three rotational degrees of freedom ($\varnothing_x$, $\varnothing_y$ and $\varnothing_z$) as shown in Figure (4.3). The plate elements are based on Mindlin's plate theory (Bathe, 1982). This theory allows for plate deflections due to shearing as well as bending. In addition, the element can change length when an axial force is applied. The material properties of plates are contained in plates material data sets and can be conveniently assigned using drag-and-drop. The forces are assessed at the integration points of the plate element and extrapolated to the element nodes. Figure (4.4) shows the mesh view

of the pipe. Table 4.2 summarizes the parameters of the PVC pipe (provided by
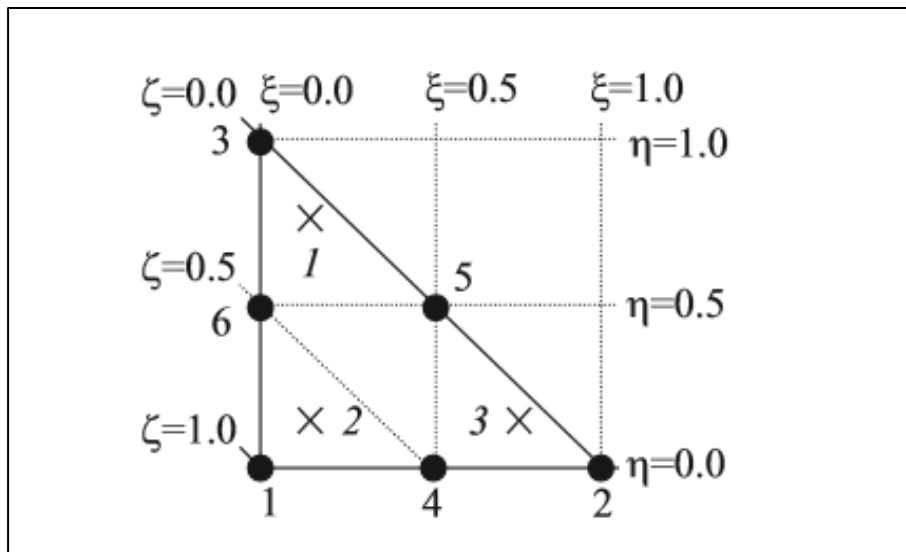
the manufacturer):

Figure 4.3 Local numbering and positioning of nodes (•) and
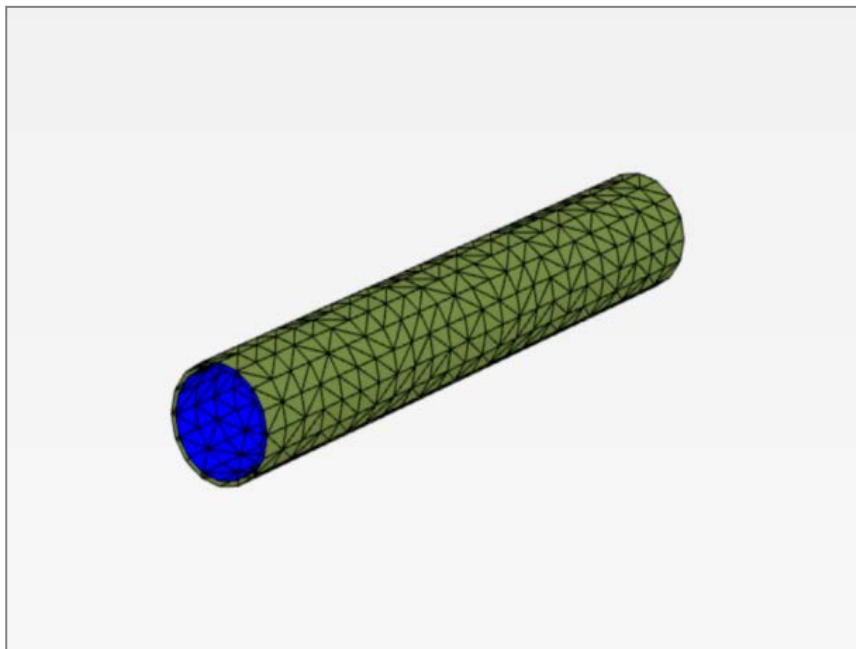integration points (x) of a 6-node triangular element.

Figure 4.4 Mesh view of the pipe.

Table 4.2 Material parameters of PVC pipe.

PVC pipe	properties
Unit weight , γ (kN/m³)	13
Modulus of elasticity, E' (kN/m²)	2700000
Thickness (mm)	1.4
Diameter (mm)	110
Poisson's ratio	0.38

4.7 Geocell modeling

The geocell reinforcement was modeled using the geogrid element, which is defined as a slender structure with an axial stiffness but with no bending stiffness. Geogrids can only sustain tensile forces and no compression. These objects are used to model soil reinforcements. Geogrids are composed triangular surface elements with 6 nodes and 3 translational degrees of freedom per node (u_x, u_y and u_z). The stiffness matrices of the element based on the materials properties defined in the data sets and numerically integrated from the three stress points of the Gaussian integration. When a tension force is applied, the element length can be changed. The basic parameter of the material is the axial stiffness, EA. Additionally, there can be a limit to tension force to allow for the simulation of failure in tension. The dimensions of the simulated geocells are the same as the dimensions of the geocells used in the experimental work. Figure (4.5) shows the 3D model of geocells. In this study, a proposed procedure is used to model the geocell reinforcement as three-dimensional reinforcement elements.
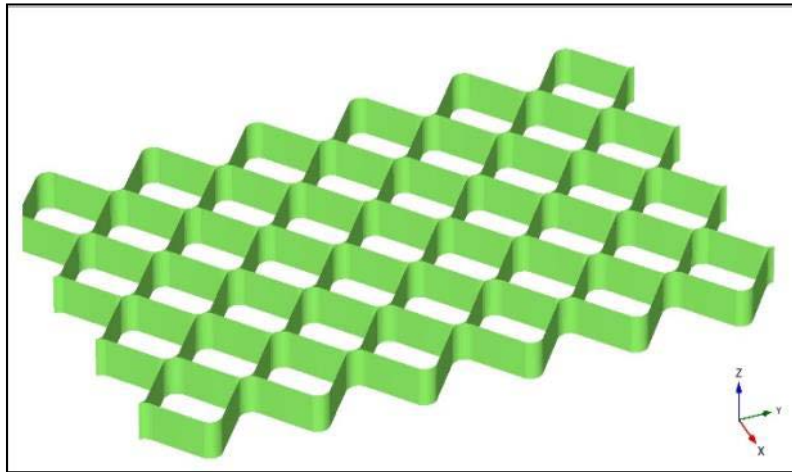
Figure 4.5 Three-dimensional modeling of geocells.

4.8 Steel footing and surface loading modeling

The steel footing was modeled using plate element, which also consists of triangular surface elements with 6 nodes and 3 translational degrees of freedom per node (u_x, u_y and u_z). As for the surface dynamic loading, PLAXIS software can either allow for harmonic signal or a signal imported from an Excel sheet. The latter signal was chosen, so the amplitude and the frequency were easily modified. Figure (4.6) shows a mesh view of the steel footing while Table (4.3) presents the properties of the steel footing. Figure (4.7) illustrates the harmonic load (half sine) function adopted in this study.

Figure 4.6 Mesh view of the steel footing.

Table 4.3 Material parameters of the steel footing.

Steel footing	properties
Unit weight , γ (kN/m³)	78.5
Modulus of elasticity, E' (kN/m²)	200,000,000
Thickness (mm)	30
Poisson's ratio	0.2

Figure 4.7 Dynamic loading signal, imported from an Excel sheet.
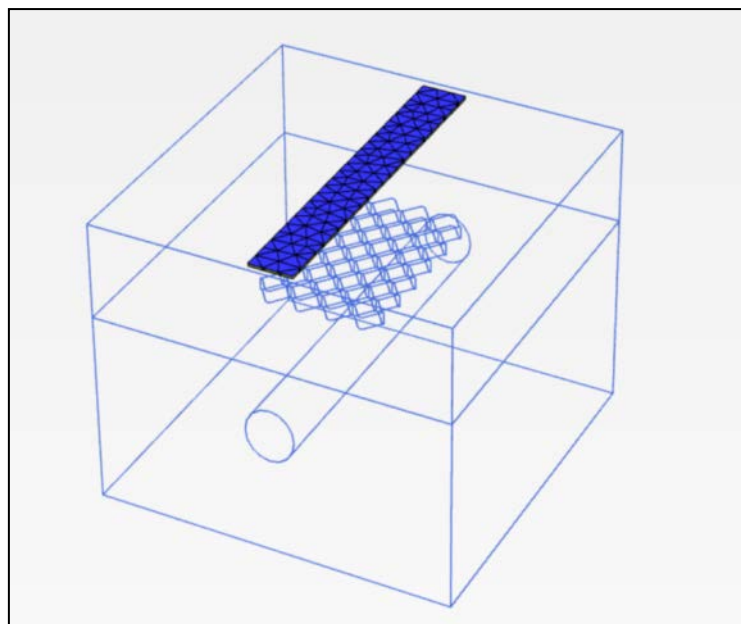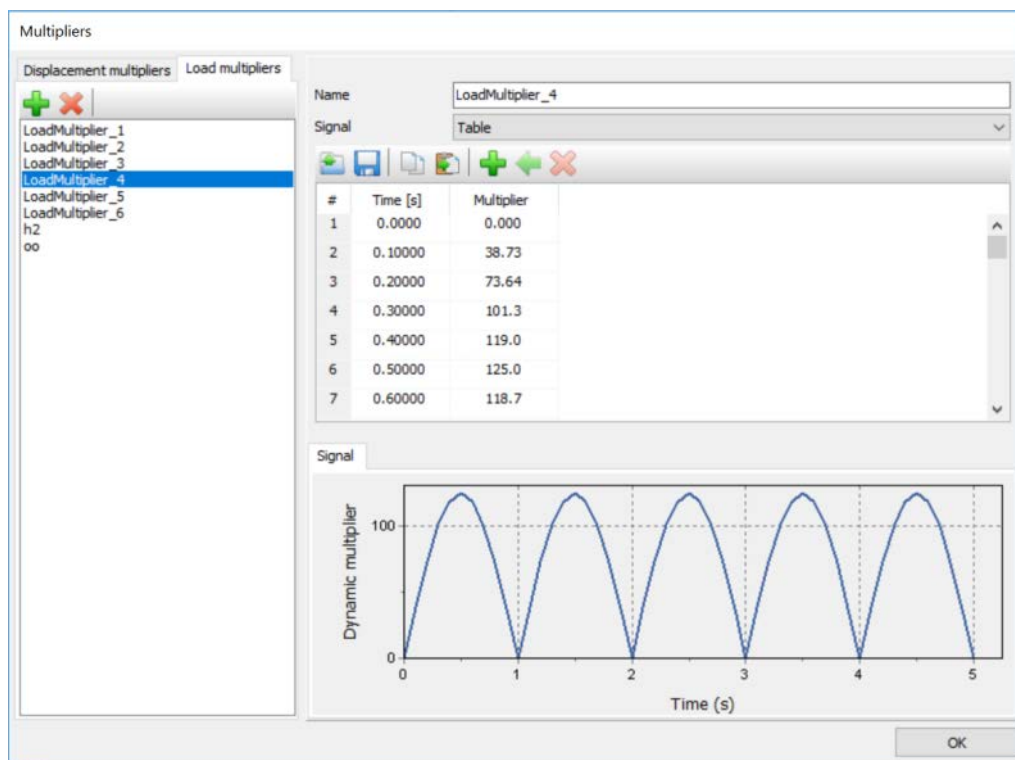
4.9 Meshing and Calculations

4.9.1 Meshing

After the modeling process of geometry is finished, the calculations can be proceeded with. This involves the mesh generation and definition of the construction phases. In the practice of engineering, a project is divided into several phases. Similarly, a calculation process in PLAXIS is also divided into calculation phases. Soil's non-linear behavior requires the application of small proportions of loadings (named load steps). It is appropriate, in most cases, to specify the state that has to be reached at the end of the calculation phase. PLAXIS can take sub-division to appropriate load steps.

A fully finite element meshes automatic generation is allowed by the PLAXIS 3D program. The process of mesh generation considers the stratigraphy of soil along with all loads, boundary conditions and structural objects. When the generation of the mesh is completed, nodes and stress points can be selected to view the results in charts. The general finite element mesh of the buried pipe problem is shown in Figure (4.8).
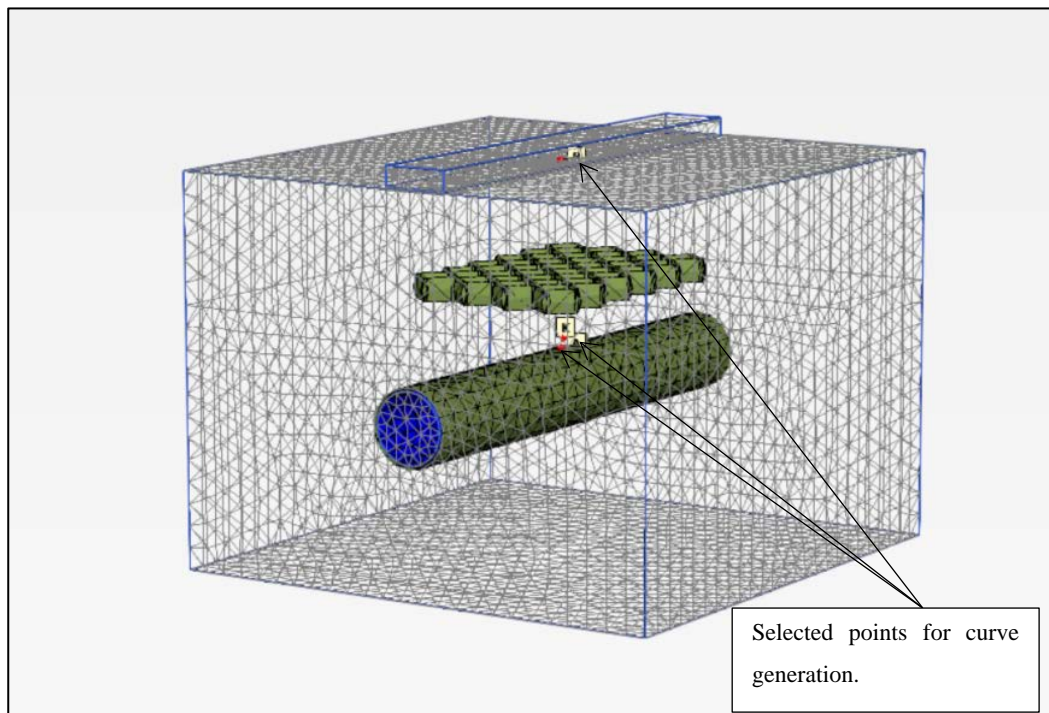

Selected points for curve generation.

Figure 4.8 Finite element mesh with selected points for curve generation.

4.9.2 Calculations

The calculations were divided into four phases:

1. Initial phase: The initial phase generates the preliminary soil stresses by the method of the K_0 procedure where K_0 is the coefficient of lateral earth pressure at rest, considering the history of loading of the soil. The required parameters in the development procedures of initial stresses are two K_0 values, one value is specified for the y-direction, and the other value is specified for the x-direction.

$$K_{0,y} = \sigma'_{yy} / \sigma'_{zz} \tag{4.5}$$

$$K_{0,x} = \sigma'_{xx} / \sigma'_{zz} \tag{4.6}$$

In engineering practice, the K_0 value for a normally consolidated soil is frequently assumed to be connected to the angle of internal friction according to Jaky's empirical expression (Jaky, 1948):

$$K_0 = 1 - \sin \phi \tag{4.7}$$

2. Plastic calculation phase: loading can be defined in this phase in the sense of changing the load combination, stress state, weight, strength or stiffness of elements, activated by changing the load and geometry configuration or pore pressure distribution by means of staged construction. In this case, the total load level that is to be reached at the end of the calculation phase is defined by specifying a new geometry and load configuration. In the verification problem, this phase includes the insertion of the pipe, geocells, and steel footing.

3. Dynamic calculation phase: The applied dynamic loading is the result of multiplying the dynamic load multiplier by the input value of the dynamic load. Absorbent (viscous) boundaries can be activated in this phase besides the dynamic loading. The critical time step is defined by the Newmark time integration scheme in which the time step is constant during the analysis. Based on the element size, time history, and material properties, the proper time step in the dynamic analysis is calculated.

4.9.3 Model boundaries

In the case of a static deformation analysis, prescribed boundary displacements are introduced at the boundaries of a finite element model. The boundaries can be completely free or fixities and can be applied in one or two directions. Particularly, the vertical boundaries of a mesh are often non-physical (synthetic) boundaries that have been chosen so that they do not actually influence the deformation behavior of the construction to be modeled.

In order to counter the reflections, special measures are needed at the boundaries especially for viscous boundaries. Various methods are used to create these boundaries, which include:

• Using of half-infinite elements (boundary elements).

• Adaptation of the material properties of elements at the boundary (low stiffness, high viscosity).

• Using of viscous boundaries (dampers).

Default fixities were chosen in favor of the viscous boundaries since the viscous boundaries move the boundary horizontally and thus produce false results.

4.9.4 Dynamic time stepping

The time step parameter used in a dynamic calculation phase is constant and equals to:

$$\delta t = \Delta t / (m \cdot n) \tag{4.8}$$

where Δt is the dynamic time interval (duration of the dynamic loading), n is the value of the number of sub-steps parameter and m is the value of maximum steps.

4.9.5 Soil damping

The main cause of damping in a material is the viscous properties of a soil, the irreversible strains development and friction. Irreversible (plastic) strains can be generated in every soil model in PLAXIS 3D, and thus cause material damping. To model realistic damping characteristics of soils in dynamic calculations, additional damping is needed, and it can be done using Rayleigh damping, which is a numerical feature that involves the composition of damping matrix C by adding a portion of the mass matrix M and a portion of the stiffness matrix K (Eq. 4.2).

The parameter that determines the influence of the mass in the system damping is determined by the parameter α_R. The higher α_R is, the more the smaller frequencies are damped. The parameter that determines the stiffness influence in the system damping is determined by the parameter β_R. The higher β_R is, the more the higher frequencies are damped.

The damping parameters can be defined for each type of the soil models, the interface and the plate elements as well. The damping ratio ξ is a commonly used engineering parameter. The damping ratio is defined as $\xi = 1$ for critical damping, which is exactly the amount of damping needed to let a single degree-of-freedom system that is released from an initial excitation u_0, smoothly stop without rebounding. A relationship can be established between the Rayleigh

damping parameters α and β and the damping ratio ξ when considering Rayleigh damping:

$$\alpha + \beta \, \omega^2 = 2 \, \omega \, \xi \tag{4.9}$$

and $\omega = 2 \, \pi \, f$ (4.10)

where ω is the angular frequency in (rad/s) and f is the frequency in Hz.

The damping ratio ξ was set to 5 % based on the PLAXIS 3D manual recommendation.

Chapter Five

Results and Discussion

5.1 Introduction

This chapter presents the results and discussion of the experimental work, followed by the results of numerical simulation. The experimental work consists of 12 models, six of them were reinforced and the other six were unreinforced, the models were subjected to two loading amplitudes (0.5 and 1) ton, and three different frequencies (0.5, 1 and 2) Hz.

The results and discussion is then followed by the numerical simulation of the experimental work models for verification purposes.

5.2 Results of experimental work

The results of 12 experimental model tests will be discussed here; the tests were carried out on dry sandy soil with a relative density of 60% and subbase layer with a degree of compaction of 80% with and without the geocell reinforcement. The models are subjected to dynamic vertical traffic load. The investigation concentrates on the effect of parameters such as loading frequency, and loading amplitude on the dynamic response of the subbase and the sand layer. The parameters that were measured during the experiments are:

1. The vertical pressure reaching the pipe crown,
2. The vertical deformation of the pipe crown and
3. The surface settlement.

The duration of all the experimental tests were set to 1000 seconds.

Six models were tested with the geocell reinforcement and the other six were tested without the geocell reinforcement for comparison purposes. The

width of geocell (b) was chosen as 3.2 B, where B is the footing width. This selected value was suggested by (Dash et al., 2003). The geocell depth was set at the bottom of the subbase layer. Two different values of loading amplitudes 0.5 ton and 1 ton, and three different frequencies 0.5 Hz, 1 Hz and 2 Hz were used.

In the following subsections, the results of the tests without and with geocells are discussed with time and compared to each other.

5.2.1 Dynamic loading effect on the surface settlement

A soil-pipe interaction can be created by the movement of the ground that acts parallel and horizontally with the longitudinal pipe axis if the pipe axial stiffness allows it to withstand the ground deformation. The relative movement between the soil and the pipe is typically focused in a thin region where the slippage and failure of shear happen at the interface between the soil and the pipe. (Ng, 1994).

I. Loading amplitude:

The variance of a surface settlement with time for the test models is shown in Figures (5.1) to (5.6). It can be shown from these figures that the curves follow a similar trend, and the settlement increases with the increment of the load amplitude. The reduction of surface settlement due to the geocell reinforcement was about (29 to 43) % when the amplitude of load is (0.5) ton, and this value turns out to be (32 to 41) % when the amplitude of load is up to (1) ton. If a rigid pipe passes through a field of soil displacement, the pipe bending stiffness will offer a specific confinement to the displacement of the pipe, which is different to the soil movement. For a more flexible pipe, the displacement profile of the pipe will be the same as the soil displacement profile.

The loading alongside the pipe can be varied based on the soil-pipe relative movement, it reaches a maximum value when the complete failure of the adjacent soil occurs. The ground movement direction (downward, upward and lateral)

influences the maximum restraint that the soil can offer, as indicated by Ng (1994).

Geogrids or geocells reinforce by laterally restraining the base or subbase and improve the bearing capacity of the system, thus decreasing shear stresses on the weak subgrade. In addition, the confinement provided by geogrids improves the distribution of the vertical stress over the subgrade and decreases vertical subgrade deformation. The proper ratio of geogrid aperture size to aggregate grain size is an important factor affecting the performance of geogrid reinforcement systems (Haas et al., 1988).

II. Frequency of load:

The results of the surface settlement are summarized in Table (5.1) after the dynamic loading application for 1000 seconds. Figures (5.1) through (5.6) show the relationship between time and settlement with the same amplitude of load and multiple frequencies. The settlement values increase proportionally with the increment of frequency value for every tested model. It may be noticed that increasing load amplitude leads to increasing the settlement under the same loading frequency.

When the soil is moving downward relative to the pipe, it inflicts a loading from the soil above the pipe. When the soil-pipe relative movement becomes too much, it leads to shear and tensile failure in the covering soil developing a soil wedge over the pipe rather than complete surrounding soil failure as indicated by (Ng, 1994). The pipe is typically assumed to be acting as a strip footing that has a shape of a cylinder for the downward direction of motion. On the other hand, if the soil moves upward relative to the pipe, the passive resistance will provide restraint of the soil under the pipe. The soil confinement will reach its maximum value when the soil adjacent to the pipe fails completely as noted by Ng (1994).

(Rajagopal et al., 1999) and (Dash et al., 2003) observed that a considerable amount of confinement is developed with the use of geocells. Rajagopal et al. (1999) showed that three interconnected cells were required to realize the full effect of geocells. The distribution of strain shows that the strain decreases significantly with distance from the load in both directions parallel and perpendicular to the opening, but around the third or fourth cell from the load the strain becomes constant.

Existing studies show that geocell reinforcement can increase the modulus and strength of the infill materials. However, limited information exists on large-scale testing of geocell-reinforced aggregates placed on poor soils to draw consistent and quantitative conclusions with regards to the degree of improvement.

Table 5.1 Results of the surface settlement.

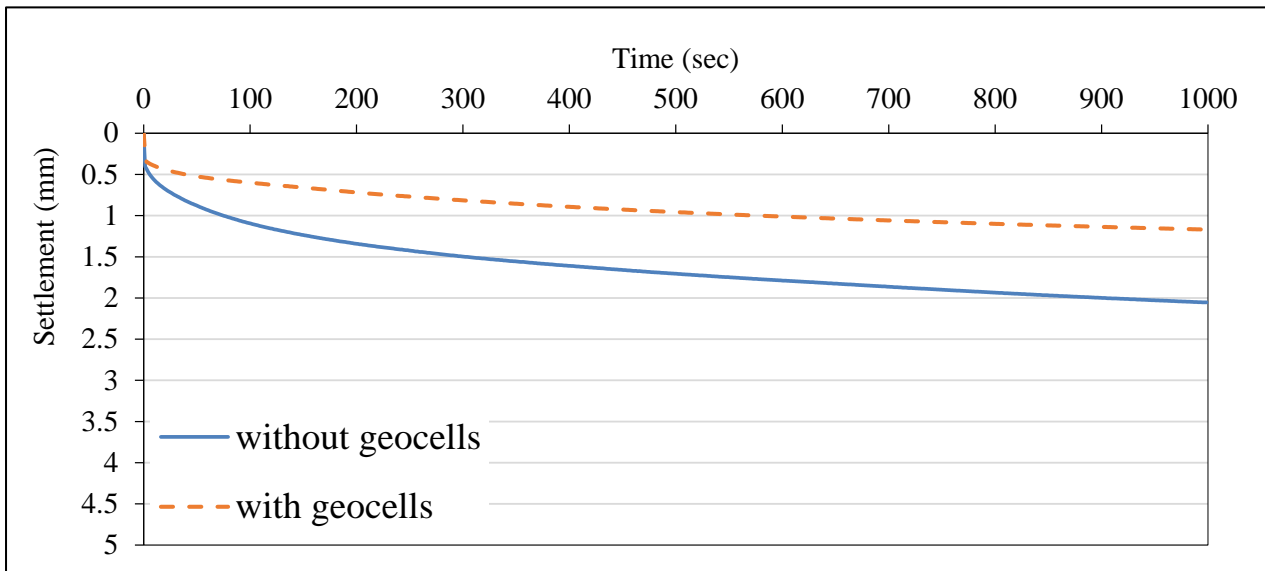| Load amplitude (ton)	Maximum surface settlement at different frequencies (mm)						Reduction percentage		
	Without the geocells			With the geocells			0.5Hz	1 Hz	2 Hz
	0.5 Hz	1 Hz	2 Hz	0.5Hz	1 Hz	2 Hz			
0.5	2.0532	3.576	3.833	1.1696	2.511	2.732	43%	30%	29%
1	10.047	12.85	16.075	6.834	7.6	10.251	32%	41%	36%

Figure 5.1 Settlement versus time with and without the geocells (a=0.5 ton, ω = 0.5 Hz).
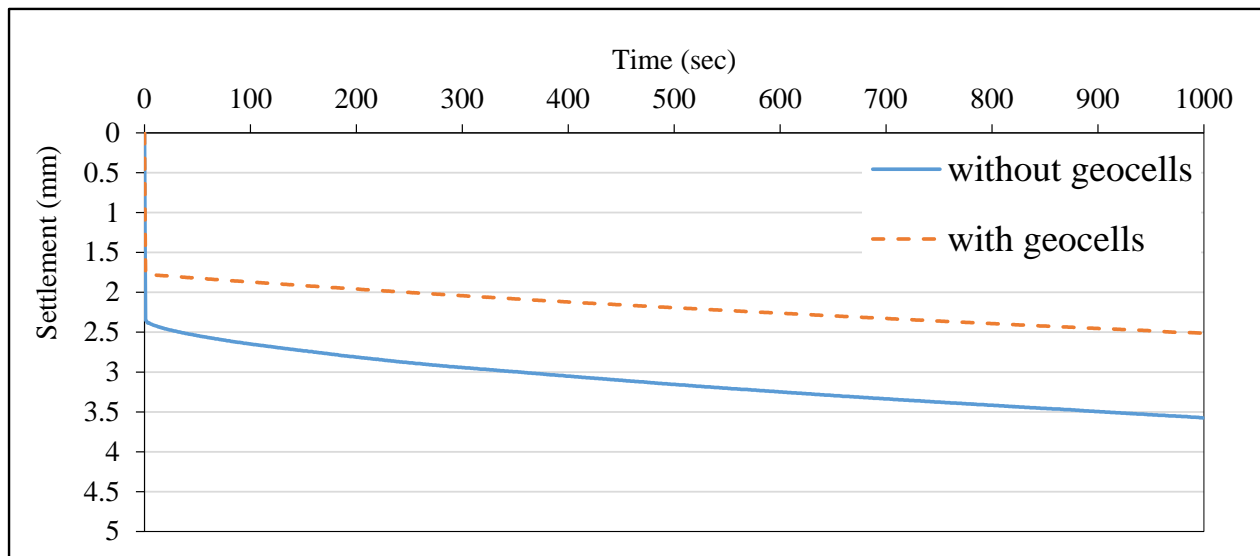

Figure 5.2 Settlement versus time with and without the geocells (a=0.5 ton, ω = 1 Hz).
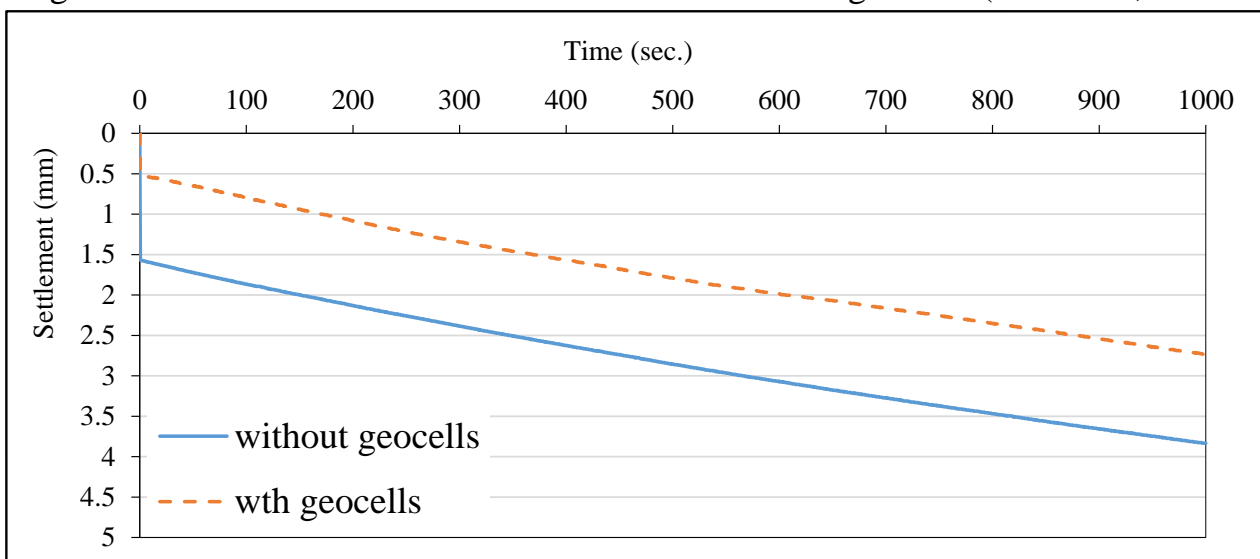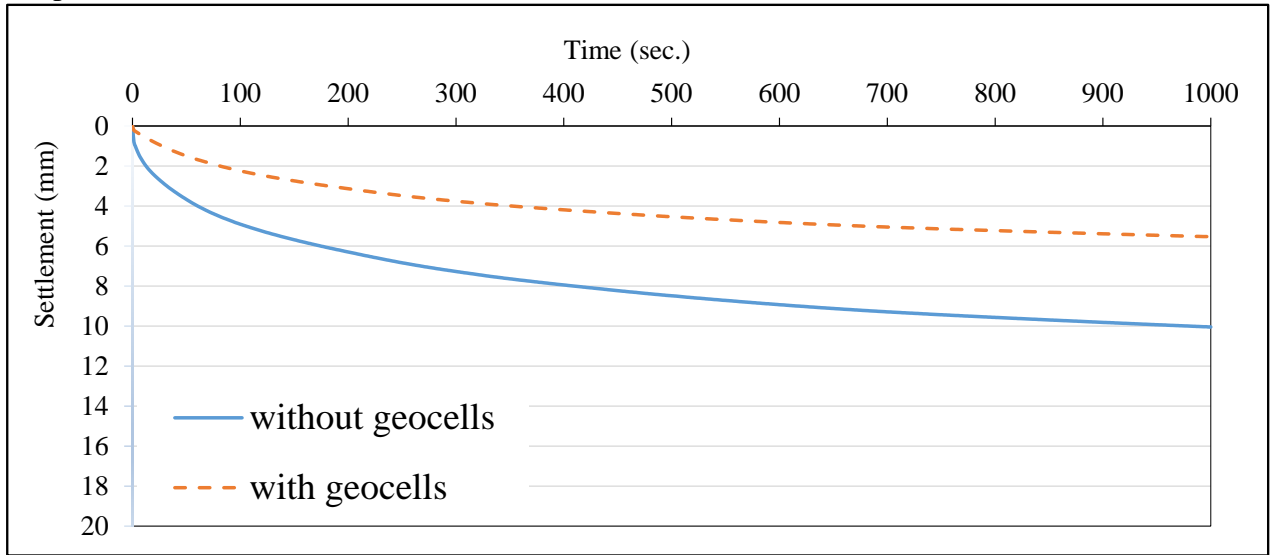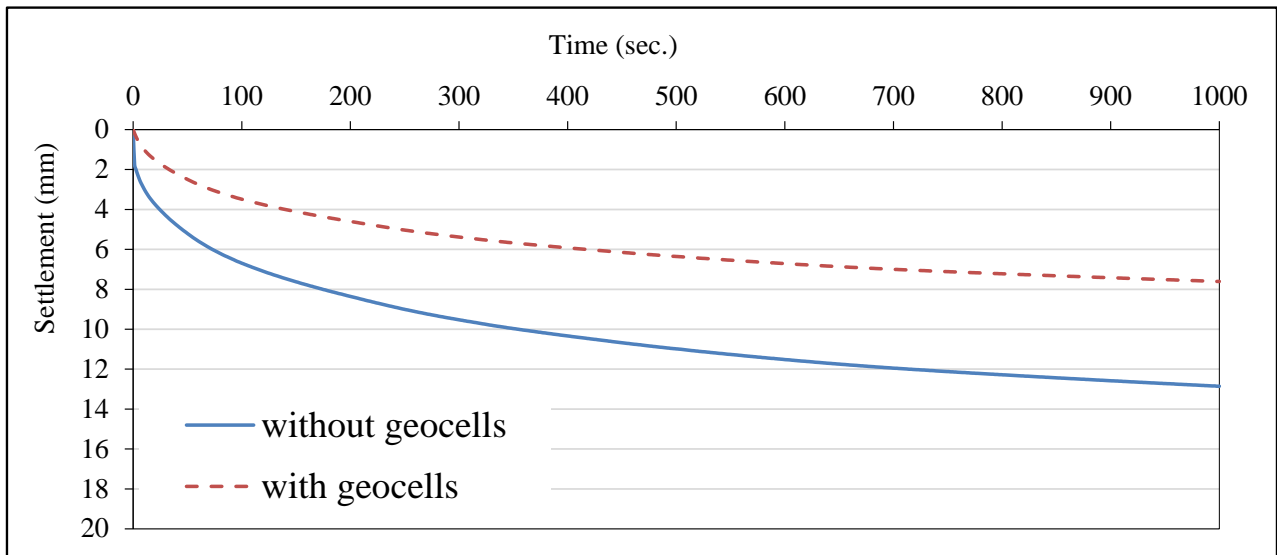

Figure 5.3 Settlement versus time with and without the geocells (a=0.5 ton, ω = 2 Hz).

Figure 5.4 Settlement versus time with and without the geocells (a=1 ton, ω = 0.5 Hz).

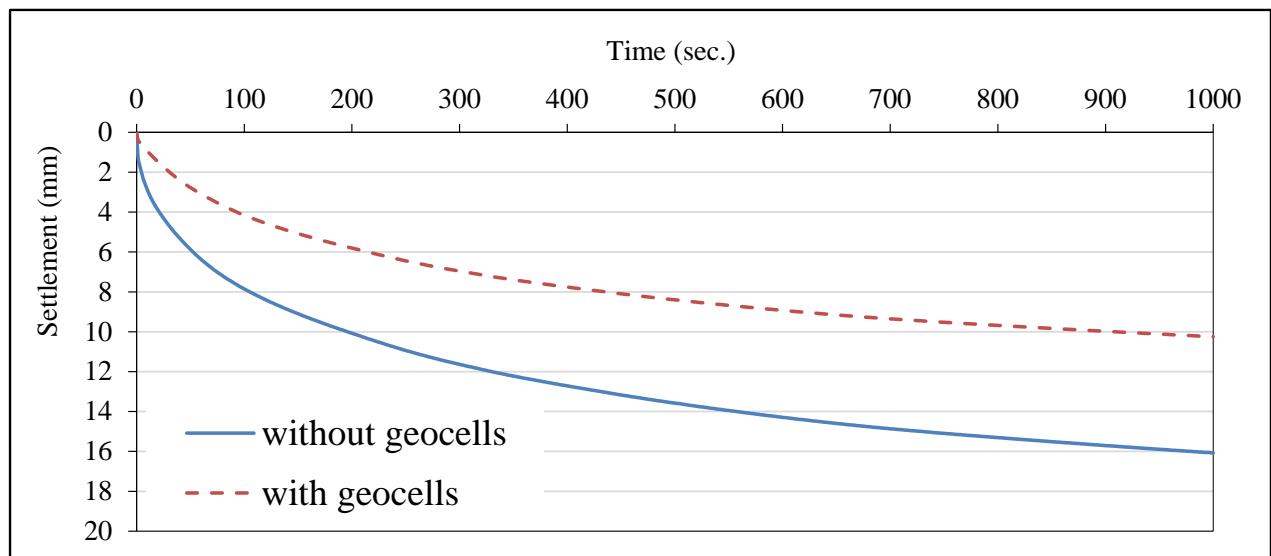Figure 5.5 Settlement versus time with and without the geocells (a=1 ton, ω = 1 Hz).

Figure 5.6 Settlement versus time with and without the geocells (a=1 ton, ω = 2 Hz).

5.2.2 Effect of dynamic load on the crown displacement:

Loading amplitude: The crown vertical displacement was measured using the vibration meter as mentioned in the previous chapter. The maximum values of displacement amplitude of motion are selected and summarized in Table (5.2). Figures (5.7) to (5.12) present the results of the vibration displacement versus time. It can be noted from these figures that the results of the tests do not show a similar trend. This can be attributed to the dynamic response of the soils and the test conditions.

When using geocell reinforcement, the displacement is reduced by about (25-35) % when the amplitude of loading is 0.5 ton and (13-18) % when the amplitude of loading is 1 ton. The reduction is attributed to the increase of the subbase stiffness induced by the geocell reinforcement which makes the subbase and the underlying layer more resistant to vibrations.

Geocell functions in two ways: reinforcement and separation which are the techniques of improving the poor soil with geocell, to increase the stiffness and load carrying capacity of the soil through frictional interaction between the soil and geocell material.

A geocell reinforced soil is stronger and stiffer and gives more strength than the equivalent soil without geocell reinforcement. Geocells provide improved aggregate interlock in stabilizing road infrastructure through subbase restraint reinforcement applications. Geogrid reinforcement provided between the base course and sub-grade soil carries the shear stress induced by vehicular loads.

I. **Frequency of Load:** The effect of load frequency on the displacement amplitude is shown in Figures (5.7) to (5.12). It may be noticed that the displacement value is increased when the frequency is increased. The amplitude of displacement increased by about (44) % when the loading frequency is changed from 0.5 Hz to

2 Hz. The increment can be credited to the dissipation of the elastic waves shifted to the underground pipe, which surges with both the dynamic load amplitude and load frequency increasing.

The test results of Lee et al. (2012) showed that use of Tensar BX1200 geogrid improved the shear strength at the interface when it is placed either between two layers of soil or between a layer of soil and a layer of aggregate. Values of the peak interface shear strength coefficient were found to be equal to 2.02 and 1.59 for the subgrade soil and the aggregate-soil samples, respectively.

The peak shear strength at the interface between the geocell and the surrounding subbase and subgrade decreases as the moisture content of the subgrade or subbase soil increases. Lee et al. (2012) found that for a normal stress of 100 kPa, the peak interface shear strength coefficient for the subgrade soil sample prepared at the OMC and compacted to relative compaction values of 94-96% was 20% less than that of the subgrade soil sample prepared at a moisture content of 4% above the OMC.

Geocell mesh provides better interlocking with the soil particles thus ensuring adequate anchorage during loading. The improvement in the load carrying capacity could be attributed to improved load dispersion through reinforced subbase on to the subgrade. This in turn, results in a lesser intensity of stresses getting the transfer to subgrade, thus leading to lesser subgrade distress.

Table 5.2 Results of the crown displacement.

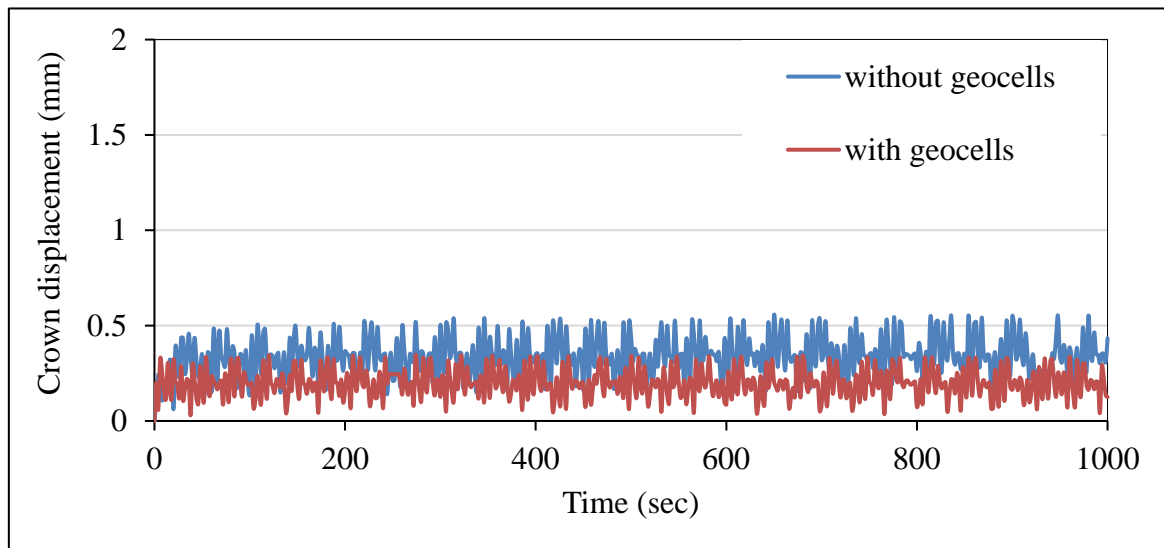| Load amplitude (ton)	Maximum crown displacement at different frequencies (mm)						Reduction percentage		
	Without the geocells			With the geocells					
	0.5 Hz	1 Hz	2 Hz	0.5 Hz	1 Hz	2 Hz	0.5 Hz	1 Hz	2 Hz
0.5	0.533	0.813	0.8365	0.344	0.5748	0.622	35%	29%	25%
1	1.269	1.623	1.8	1.033	1.41	1.48	18%	13%	17%

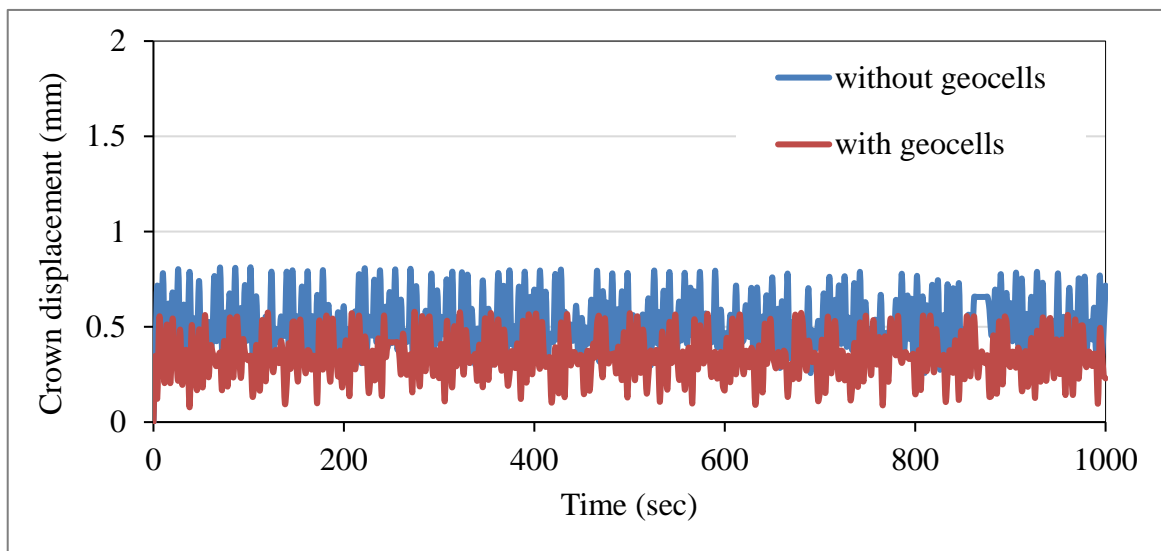Figure 5.7 Vibration of the pipe crown versus time (a = 0.5 ton, ω = 0.5 Hz).

Figure 5.8 Vibration of the pipe crown versus time (a = 0.5 ton, ω = 1 Hz).
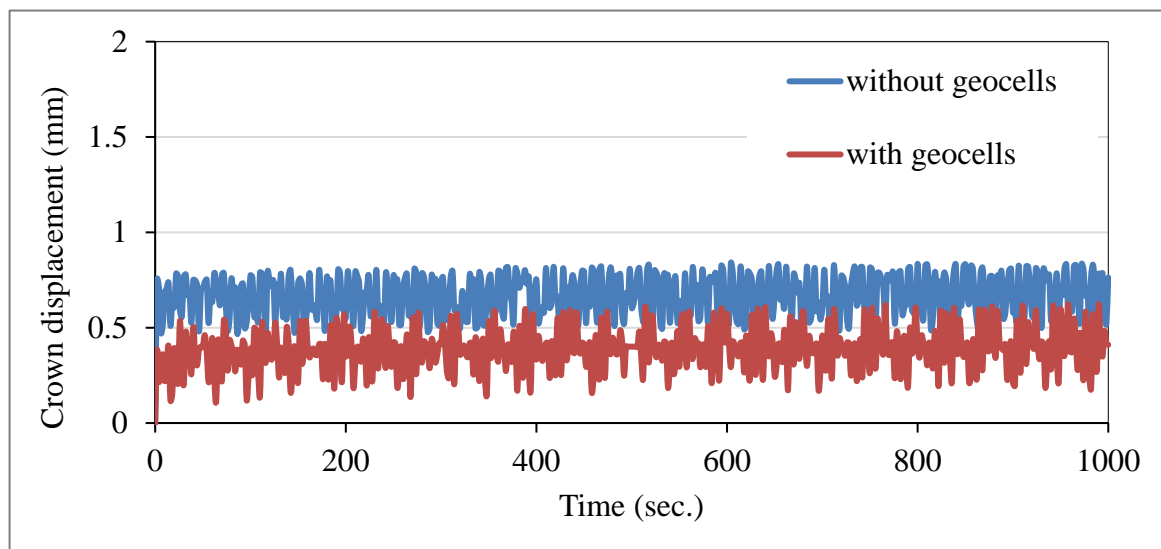

Figure 5.9 Vibration of the pipe crown versus time (a = 0.5 ton, ω = 2 Hz).

69

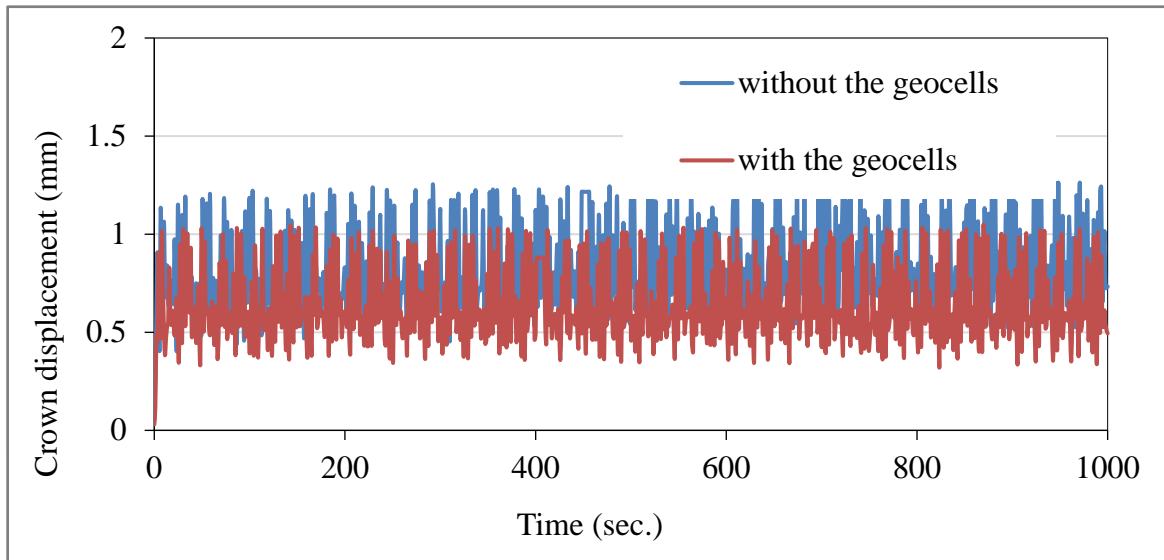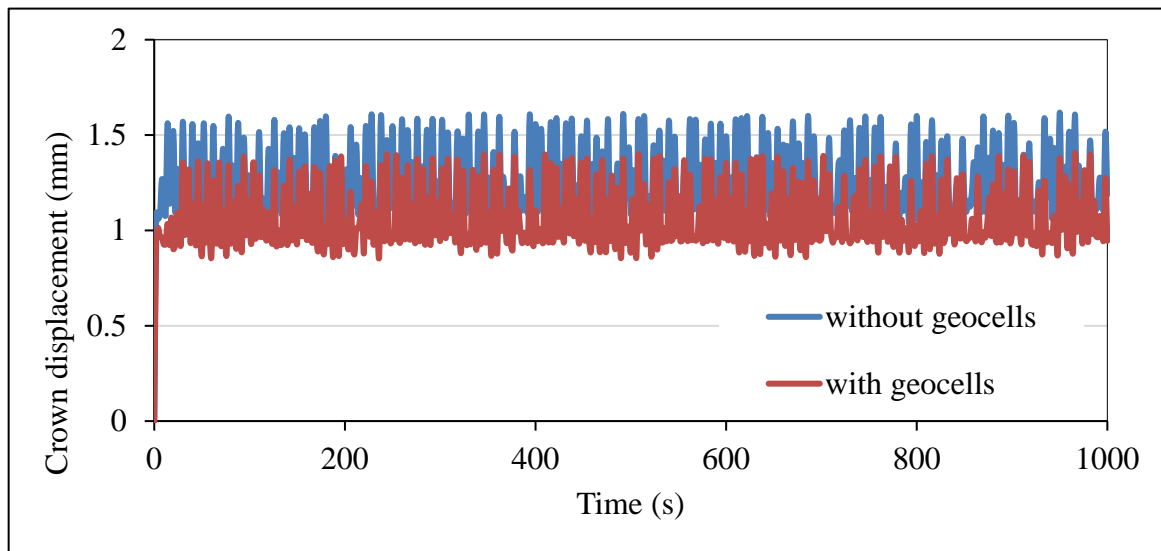Figure 5.10 Vibration of the pipe crown versus time (a = 1 ton, ω = 0.5 Hz).

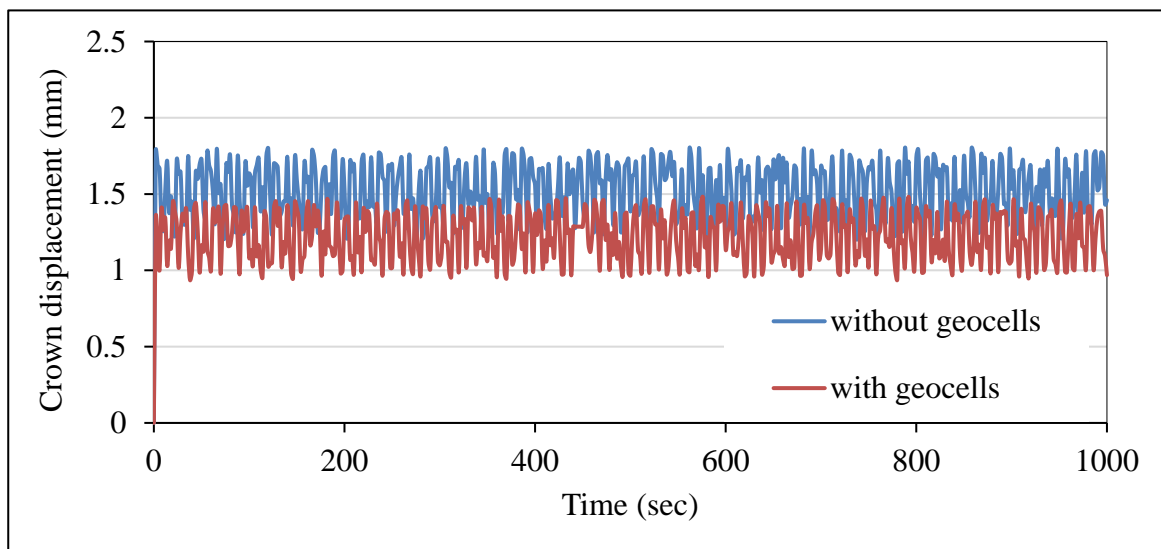Figure 5.11 Vibration of the pipe crown versus time (a = 1 ton, ω = 1 Hz).

Figure 5.12 Vibration of the pipe crown versus time (a = 1 ton, ω = 2 Hz).

70

The mechanism of reinforcement of shear-resisting interface or a lateral restraint, are developed due to the soil-geosynthetic reinforcement shear interaction (Figure 5.13).
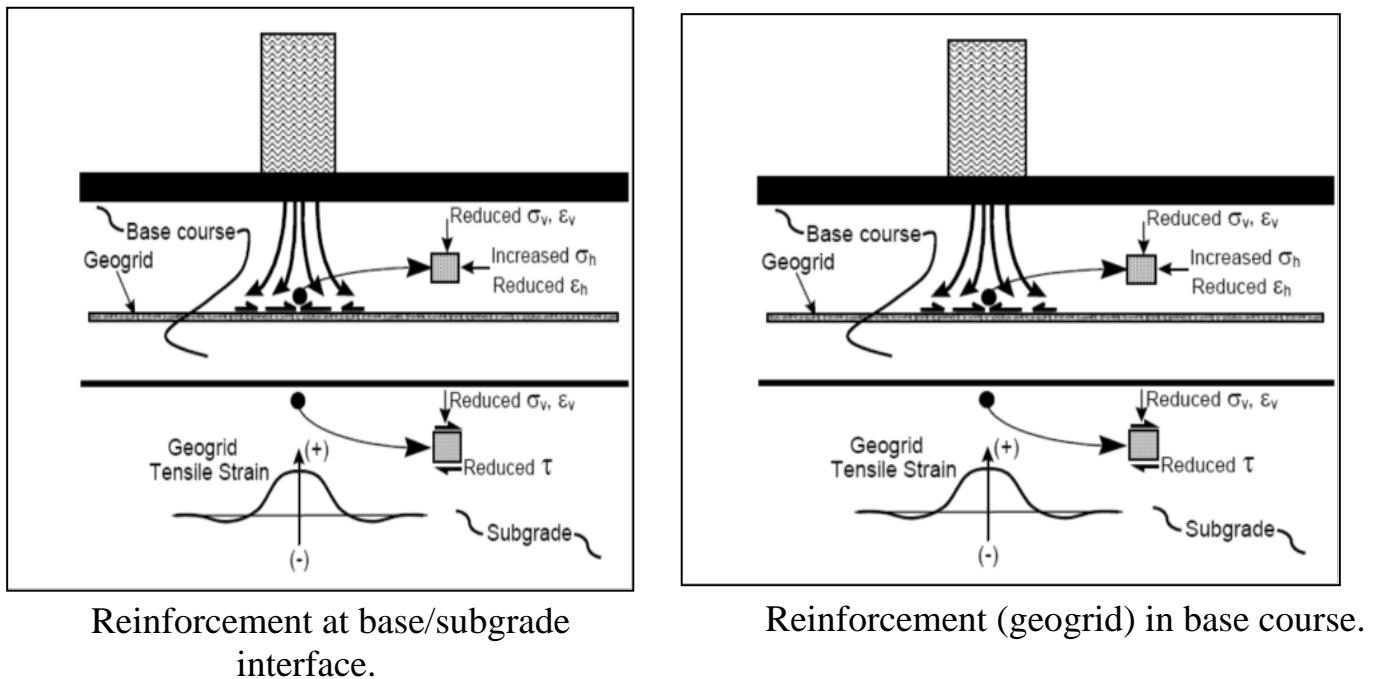

Reinforcement at base/subgrade interface.

Reinforcement (geogrid) in base course.

Figure 5.13 Illustration of reinforcement mechanisms (Berg et al., 2000).

5.2.3 Dynamic loading effect on the vertical pressure:

Loading amplitude: Table (5.3) summarizes the values of pressure on the pipe crown induced by the externally applied load. Values of the vertical pressure reaching the crown of the pipe are shown in Figures (5.14) to (5.20). The vertical pressure increases by about (30) % when the amplitude of load is changed from (0.5 to 1) ton. When using geocell reinforcement, the value of vertical pressure is decreased by about (13-41) % when the load amplitude is 0.5 ton and by about (25-32) % when the load amplitude is 1 ton.

Based on the conclusions of Tafreshi and Dawson (2010), the geocell reinforcement is keeping the encapsulated soil from being directly displaced from under load via the geocells walls induced hoop action, thus increasing the system

shear strength. The load distribution of the confined zone involves a subbase-geocell three-dimensional interaction.

The applied vertical stress to the soil infill inside the geocell prompts an active horizontal pressure at the geocell walls. The friction of interface of the soil infill wall transfers load into the stricter of the geocell, which activates resistance in the geocells surrounding the subbase. It can also be noted that the cells surrounding a geocell provide larger passive resistance as a result of the larger lateral strain in the loading area. The combination of these mechanisms results in a large mat spreading the load over a larger area rather than a smaller contact area, and affords a compound slab having load support capabilities and large flexural stiffness value within the reinforcement; subsequently, resulting in an overall performance enhancement.

Placement of a geosynthetic layer or layers in or at the bottom of the base course allows for shear interaction to develop between the aggregate and the geosynthetic, as the base attempts to spread laterally. The shear load is transmitted from the base aggregate to the geosynthetic and places the geosynthetic in tension. The relatively high stiffness of the geosynthetic acts to retard the development of lateral tensile strain in the base adjacent to the geosynthetic. Lower lateral strain in the base results in less vertical deformation of the roadway surface. Hence, the first mechanism of reinforcement corresponds to direct prevention of lateral spreading of the base aggregate.

I. **Frequency of load:** The vertical pressure variation that reaches the pipe crown due to the variation of frequency is shown in Figures (5.14) to (5.19). It can be observed that the vertical pressure value is increased by (40) % when the loading frequency is increased from 0.5 Hz to 2 Hz when there is no geocell reinforcement. When the geocell reinforcement was used, the vertical pressure increased by (33) % when the loading frequency is changed from (0.5 to 2) Hz.

This behavior may be credited to the load intensity in a limited period which will be more prominent when the frequency of loading is increased, which will lead to the increment of the transferred pressure to the pipe. The experimental results agree with the conclusions of Al-Ameri (2014) and Fattah and Redha (2016) who witnessed that the dynamic stress (σ_{dy}), at a certain depth, increases with the operating frequency (ω_r) increment for every tested soil state.

Table 5.3 Results of the crown pressure reaching the pipe crown.

Load amplitude (ton)	Maximum pressure reaching the crown at different frequencies (kN/m^2)						Reduction percentage		
	Without the geocells			With the geocells					
	0.5 Hz	1 Hz	2 Hz	0.5 Hz	1 Hz	2 Hz	0.5 Hz	1 Hz	2 Hz
0.5	15.25	15.81	19.87	8.86	13.6	14.79	41%	13%	25%
1	20.37	22.65	27.95	13.78	15.6	20.85	32%	31%	25%
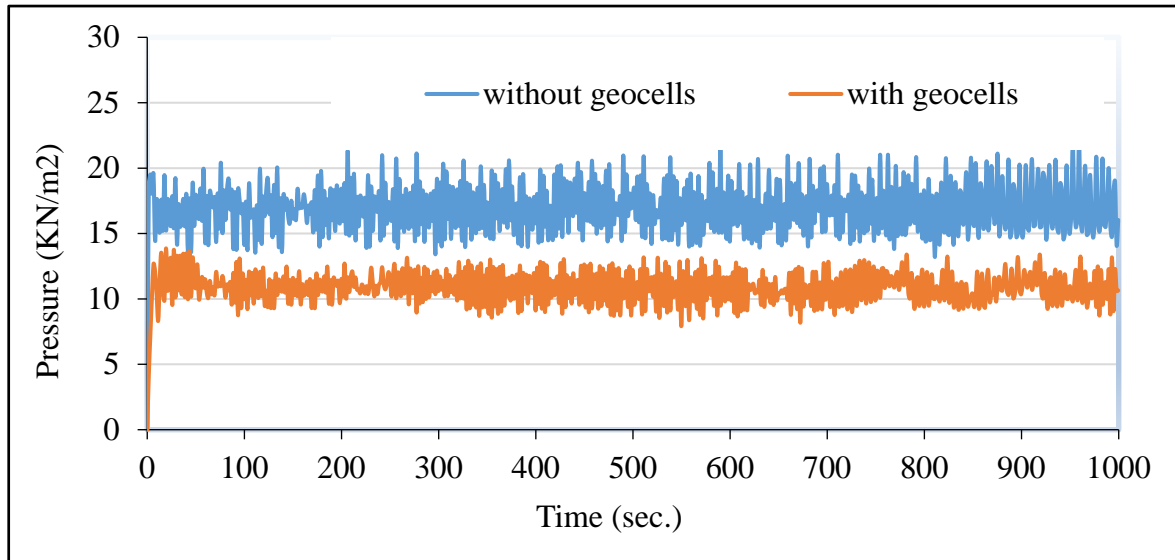
Figure 5.14 Vertical pressure at the pipe crown versus time (a = 0.5 ton, ω = 0.5 Hz).
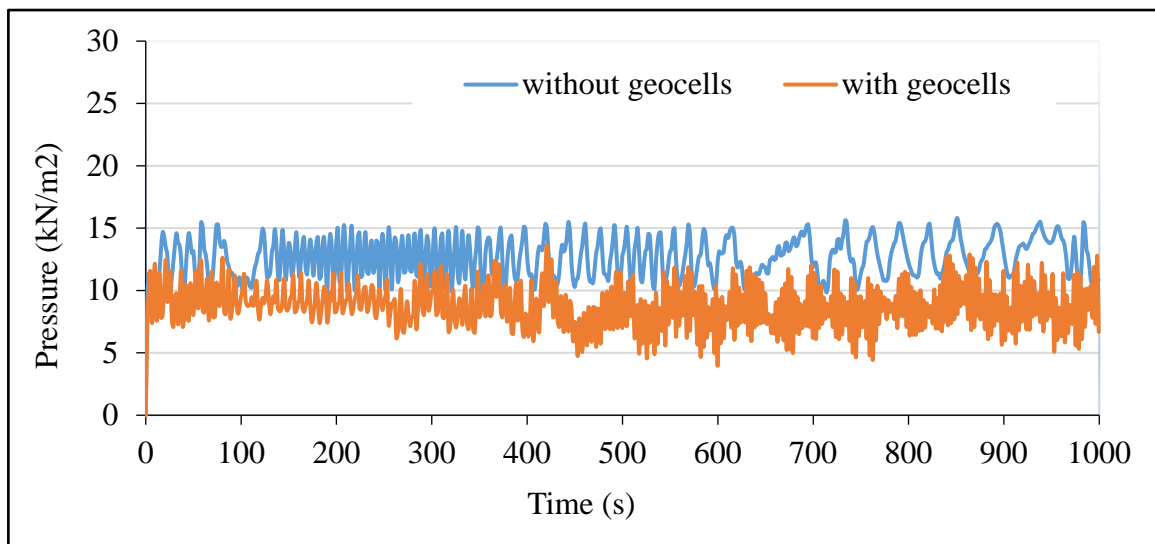

Figure 5.15 Vertical pressure at the pipe crown versus time (a = 0.5 ton, ω = 1 Hz).
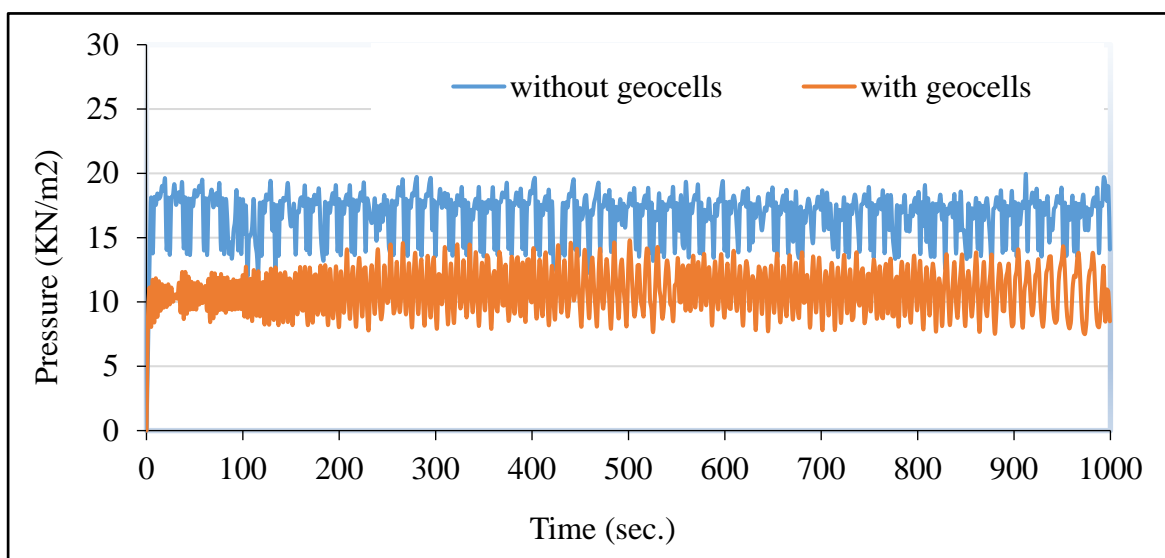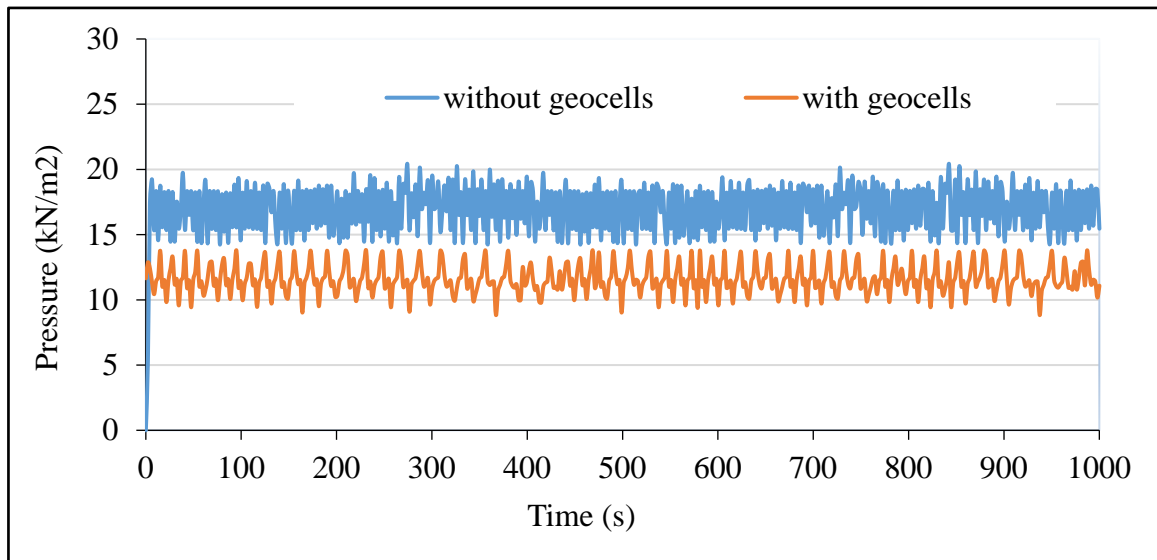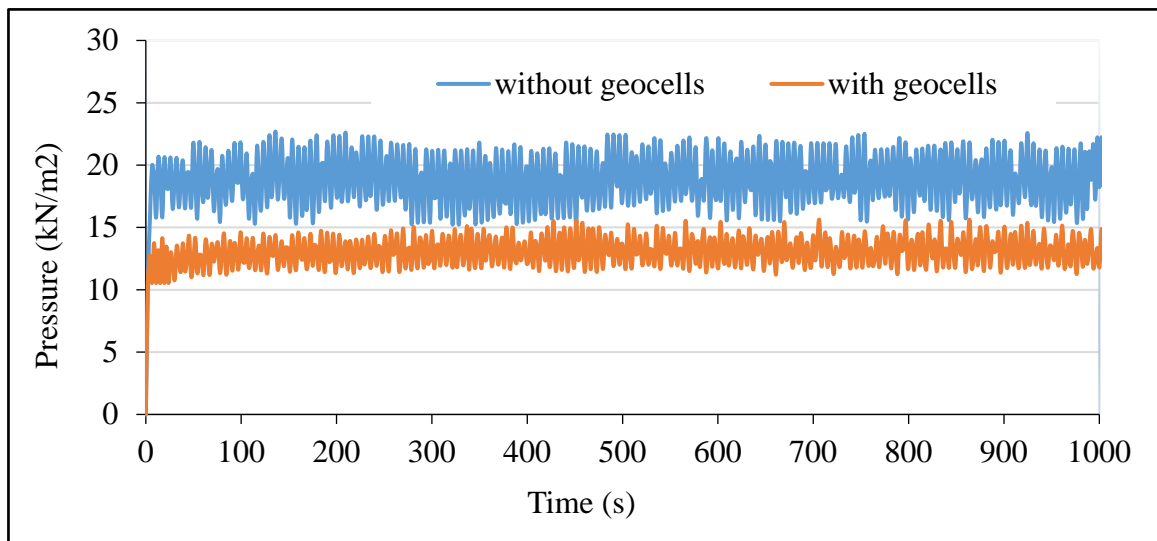

Figure 5.16 Vertical pressure at the pipe crown versus time (a = 0.5 ton, ω = 2 Hz).

Figure 5.17 Vertical pressure at the pipe crown versus time (a = 1 ton, ω = 0.5 Hz).

Figure 5.18 Vertical pressure at the pipe crown versus time (a = 1 ton, ω = 1 Hz).
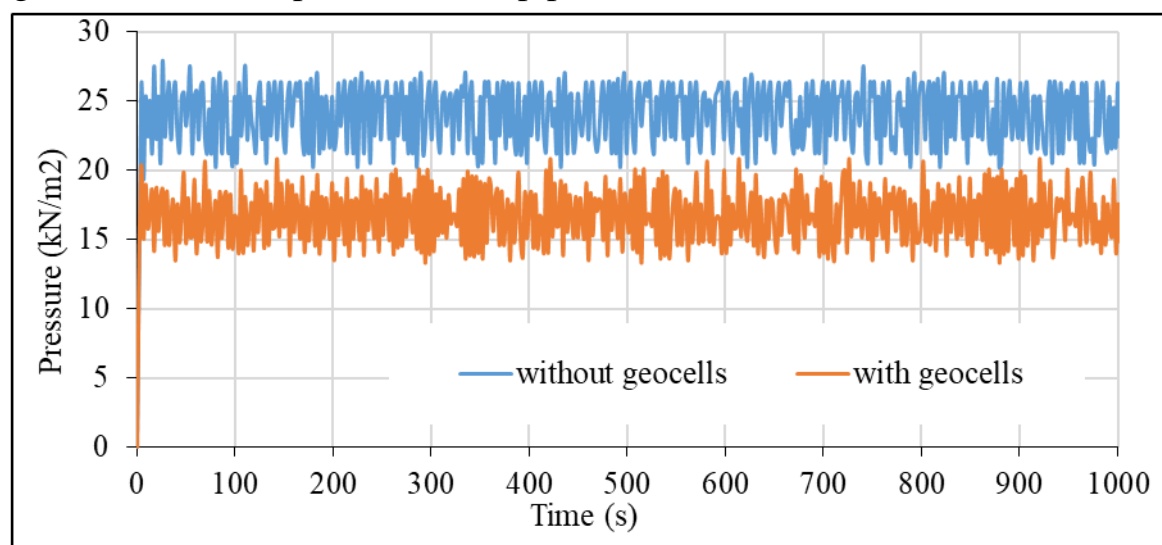

Figure 5.19 Vertical pressure at the pipe crown versus time (a = 1 ton, ω = 2 Hz).

75

The developed shear stress between the geosynthetic and the base course aggregate provides a lateral confining stress increment within the base. An increment in elastic modulus is exhibited in granular materials when the confining stress is increased. The component of subbase reinforcement results from the subbase stiffness being increased when the proper subbase-geocell interaction develops. The increased subbase stiffness reduces the vertical subbase deformations and the vertical surface deformations. Models of reinforcement relying upon an increase in confinement and modulus of the base as illustrated by Sellmeijer (1990) and Kinney et al. (1998)

5.3 Model Calibration

For the analysis of the buried pipes, theoretical methods are as valuable as the experimental methods, because they can directly provide the analytical formulas used in engineering design. The theoretical methods involve two principal techniques: numerical solution and analytical solution. The calibration study will be done in this chapter to verify the simulation procedure adopted in the current study. The experimental work results have been selected to be a matter of calibration study because it contains all the properties needed by the program such as modulus of elasticity, Poisson's ratio, angle of internal friction, soil unit weight, etc.

5.3.1 Experimental work simulation

Four models were selected from the experimental work for the verification problem, two models with a load amplitude of 0.5 ton and a load frequency of 0.5 Hz with and without geocell reinforcement. For the other two models, the load amplitude was 1 ton, and the load frequency was 1 Hz with and without geocell reinforcement.

The results of the analysis performed are graphically presented by listing the maps of model deformation, maps of stress and strain of the soil mass and

pipe structure and diagrams of displacements of the pipe points, and the diagrams of generalized internal forces in the pipeline.

5.3.2 Results of the numerical modelling

Figures (5.20) and (5.21) show a comparison of the surface settlement between the experimental work and the numerical modeling with PLAXIS 3D software. The results showed that the maximum percentage of error between experimental work and numerical simulation is about 10%.

Figures (5.22) and (5.23) present a comparison of crown displacement between the experimental work and the numerical finite element analysis. The results indicated that the maximum percentage of error between experimental work and numerical simulation is about 11%.

Figures (5.24) and (5.25) show a comparison of vertical pressure at the pipe crown between the experimental work and the numerical results. The results indicated that the maximum percentage of error between experimental work and numerical simulation is about 6%.

.

The error can be attributed to many reasons, such as the test conditions, the use of Mohr-Columb model, which cannot predict the soil behavior accurately, mesh size, damping and some soil properties, which are assumed due to the lack of testing devices.

The inclusion of the geocell reinforcement in the subbase layer can also improve and distribute the loading over a larger area of the subgrade. In general, as the subbase stiffness increases, the vertical load in the subgrade under the geocell layer should decrease. The surface deformation will be less and more uniform due to the applied loading being spread over a larger area, thus results in

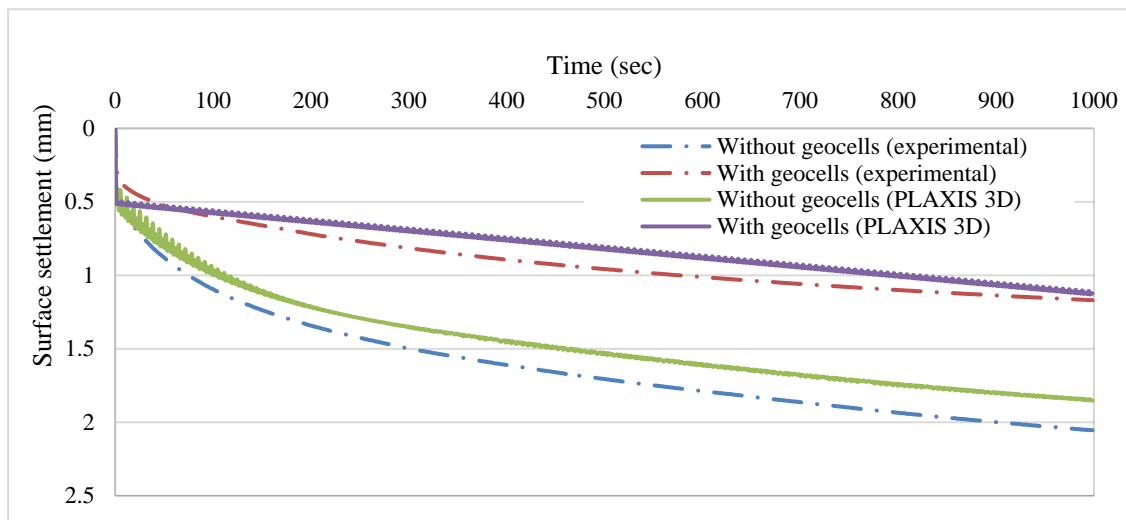a third reinforcement component from the improved stress distribution over the subgrade.

Figure 5.20 Comparison between the experimental and the numerical simulation for surface settlement versus time (a = 0.5 ton, ω = 0.5 Hz).
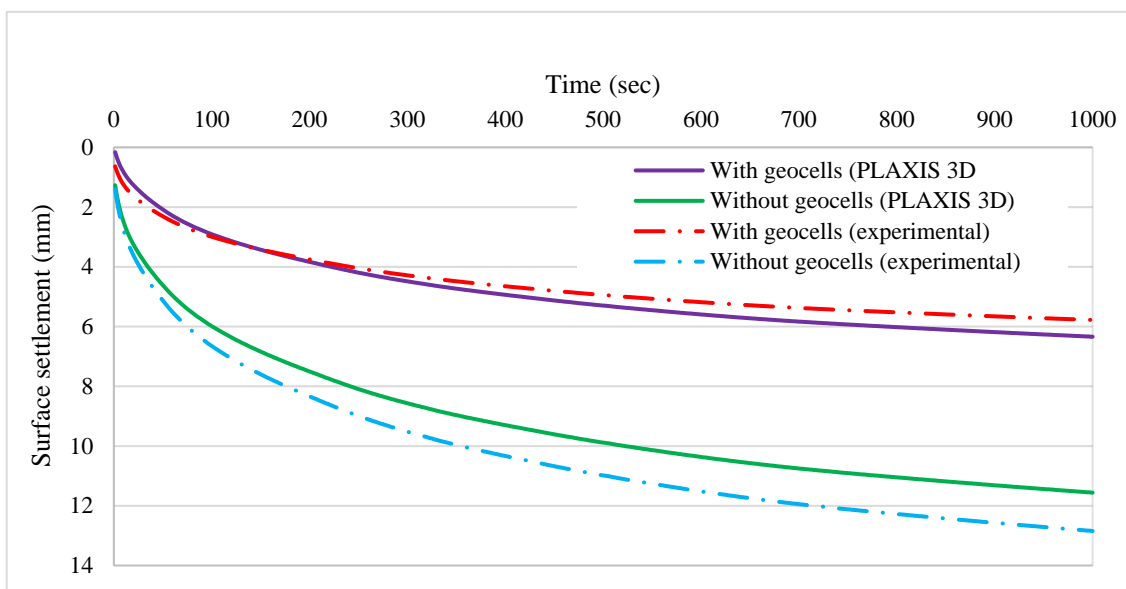

Figure 5.21 Comparison between the experimental and the numerical simulation for surface settlement versus time (a = 1 ton, ω = 1 Hz).
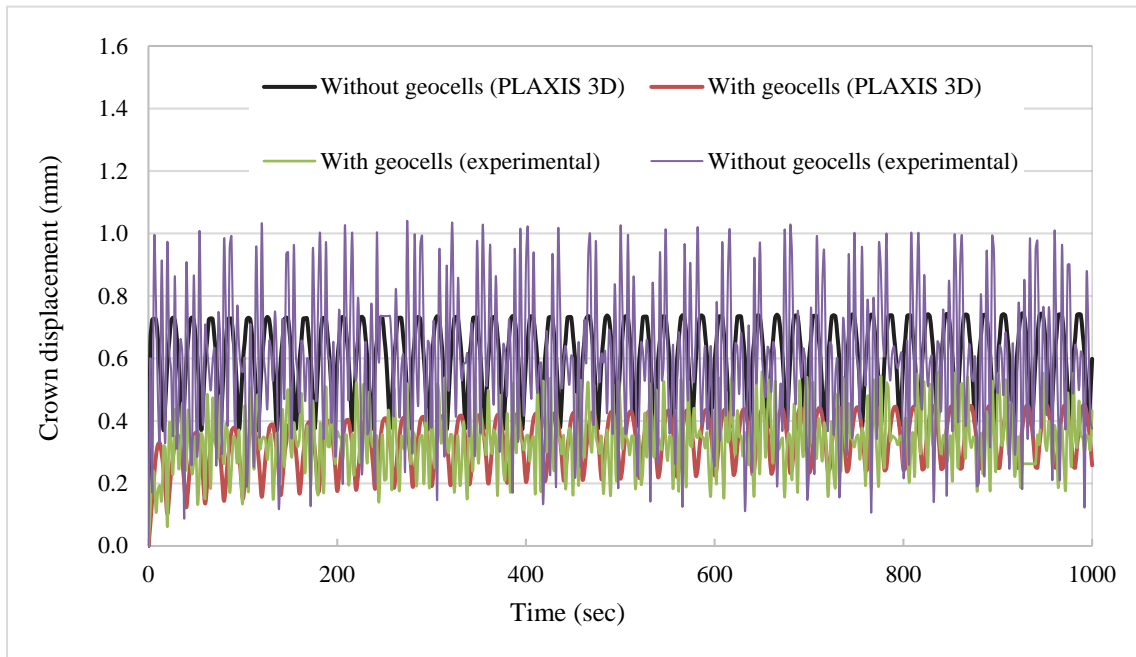
Figure 5.22 Comparison between the experimental and the numerical simulation for crown displacement versus time (a = 0.5 ton, ω = 0.5 Hz).
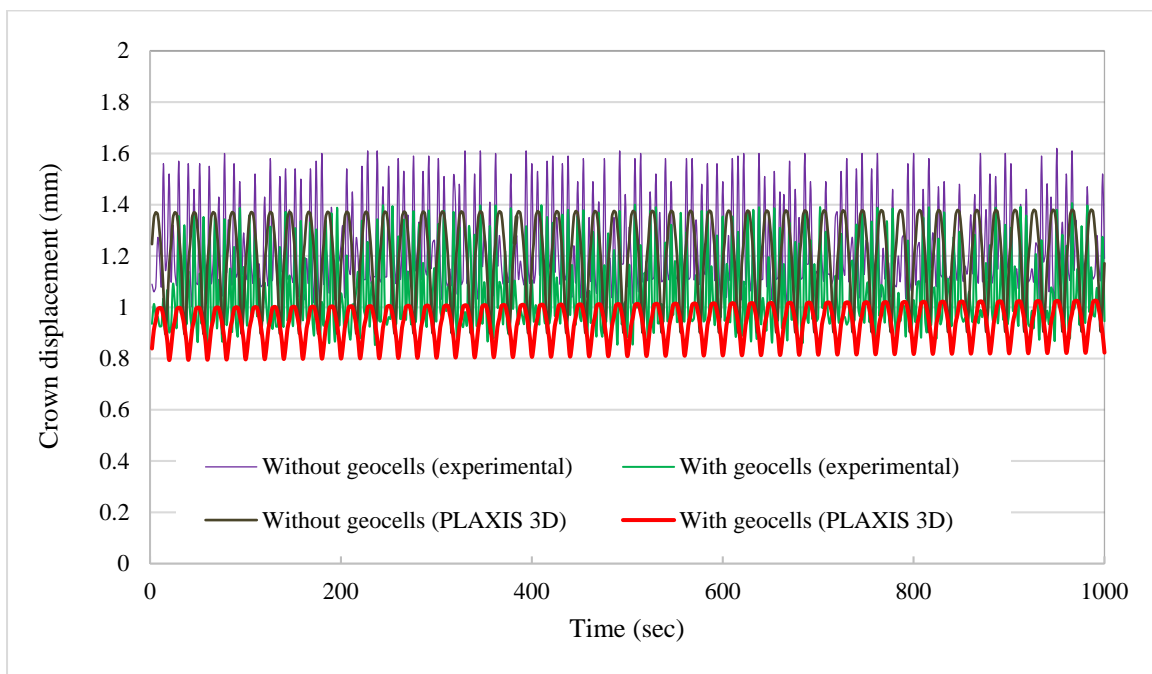

Figure 5.23 Comparison between the experimental and the numerical simulation for crown displacement versus time (a = 1 ton, ω = 1 Hz).
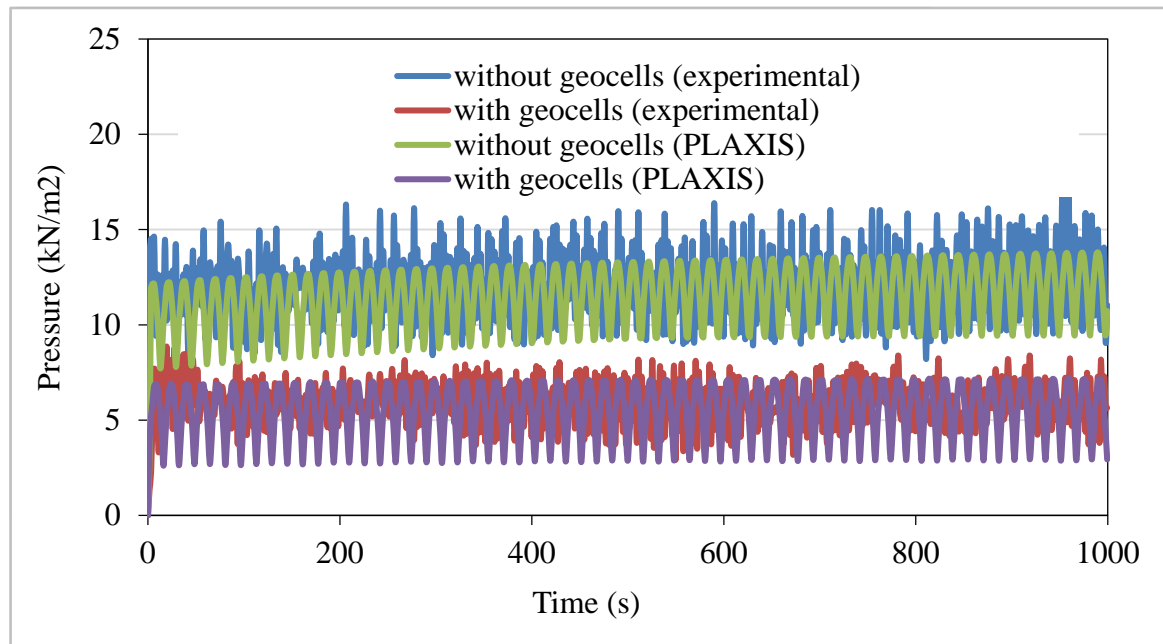
Figure 5.24 Comparison between the experimental and the numerical simulation for vertical pressure versus time (a = 0.5 ton, ω = 0.5 Hz).
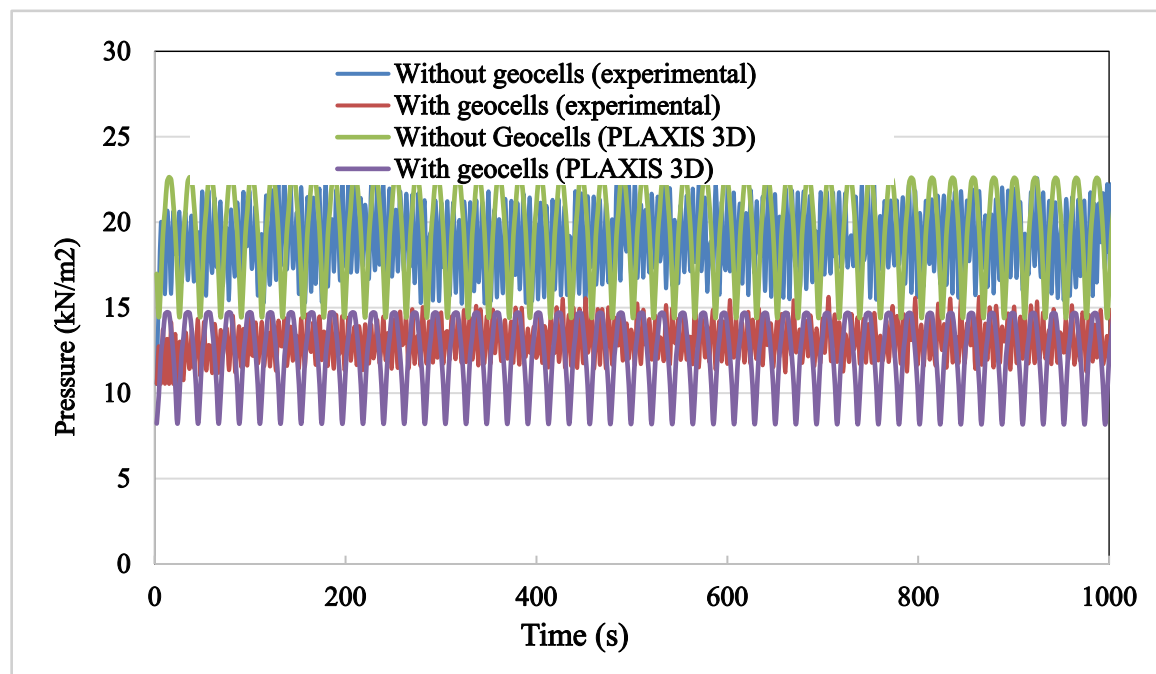

Figure 5.25 Comparison between the experimental and the numerical simulation for vertical pressure versus time (a = 1 ton, ω = 1 Hz).

The following figures show a comparison between reinforced and unreinforced models (a = 1 ton, ω = 2 Hz) at the end of 50 seconds. Figure (5.26) shows the surface settlement U_z, Figure (5.27) shows the plastic points, Figure (5.28) presents the total displacement of the pipe, while Figure (5.29) shows the axial force imposed on the pipe.
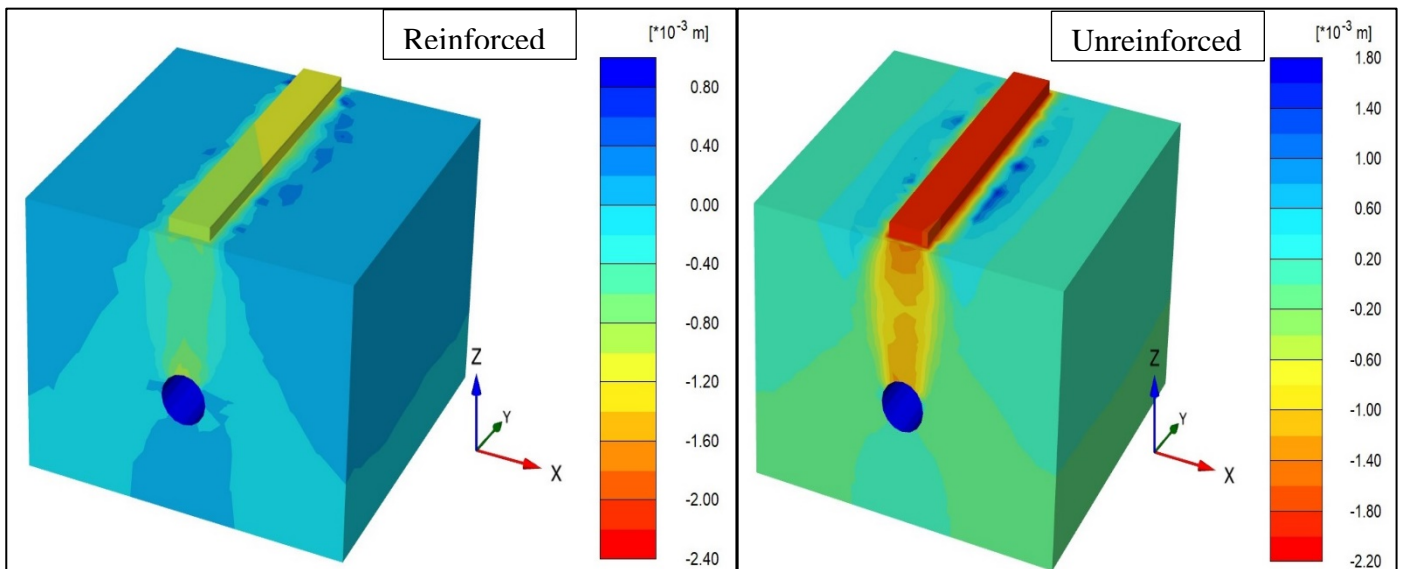
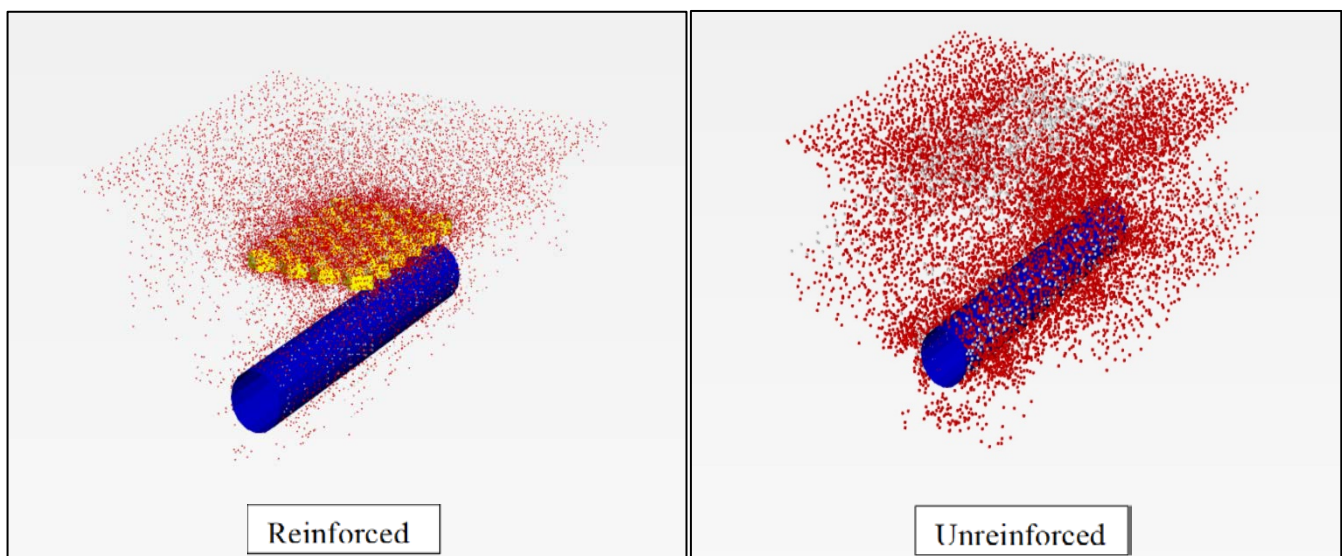

Figure 5.26 Surface settlement.

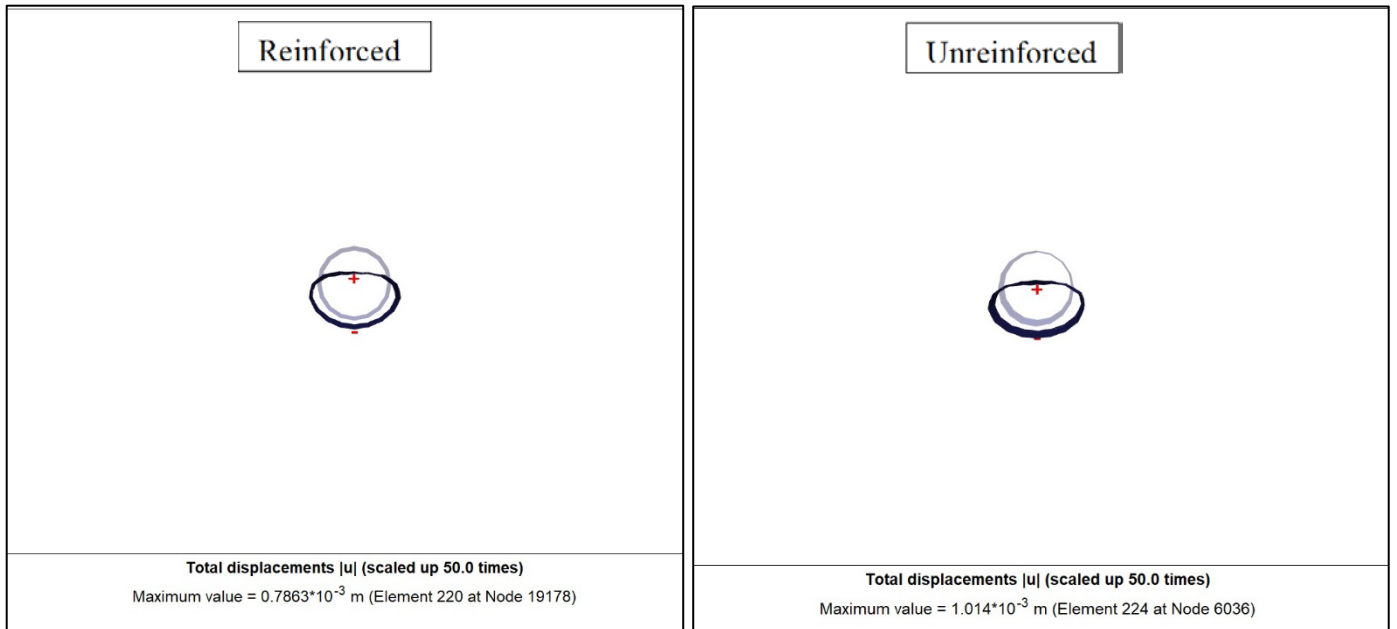Figure 5.27 Plastic points.

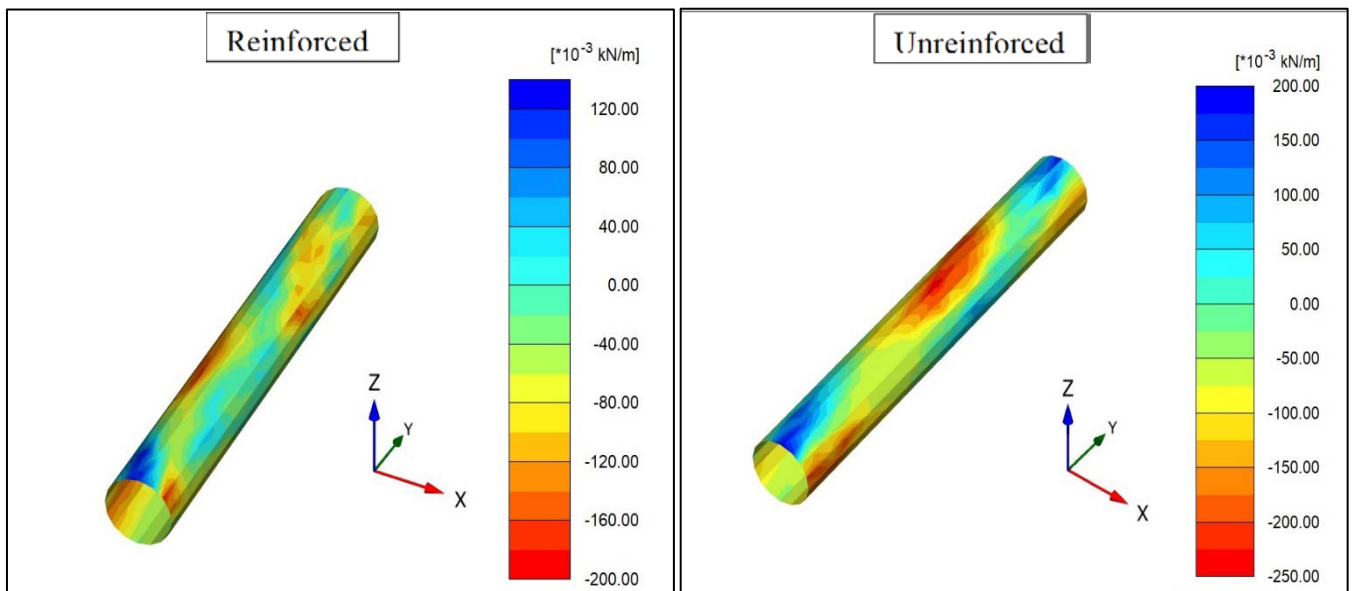Figure 5.28 Total displacement of the pipe.

Figure 5.29 Axial force.

The crown of the pipe has been deflected significantly and has shed load to the adjacent pipe sections.

There are two significant points when discussing the pipeline damage. First, how much material has yielded and secondly how much length of the pipe enters in the plastic stage. This has great significance in case of post-event repair and maintains. This large longitudinal strain in the pipe material further causes a reduction in the wall thickness (developing upon Poisson's ratio), which may not be safe design thickness for the internal pressure and another load.

Chapter Six

Parametric Study on the Buried Pipe Problem

6.1 Introduction

The numerical analysis presented in Chapter four was based on the experimental tests conducted in the laboratory. Due to the limitations of large-scale tests, limited tests were conducted. To evaluate the effects of few key influence factors on the benefits of using geosynthetics to protect pipes, a parametric study was developed based on the literature review, the experimental results, and the calibrated numerical models. The numerical model of the test section was used as the baseline for the parametric study. This chapter presents the selection of parameters, the results of the parametric study, and the conclusions.

6.2 Selection of Parameters

The purpose of this study is to study the influence of numerous factors in the prediction of the buried pipeline behavior when subjected to traffic loading, including the material properties, depth of pipe, the depth of the geocell reinforcement, the relative density of the subbase layer and traffic speed.

6.2.1 Material of pipe

The material that was chosen to represent the pipe is glass fiber reinforced plastics (GRP), as it is widely used in underground pipe systems.

6.2.2 Soil layers

The subbase relative density was chosen on the basis of relative compaction and was set to 95% and the thickness was chosen to be 300 mm above the subgrade. The properties of the sand layer were kept the same as the ones used in Chapter Four, the thickness of the sand layer was set to 5 m for all tests.

6.2.3 Surface layer

The surface layer was modeled as an asphaltic layer of 50 mm thickness and a base layer of 100 mm thickness based on (Lay, 2009). The surface layer was modeled as linear elastic since the study is for a short period; therefore, the creep effect is not taken into consideration.

6.2.4 Geocell reinforcement

The geocell reinforcement is assumed to be installed at a rather restricted elevation, typically at a sand-subbase interface. This study focused on a geocell layer of a thickness of 150 mm, which is consistent with the grain size of the gravel infill. Thus, the stiffness of geocell became a major item of the parametric study.

6.2.5 Live load

Despite the fact that wheel loads from cars and other vehicles may be frequent, these types of loads generally have minimum impact on underground pipes when compared to significantly heavier loads with less frequent from trains, trucks or other heavy vehicles. For the pipe design below highways and streets, only the loadings from these heavier vehicles are taken into account. The transmitted pressure to a pipe by a vehicle depends on the tire size and pressure, the pipe depth, the weight of the vehicle, speed of vehicle, smoothness of surface, soil type, the type and amount of paving, and the distance from the point of loading to the pipe. For the more common cases, such as American Association of State Highway and Transportation Officials-AASHTO, HL-93 design truck traffic on paved roads and E-80 rail loading, the maximum wheel load takes place at the surface and attenuates with depth. Buried pipes should be installed at the greater value of depth of minimum of one diameter or 450 mm, under the road surface. The pipe, at this depth, is far enough under the wheel load to significantly diminish the pressure of soil and the pipe can fully make use of the embedment soil for load resistance. Loads from vehicles are typically based on the AASHTO

standard truck loadings. The loading is normally assumed to be HL-93 design truck when calculating the pressure of soil above the flexible pipe. Design Truck consists of three axles, front and two rear axles with front axle weighing 8 kip (35 kN) and two rear axles weighing 32 kip (145 kN). The distance between front and rear axle is 14 ft (4.3 m) and that of two rear axles can be varied between 14 ft (4.3 m) to 30 ft (9.0 m) to obtain the worst design force. The tire to tire distance in any axle is 6 f-t (1.8 m) (Plastics Pipe Institute (PPI), 1950) as shown in Figures (6.1) and (6.2).
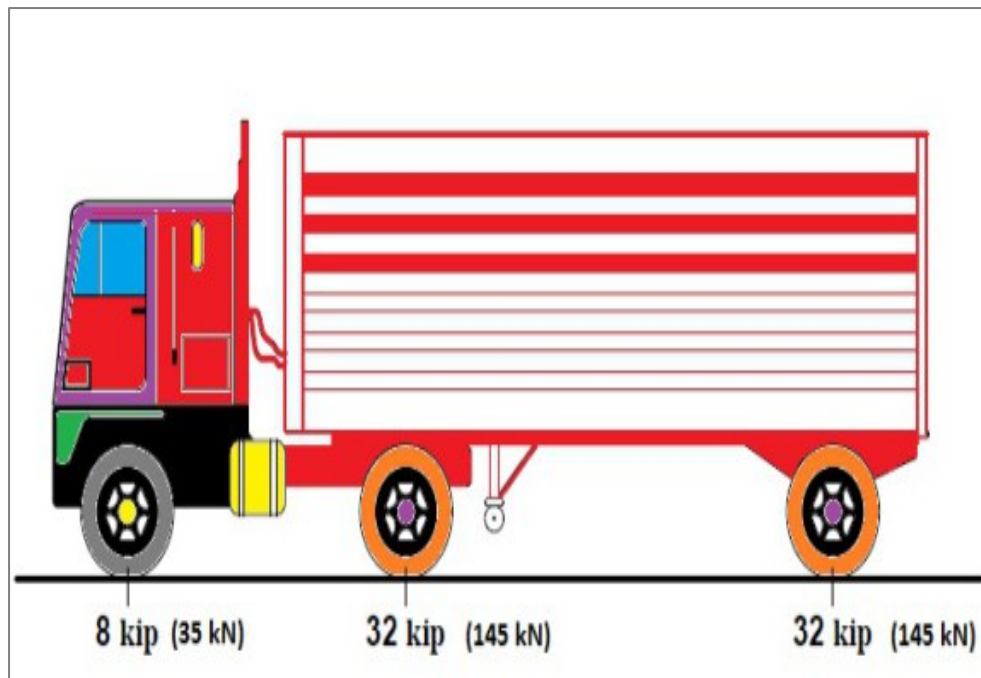

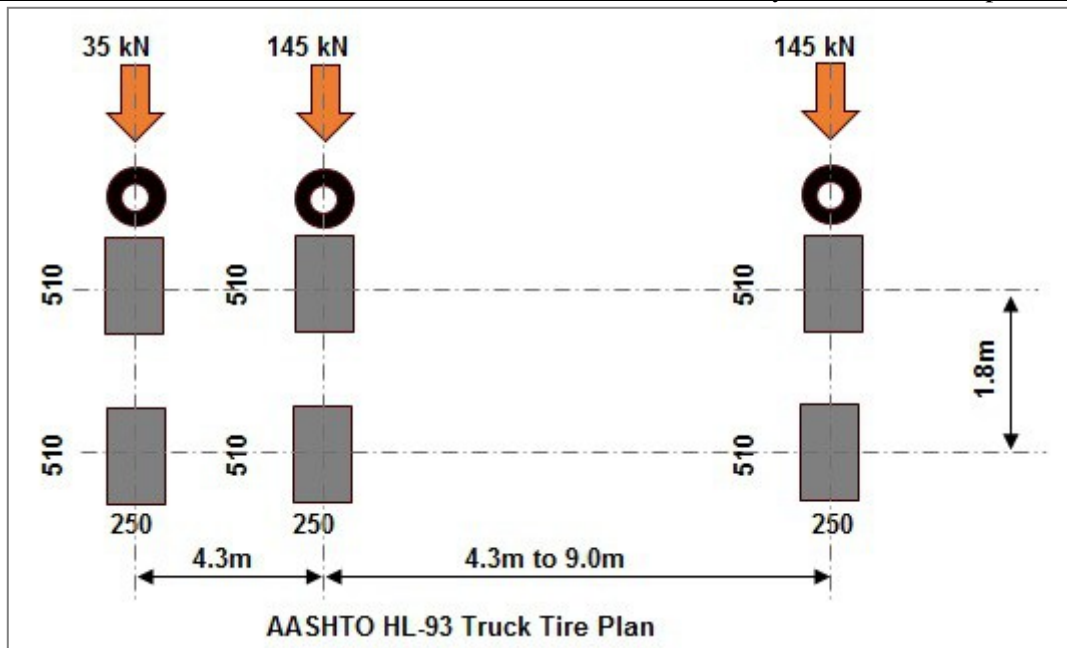Figure 6.1 HL-93 design truck (AASHTO Bridge Design Specifications Cl 3.6.1.2).

Figure 6.2 HL-93 design truck tire plan (AASHTO Bridge Design Specifications Cl 3.6.1.2).

6.2.6 Tire contact area

The length of tire contact can be considered using AASHTO's LRFD (2010), which yields a 250 mm length and a 50 mm width (based on a wheel load of 71 kN) and a 33 percent impact factor at the surface and dispelling to zero at 2.45 m depth. A design case for a highway pavement typically assumes a two-lane paved road with an HL-93 design truck centered in each 3.65 m wide lane (Figure 5.3). Two wheels from passing trucks will give the greatest load, and this load case should be used for buried pipes design. The pipe may be parallel or perpendicular to the truck travel direction, or any in-between position. Other design truck loads can be specified as required by local practice and project needs.(Richard and Furest, 2013).

Figure (6.3) shows a schematic representation of Two HL-93 trucks located in adjacent lanes, while Figure (6.4) presents the distribution of HL-93 live load through the fill. Three different speeds of vehicles were chosen for comparison in the study, they are 20, 40 and 60 km/hr.
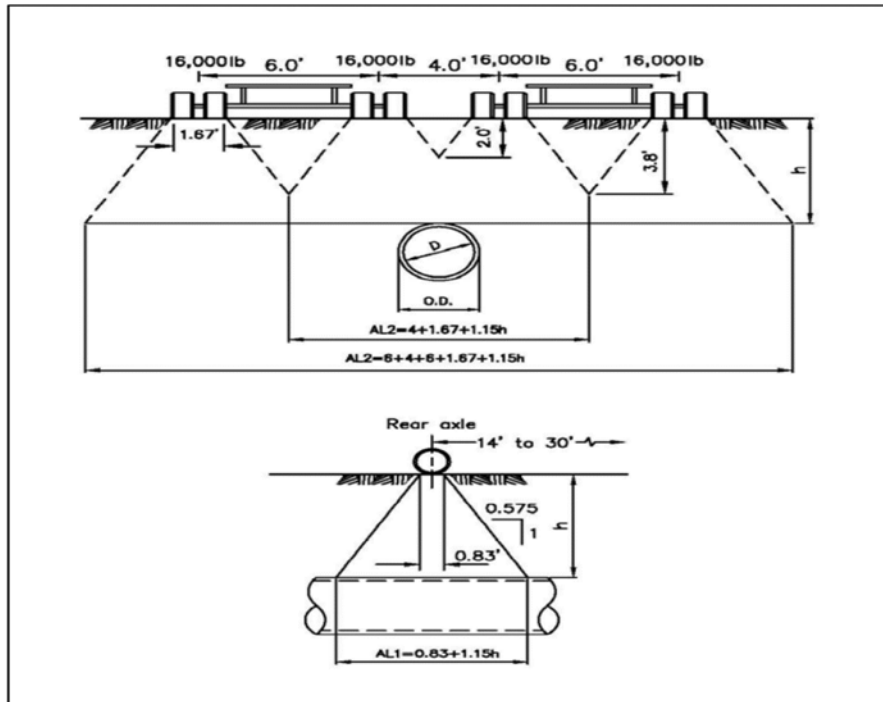
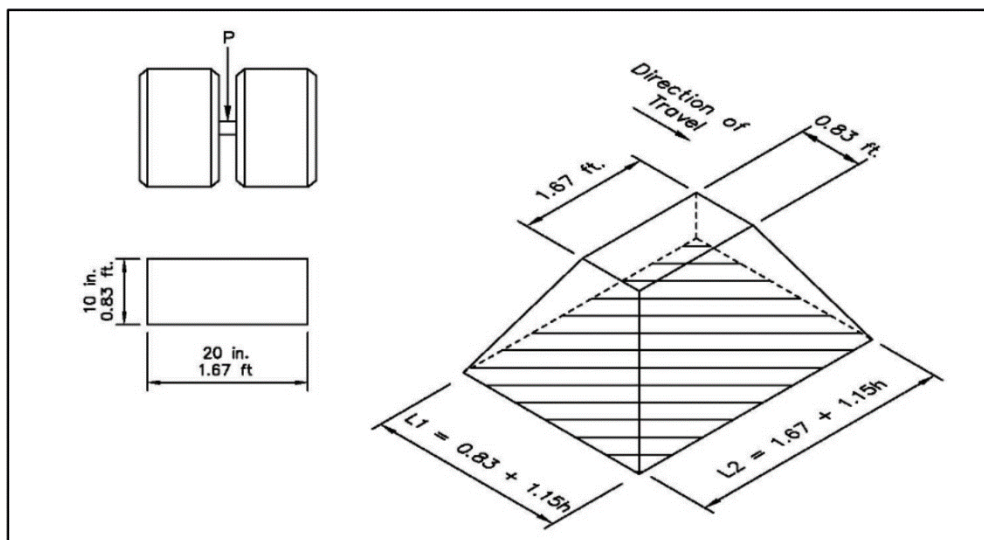Figure 6.3 Two HS-20 trucks located in adjacent lanes (Richard and Furest, 2013).

Figure 6.4 Distribution of HS-20 live load through fill (Richard and Furest, 2013).

6.3 Simulation Program

A total of 18 models shall be simulated in this study. Nine of them are unreinforced and the other nine are reinforced, three different pipe diameters were selected (600, 800 and 1000) mm. The depth of each pipe was set as (1D) and

three speeds of vehicles were chosen (20, 40 and 60) km/hr. The geocell reinforcement was modeled at the sand-subbase interface.

Figure (6.5) presents a summary of the numerical analysis program conducted in the parametric study and Figure (6.6) shows a cross section of the model. Figure (6.7) shows the mesh view of the model including the location of points for presentation of the results.
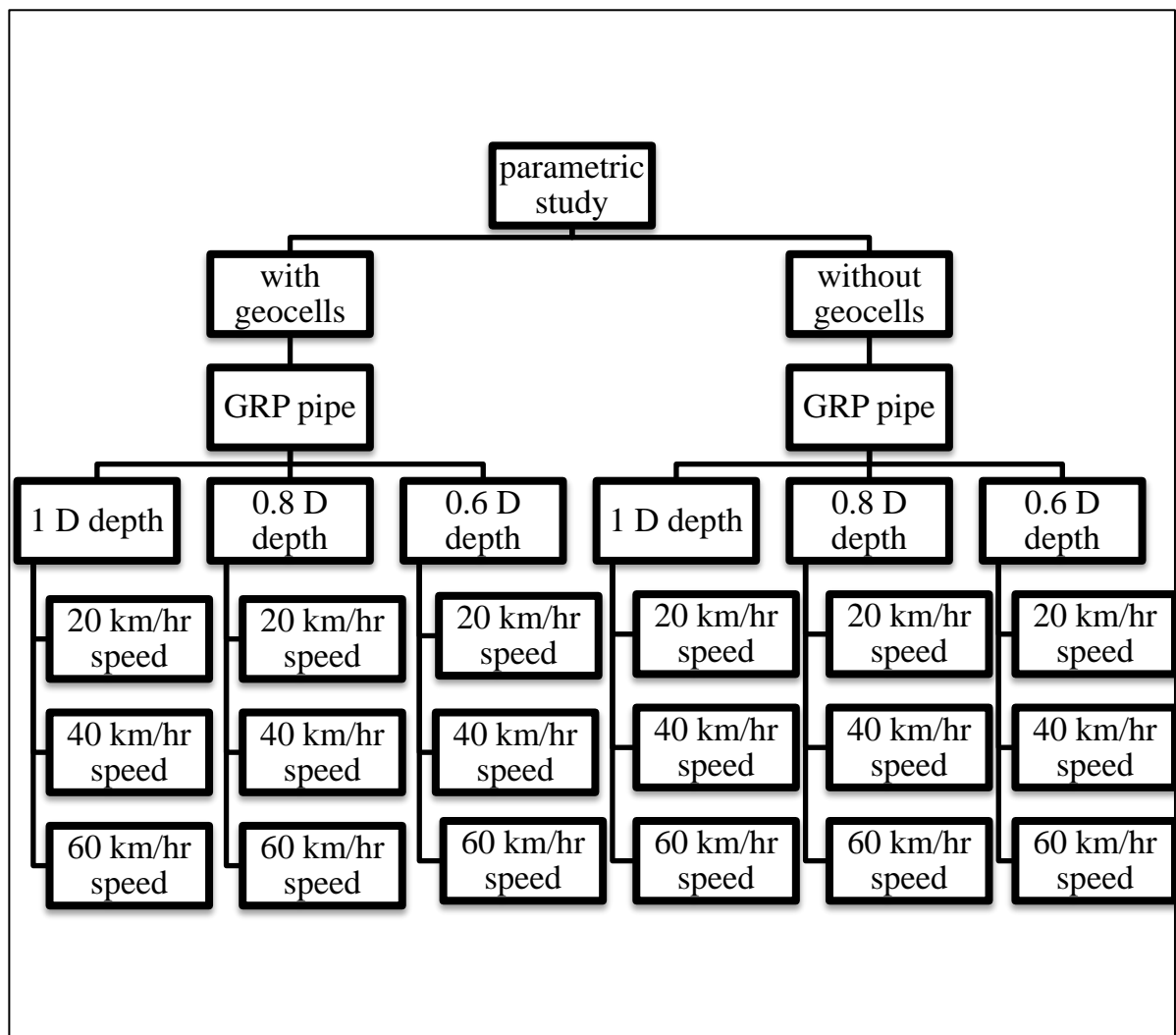
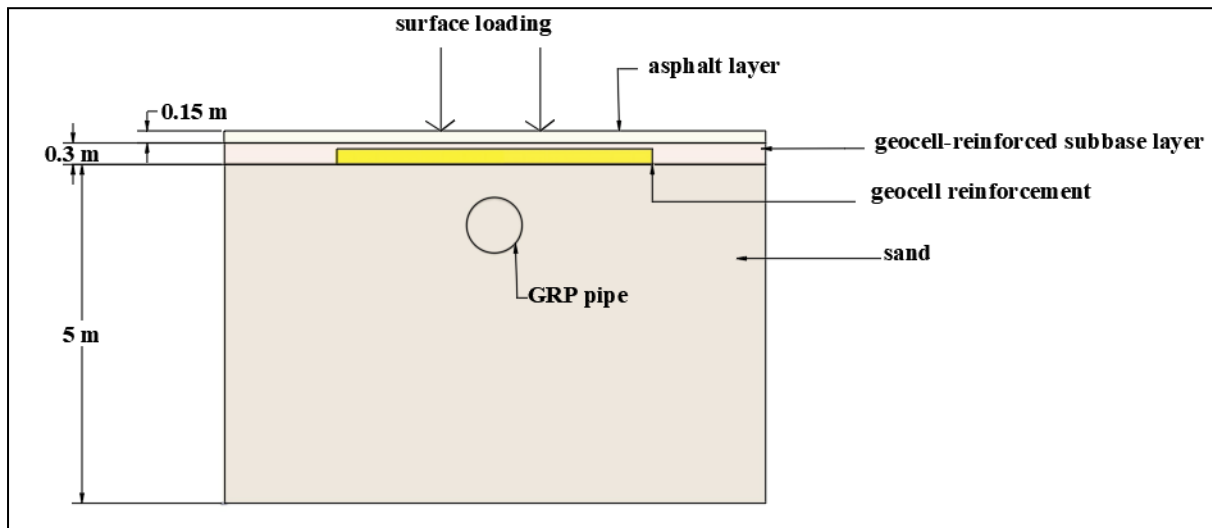Figure 6.5 Summary of the finite element analysis models.
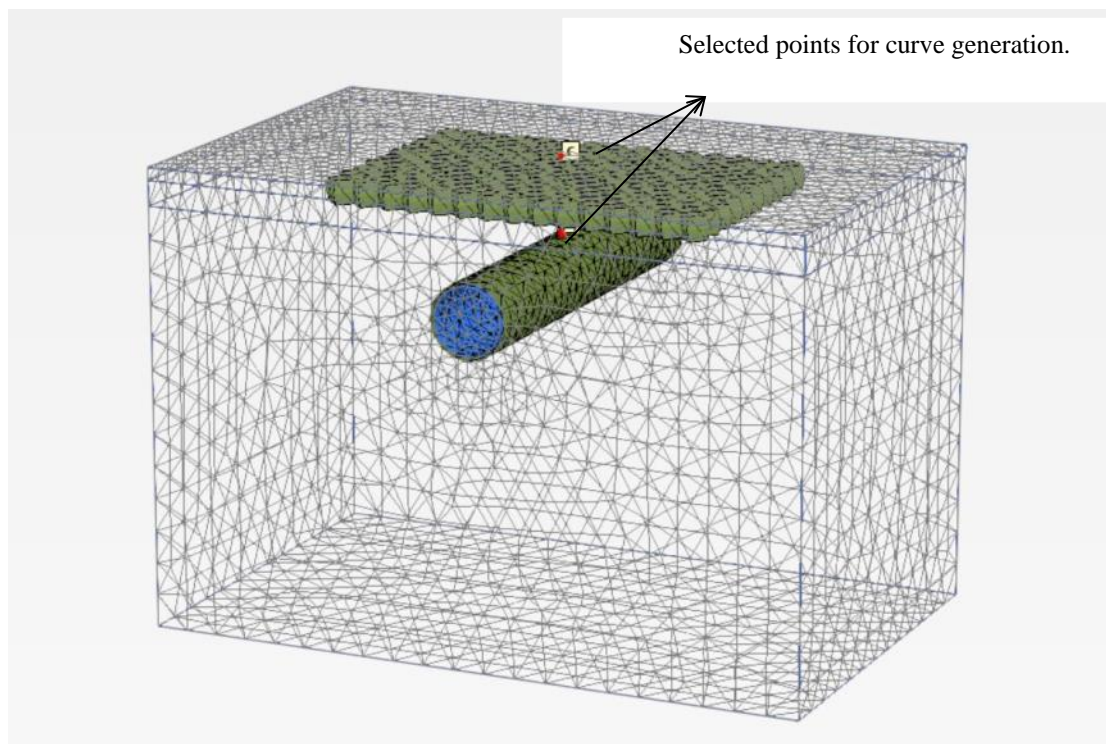
Figure 6.6 Cross section of the model.

Figure 6.7 Mesh view of the model showing the location of points for curve generation.

Figures (6.8) to (6.10) show the traffic-loading wave for all the simulated speeds of vehicles. Table 5.1 presents the properties of the soils, asphalt, GRP pipe and geocells materials used in the parametric study. Some of the parameters of the asphalt and subbase layers are assumed and the parameters of the GRP pipe are provided by the manufacturer.
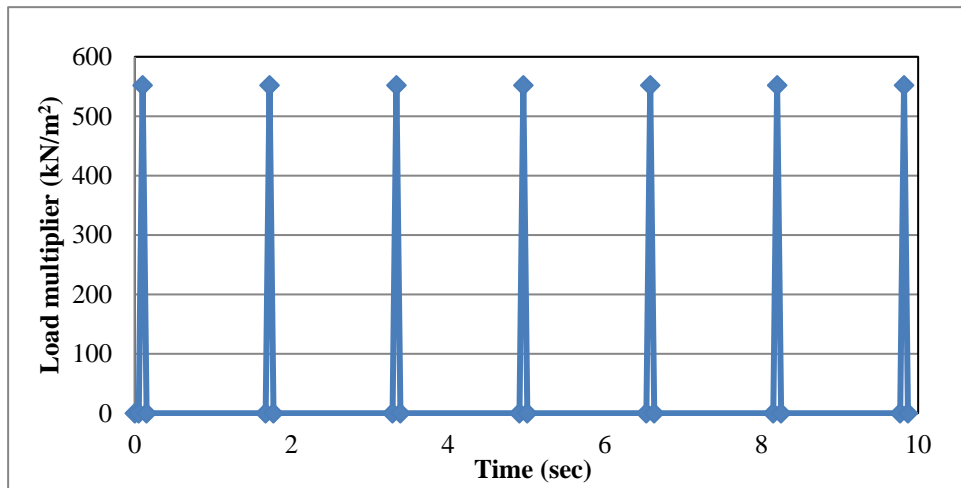
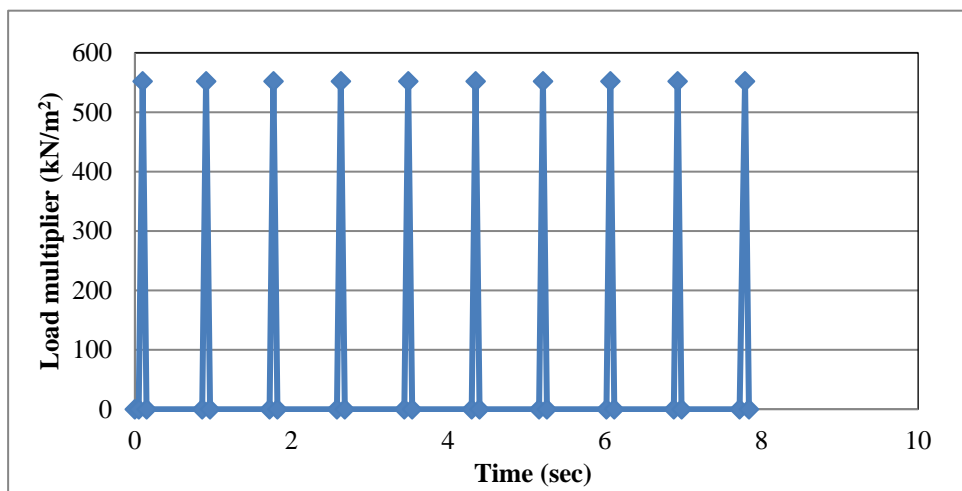Figure 6.8 Dynamic loading wave (speed = 20 km/hr).

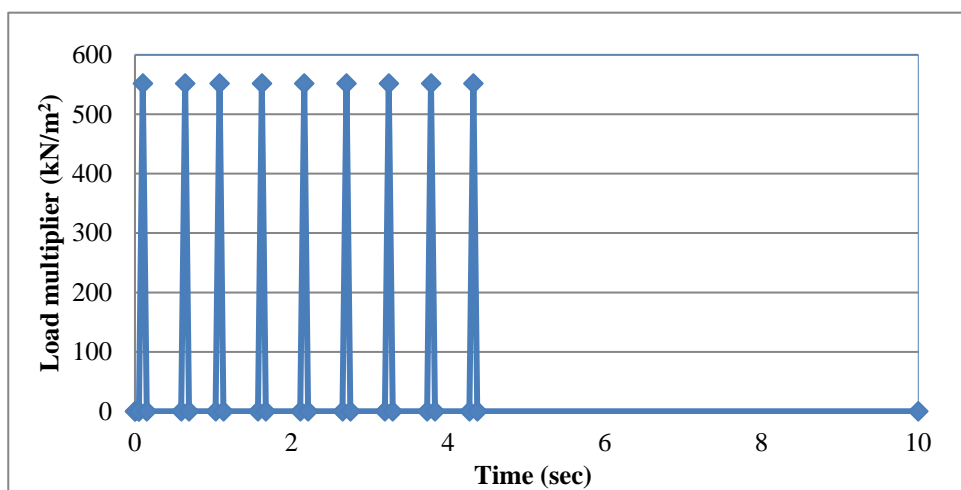Figure 6.9 Dynamic loading wave (speed = 40 km/hr).

Figure 6.10 Dynamic loading wave (speed = 60 km/hr).

Table 6.1 Material properties.

Soil	Sand	Subbase	Asphalt	GRP pipe
Model	Mohr-Coulomb	Mohr-Coulomb	Linear elastic	Plate element
Unit weight $\gamma(kN/m^3)$	17.2	22.06	23.5	15.8
Modulus of elasticity E' (kN/m^2)	35,000	120,000	12,000,000	41,000,000
Angle of internal friction ϕ'' (°)	38	40	-	-
Dilatancy angle ψ (°)	8	10	-	-
Poisson's ratio	0.3	0.35	0.3	0.159

6.4 Results of the Parametric Study

6.4.1 Crown displacement

Table (6.1) and Figures (6.11) to (6.19) present the results for crown displacement. When the pipe diameter is (600) mm and when using the geocell reinforcement, the crown displacement decreases by 75 % for all vehicle speeds.

When increasing the pipe diameter to (800) and (1000) mm. respectively, the percentage of decrement becomes 72%.

Table 6.2 Results of crown displacement for the parametric study.

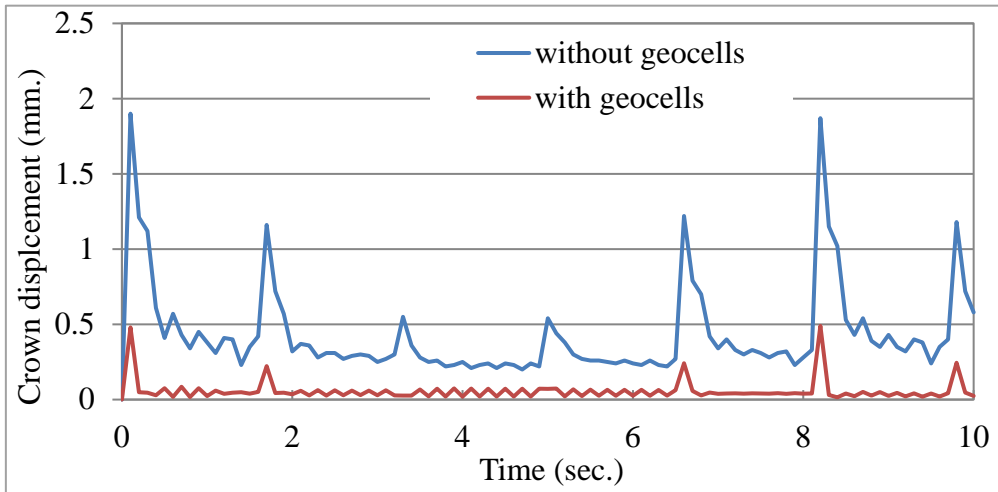| Pipe diameter (mm)	Crown displacement (mm)						Reduction percentage		
	With geocells			Without geocells					
	20 km/hr.	40 km/hr.	60 km/hr.	20 km/hr.	40 km/hr.	60 km/hr.	20 km/hr.	40 km/hr.	60 km/hr.
600	0.48	0.48	0.48	1.9	1.9	1.9	74.74%	74.74%	74.74%
800	0.46	0.46	0.46	1.64	1.64	1.64	71.95%	71.95%	71.95%
1000	0.41	0.41	0.41	1.46	1.46	1.46	71.92%	71.92%	71.92%

Figure 6.11 Crown displacement versus time when (D=600 mm, S=20 km/hr).

Figure 6.12 Crown displacement versus time when (D=600 mm, S=40 km/hr).

Figure 6.13 Crown displacement versus time when (D=600 mm, S=60 km/hr).

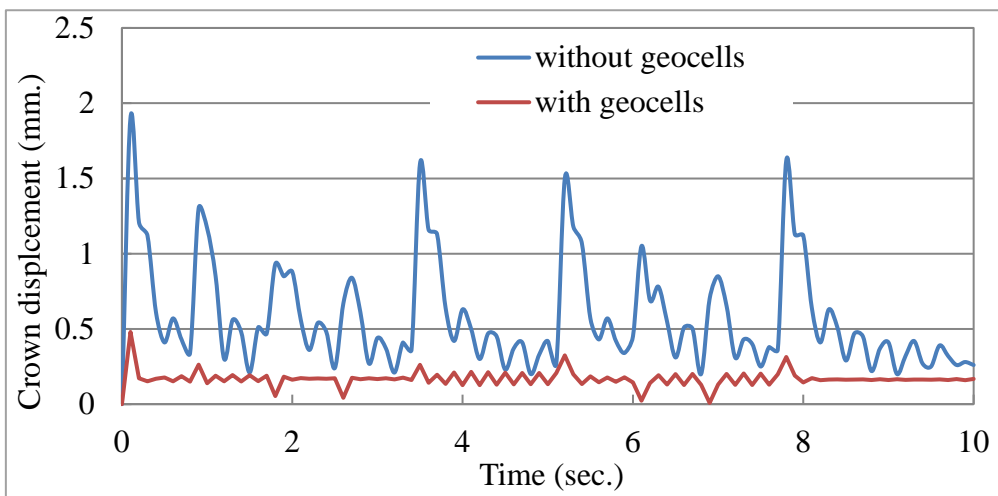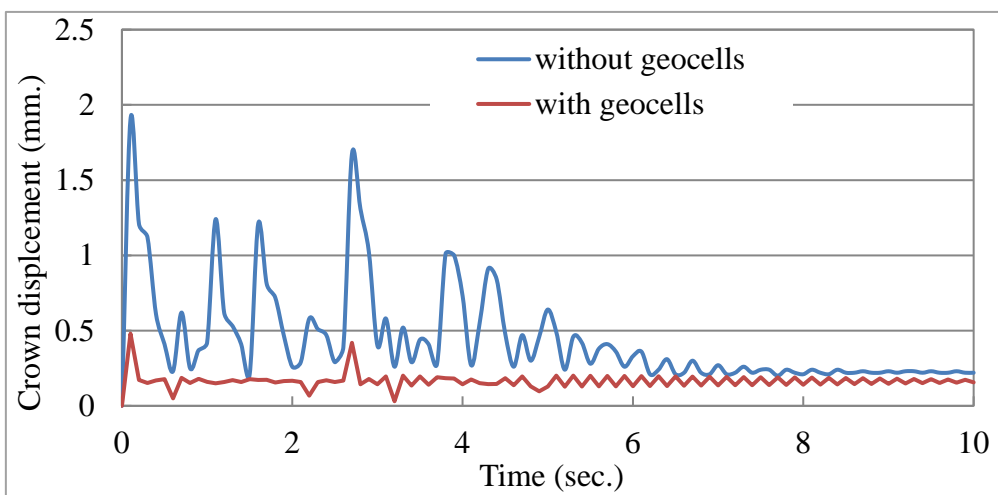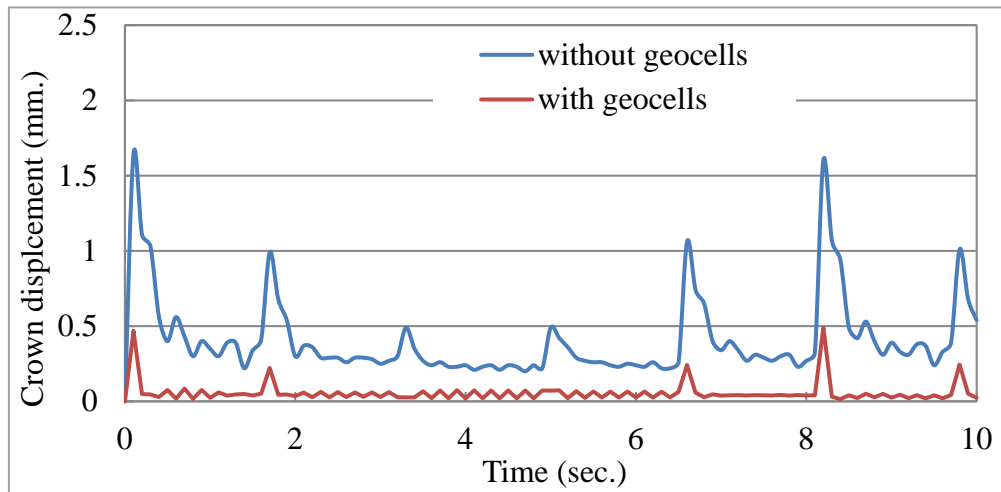Figure 6.14 Crown displacement versus time when (D=800 mm, S=20 km/hr).

Figure 6.15 Crown displacement versus time when (D=800 mm, S=40 km/hr).

Figure 6.16 Crown displacement versus time when (D=800 mm, S=60 km/hr).

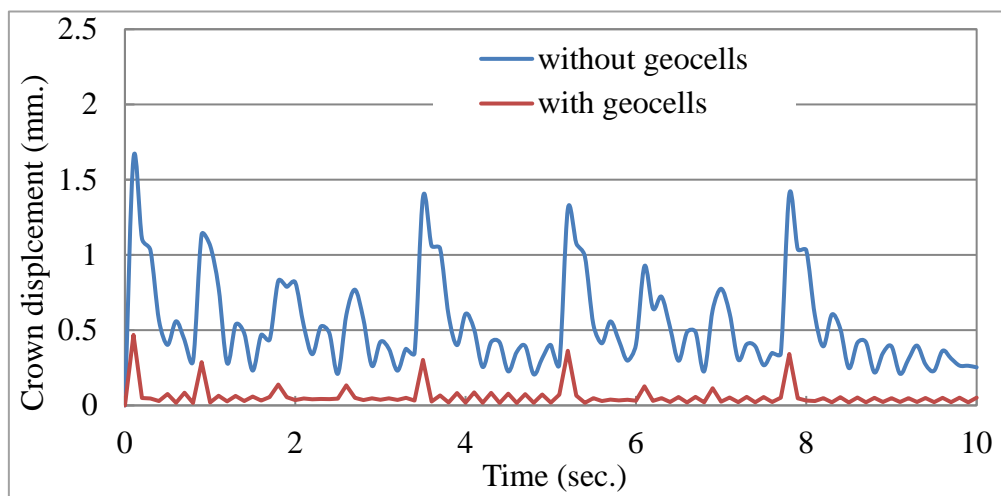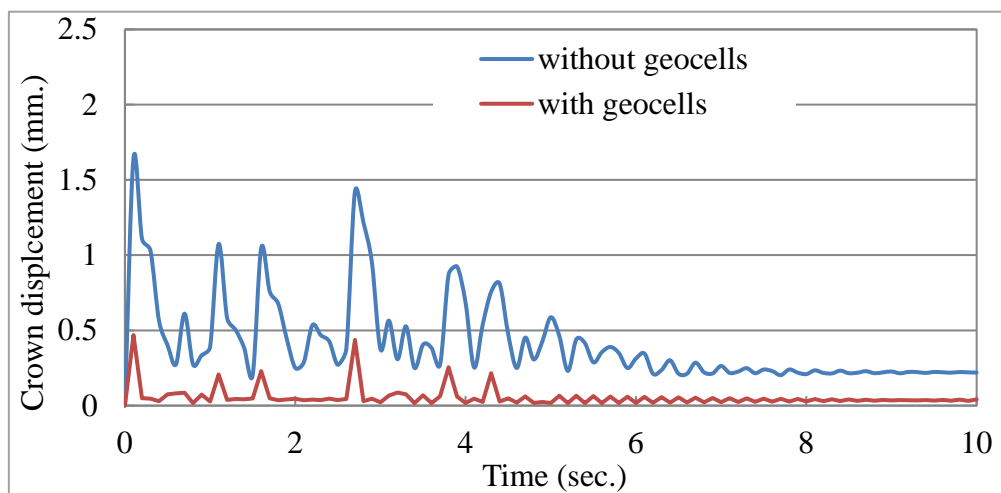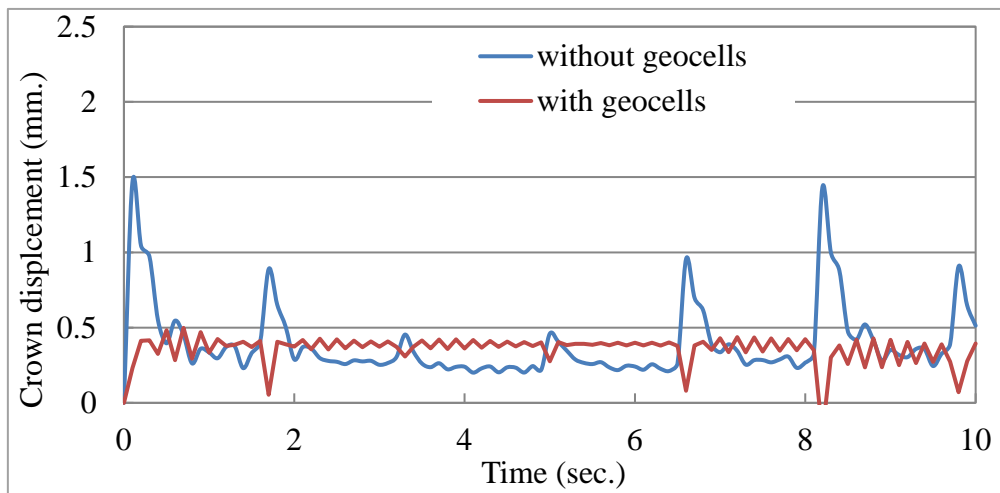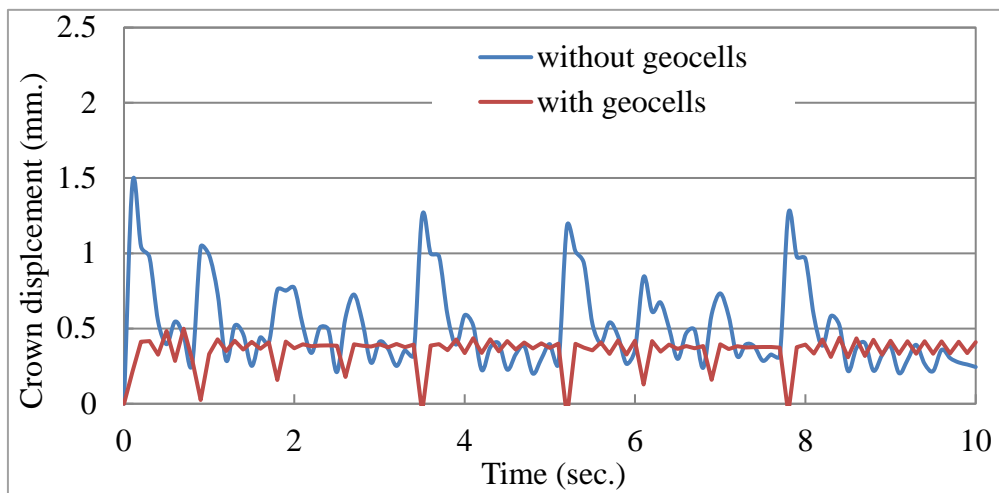Figure 6.17 Crown displacement versus time when (D=1000 mm, S=20 km/hr).

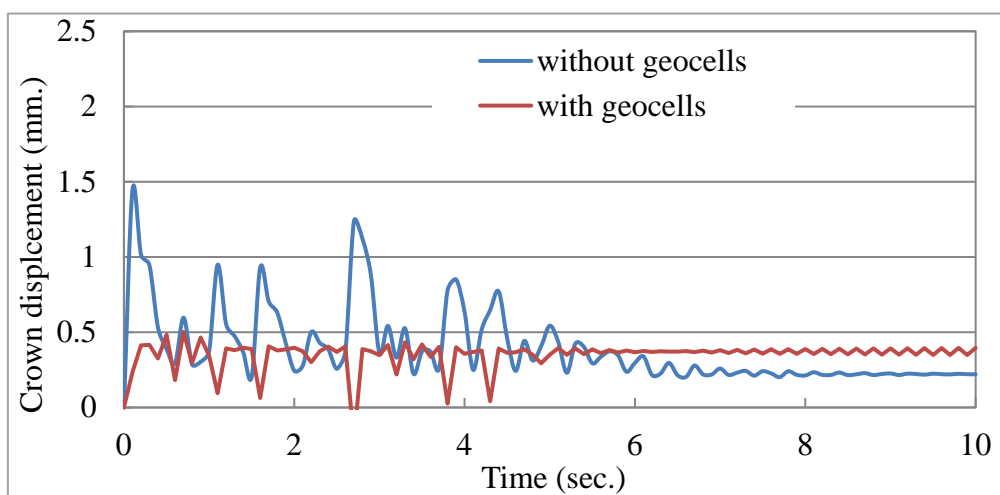Figure 6.18 Crown displacement versus time when (D=1000 mm, S=40 km/hr).

Figure 6.19 Crown displacement versus time when (D=1000 mm, S=60 km/hr).

6.4.2 Surface settlement

Table (6.3) and Figures (6.20) to (6.28) present the results for surface settlement. When the pipe diameter is (600) mm and when using the geocell reinforcement, the surface settlement decreases by 51% when the speed of vehicle is (20) km/hr. This value stays the same for the other vehicle speeds. Changing the pipe diameter to 800 and 1000 mm increases the reduction percentage to 53% and 54% respectively.

Table 6.2 Results of surface settlement for the parametric study

Pipe diameter (mm)	Surface settlement (mm)						Reduction percentage		
	With geocells			Without geocells					
	20 km/hr.	40 km/hr.	60 km/hr.	20 km/hr.	40 km/hr.	60 km/hr.	20 km/hr.	40 km/hr.	60 km/hr.
600	1.75	1.75	1.75	3.57	3.57	3.57	50.98%	50.98%	50.98%
800	1.71	1.71	1.71	3.63	3.63	3.63	52.89%	52.89%	52.89%
1000	1.69	1.69	1.69	3.66	3.66	3.66	53.83%	53.83%	53.83%

Figure 6.20 Surface settlement versus time when (D=600 mm, S=20 km/hr).

Figure 6.21 Surface settlement versus time when (D=600 mm, S=40 km/hr).

Figure 6.22 Surface settlement versus time when (D=600 mm, S=60 km/hr).

Figure 6.23 Surface settlement versus time when (D=800 mm, S=20 km/hr).

Figure 6.24 Surface settlement versus time when (D=800 mm, S=40 km/hr).

Figure 6.25 Surface settlement versus time when (D=800 mm, S=60 km/hr).

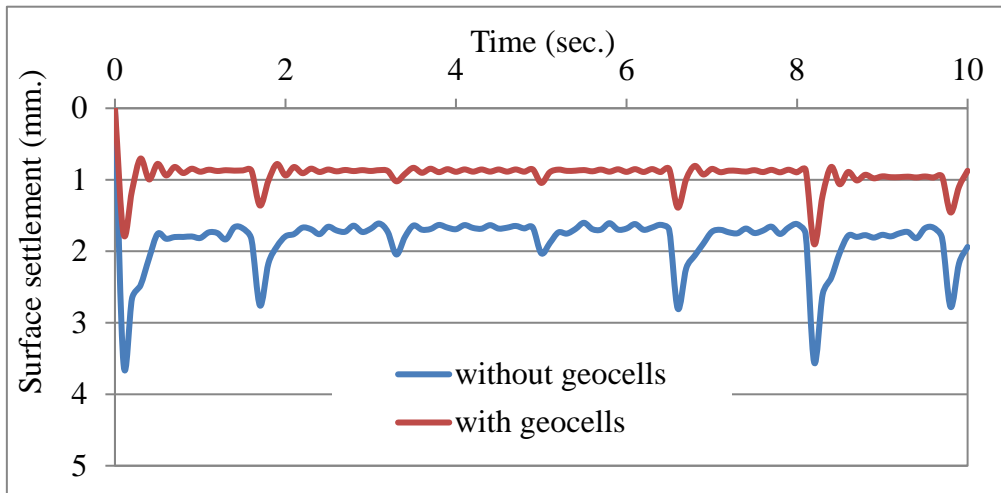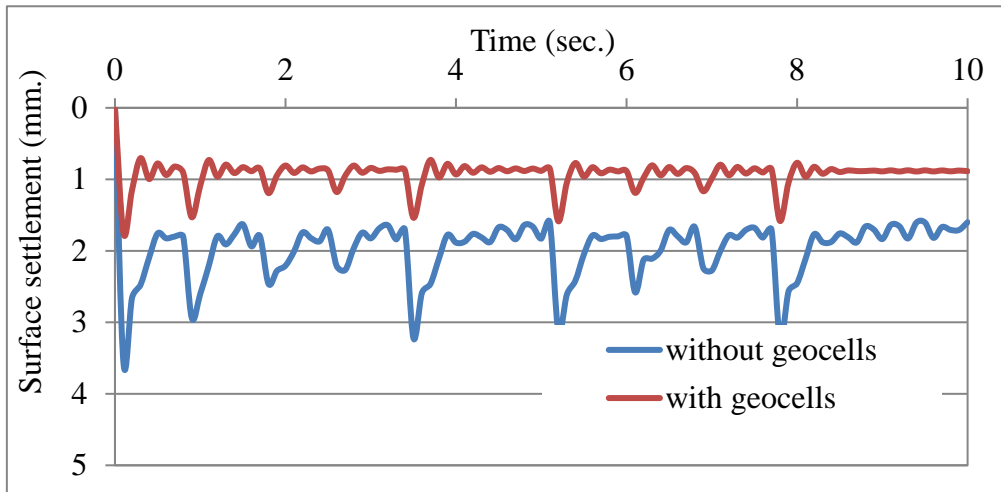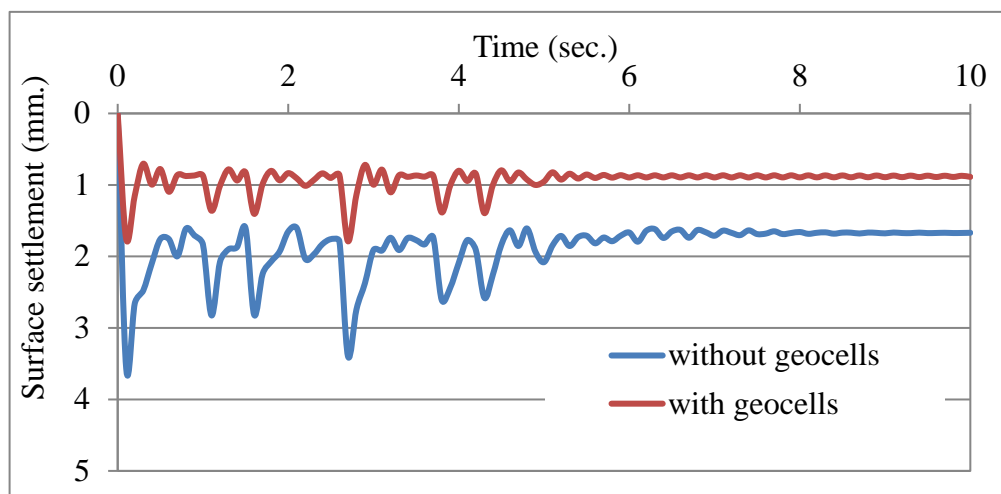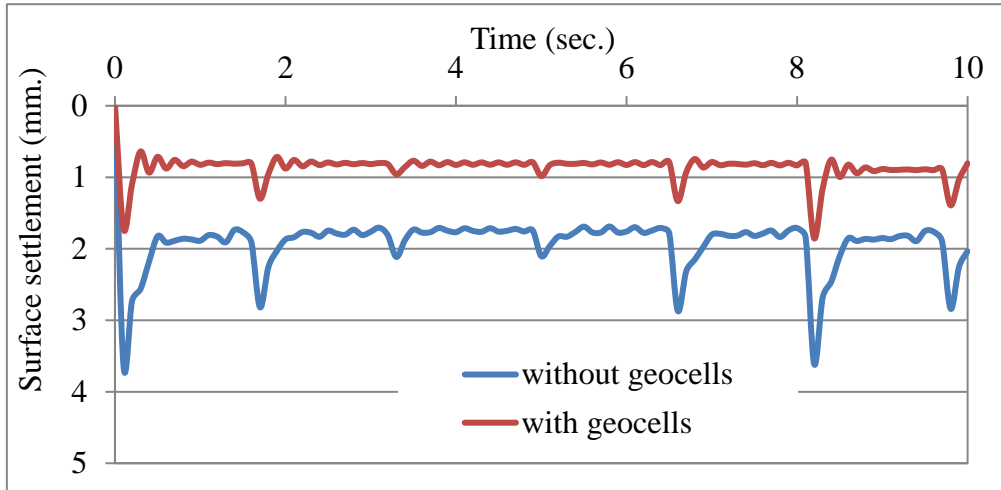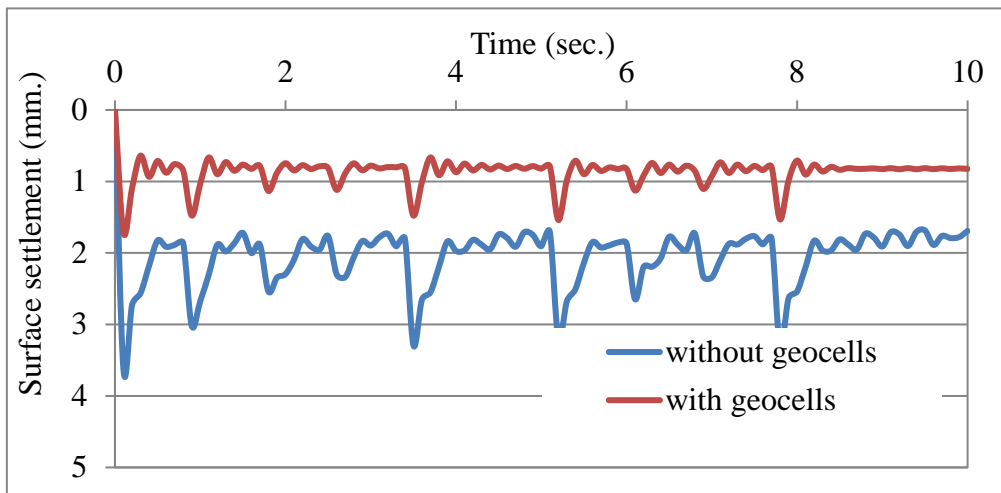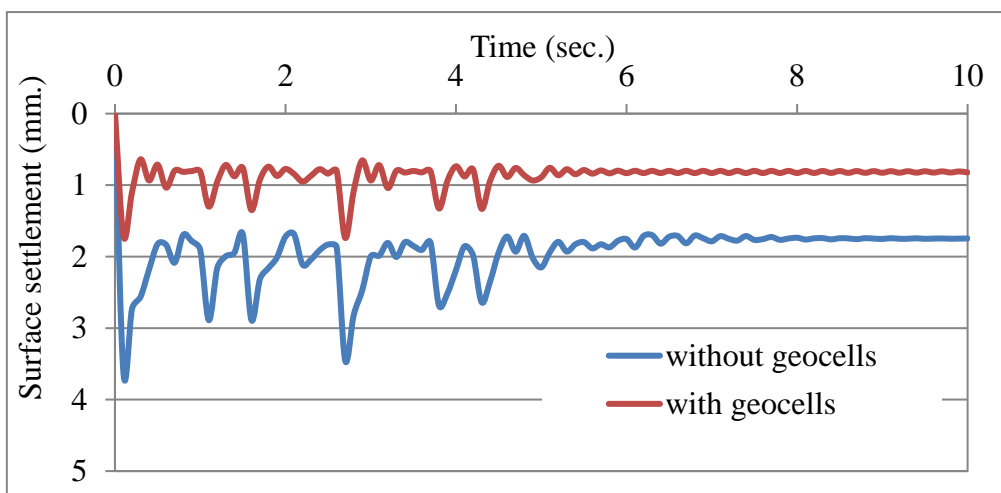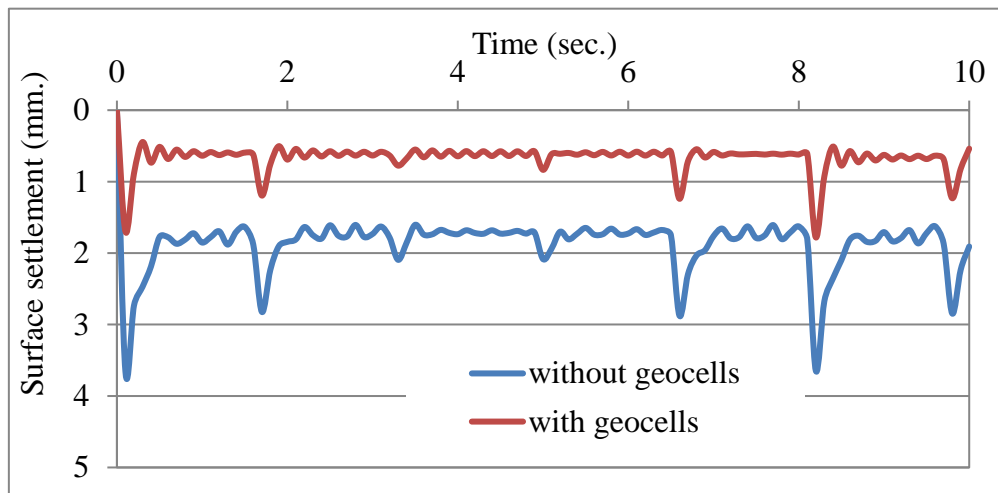Figure 6.26 Surface settlement versus time when (D=1000 mm, S=20 km/hr).
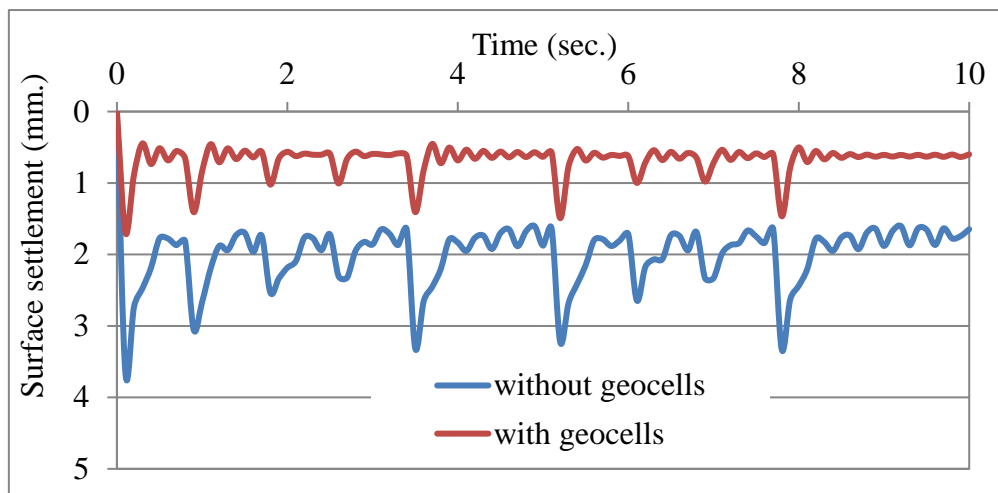
Figure 6.27 Surface settlement versus time when (D=1000 mm, S=40 km/hr).
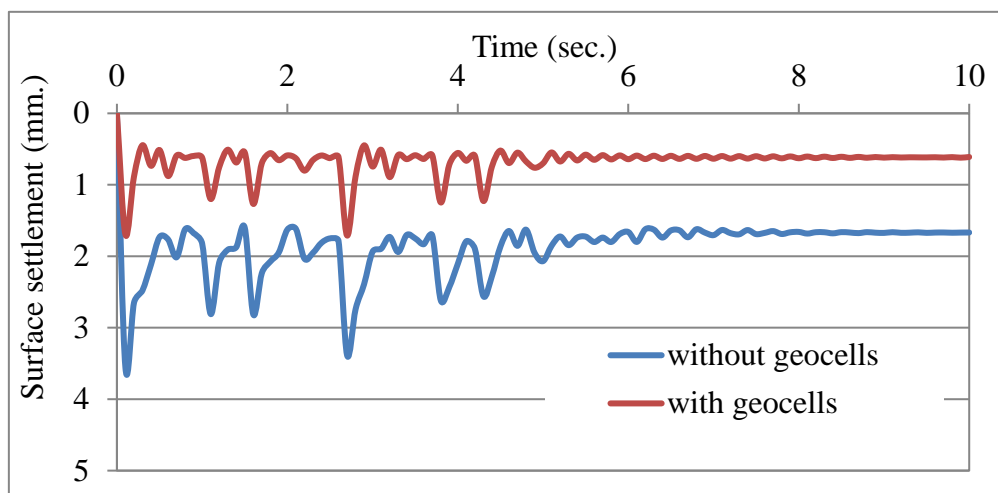
Figure 6.28 Surface settlement versus time when (D=1000 mm, S=60 km/hr).

6.4.3 Vertical pressure

Table (6.4) and Figures (6.29) to (6.37) present the results of vertical stress at the pipe crown. When the pipe diameter is (600) mm, and when using the geocell reinforcement, the vertical pressure decreases by 42% when the speed of the vehicle is (20) km/hr. and by 41 % when the speed of the vehicle is (40) and (60) km/hr.

When the pipe diameter is (800) mm and when using the geocell reinforcement, the percentage becomes (75) % when the speed of the vehicle is (20) km/hr. and (75) % when the speed of the vehicle is (40) km/hr. and (97) % when the speed of the vehicle is (60) km/hr.

When increasing the pipe diameter to (1000) mm and when using the geocell reinforcement, the values of decrement become 43% when the speed of the vehicle is (20) km/hr. and 44 % when the speed of the vehicle is (40) and (60) km/hr.

It can be shown from the results that the value of vertical stress is decreasing when the diameter increases due to the stress being distributed on a wider area.

Table 6.3 Results of vertical pressure at the pipe crown for the parametric study.

| Pipe diameter (mm) | Crown vertical stress (kN/m^2) | | | | | | Reduction percentage | | |
| | With geocells | | | Without geocells | | | | | |
	20 km/hr.	40 km/hr.	60 km/hr.	20 km/hr.	40 km/hr.	60 km/hr.	20 km/hr.	40 km/hr.	60 km/hr.
600	25.26	25.78	25.78	43.76	43.76	43.76	42.28%	41.09%	41.09%
800	22.74	22.47	22.46	40.22	40.12	40.06	43.46%	43.99%	43.93%
1000	14.08	14.08	14.08	32.5	32.5	32.5	56.68%	56.68%	56.68%

Figure 6.29 Vertical pressure versus time when (D=600 mm, S=20 km/hr).

Figure 6.30 Vertical pressure versus time when (D=600 mm, S=40 km/hr).

Figure 6.31 Vertical pressure versus time when (D=600 mm, S=60 km/hr).

Figure 6.32 Vertical pressure versus time when (D=800 mm, S=20 km/hr).

Figure 6.33 Vertical pressure versus time when (D=800 mm, S=40 km/hr).
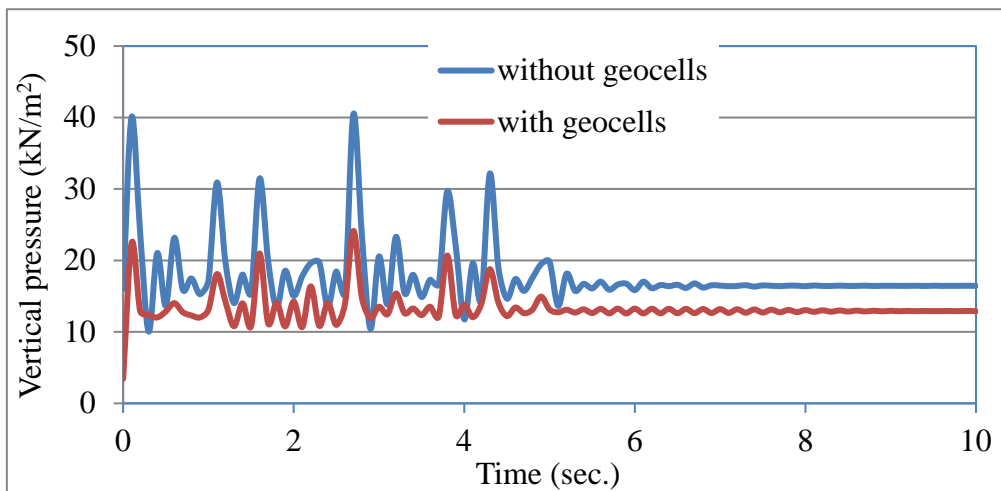
Figure 6.34 Vertical pressure versus time when (D=800 mm, S=60 km/hr).
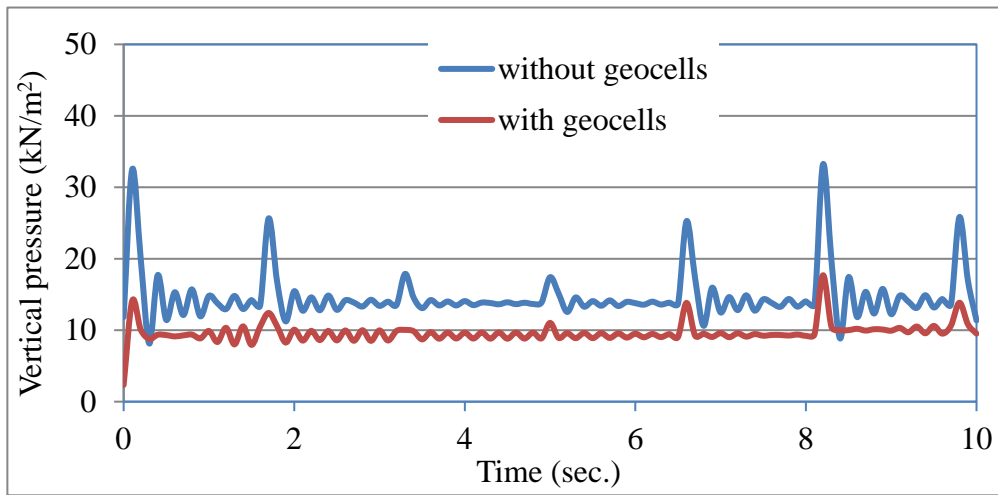
Figure 6.35 Vertical pressure versus time when (D=1000 mm, S=20 km/hr).
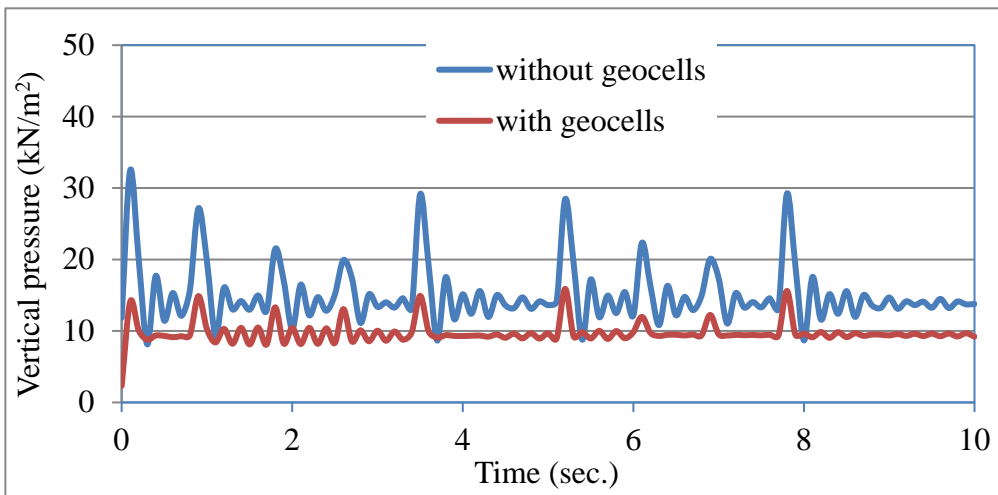
Figure 6.36 Vertical pressure versus time when (D=1000 mm, S=40 km/hr).
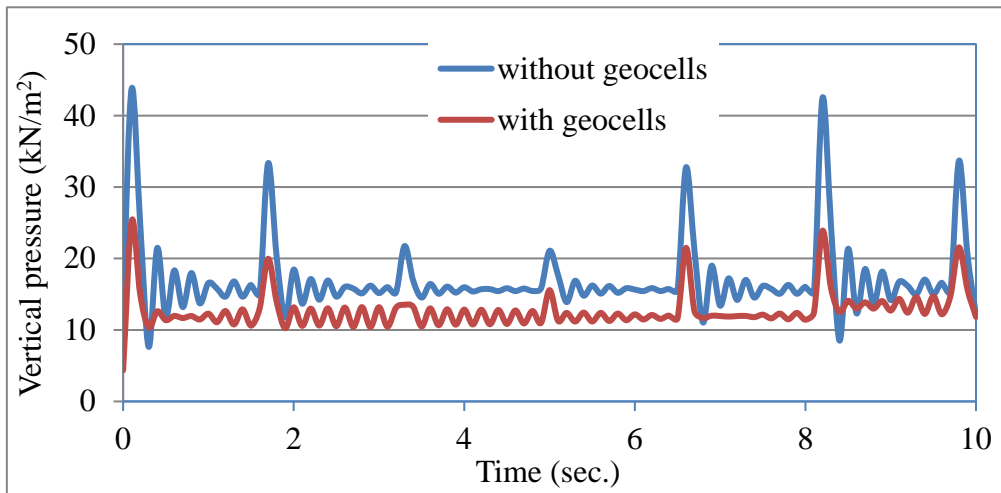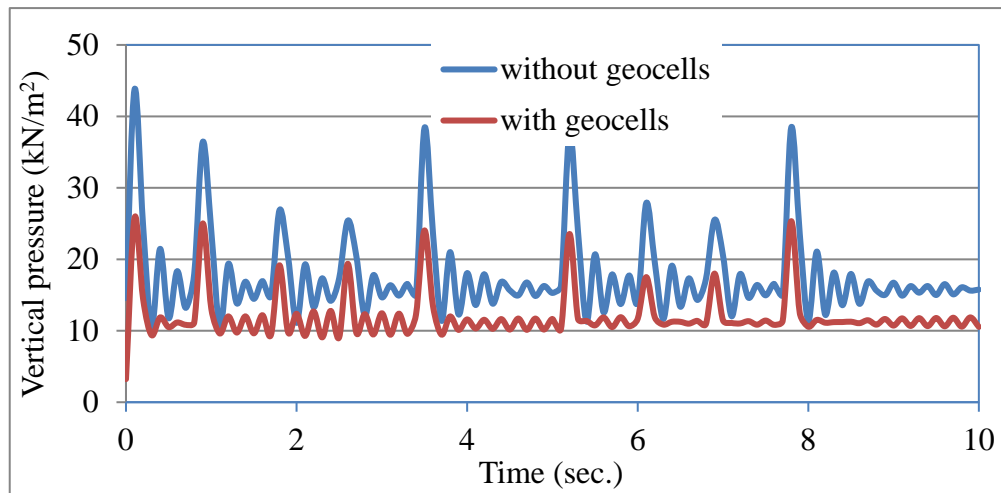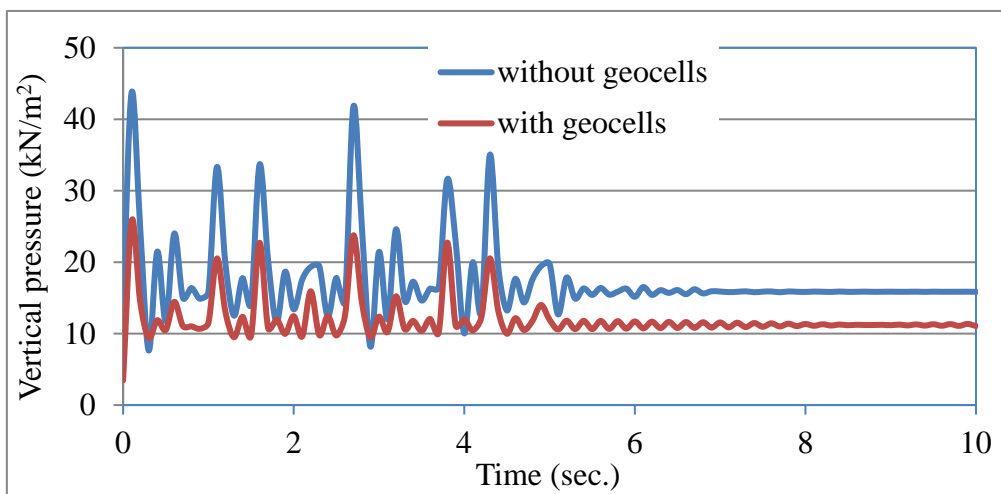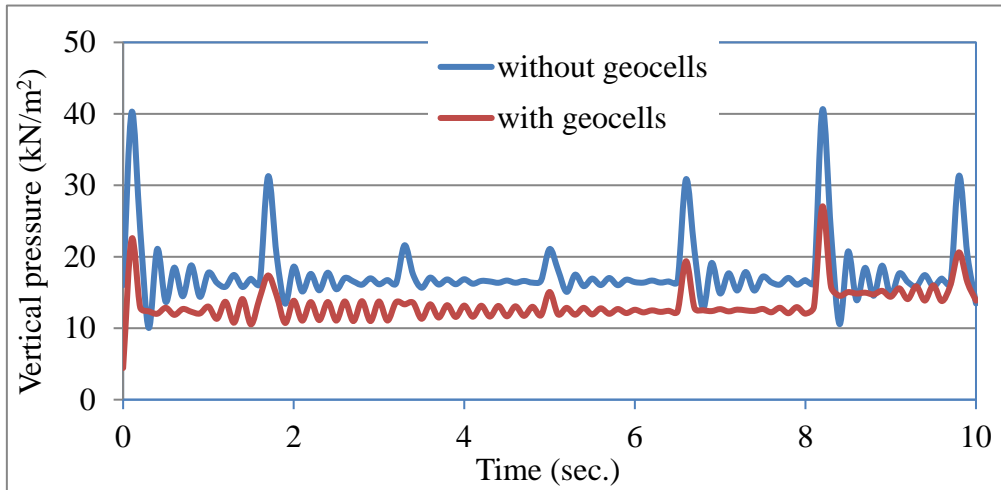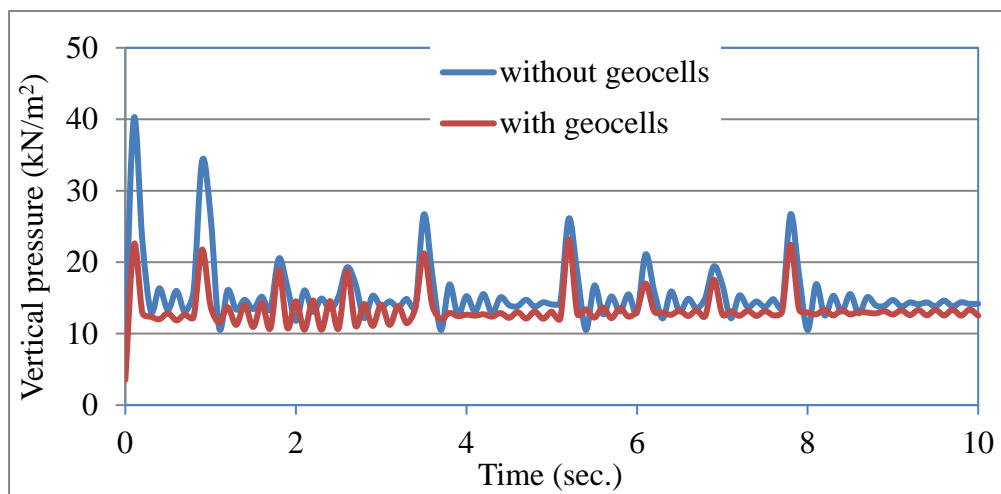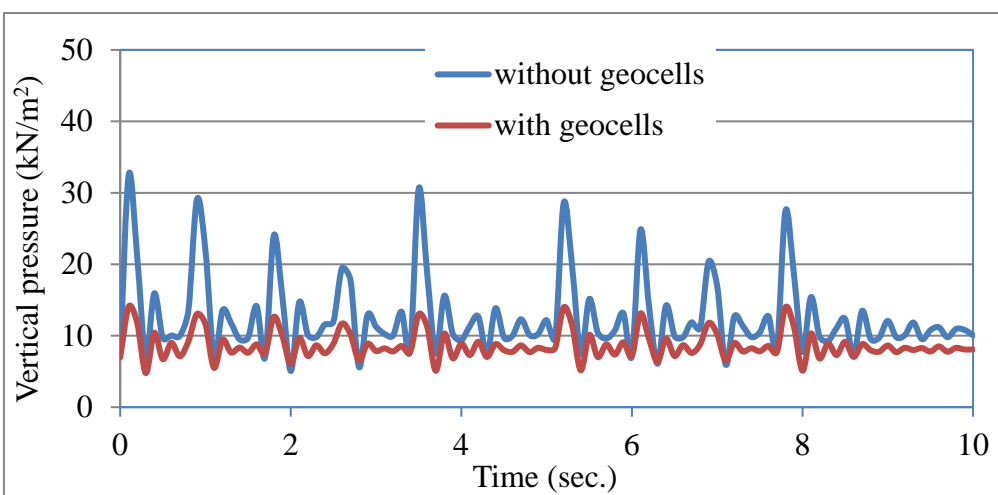

Figure 6.37 Vertical pressure versus time when (D=1000 mm, S=60 km/hr).

6.5 Contours of displacement and stress

Distribution of total displacements in ux, uy, and uz are illustrated in Figures (6.38), (6.39), and (6.40), respectively. It can be noticed that the maximum displacement occurs directly under the surface loading area. Figure (6.41) shows the contours of the cartesian strain ε_{xx}, Figures (6.42) to (6.45) present principal effective stresses σ_1, σ_2, σ_3 and the relative shear stress τ_{rel}. The deformed mesh of the model and the pipe deformation at the maximum applied loading are shown in Figures (6.46) and (6.47), respectively. It can be noted that all the figures are selected arbitrarily when the geocell reinforcement is inserted and (speed = 40 km/hr, D = 800 mm).

It is clear that the major principal stress from the FEA was the highest below the edge of the loading plate and adjacent to the center of the loading plate. The stress concentration from the edge of the loading plate headed towards the quarter point of the pipe. Such a pattern of stress development could be expected of granular soil, which is conducive to arching. The crown of the pipe, having deflected significantly has shed load to neighboring pipe sections.

The arching effect does not take into consideration the effect of friction of the backfill material on the pipe's surface. The arching effect is related to the relative movement of the backfill directly above the pipe with respect to the soil on both sides of the trench. The rigidity of the pipe and the density of the backfill have a considerable effect on the arching. For instance, a loose soil placed above the pipe will settle more than the side fills. The friction between the sides fills and the loose soil will reduce the load applied on the top of the pipe resulting in arching. However, the numerical analysis with interface elements generated greater arching than the analysis without interface elements.

104
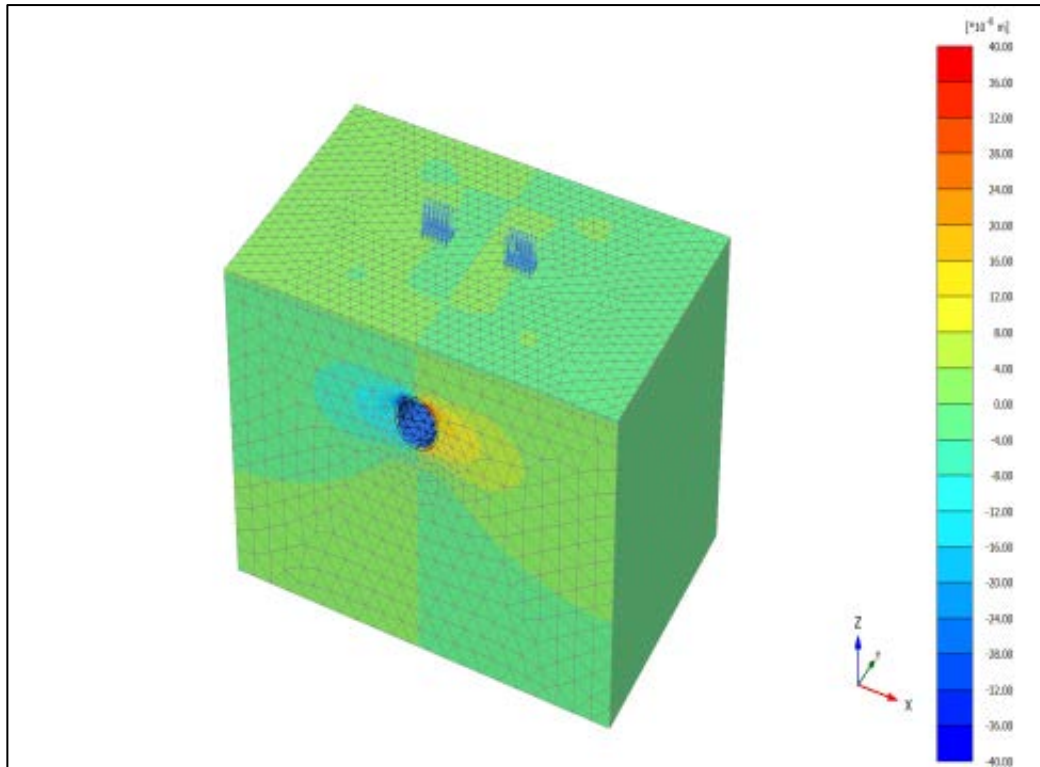
Figure 6.38 Total displacements u_x (m).
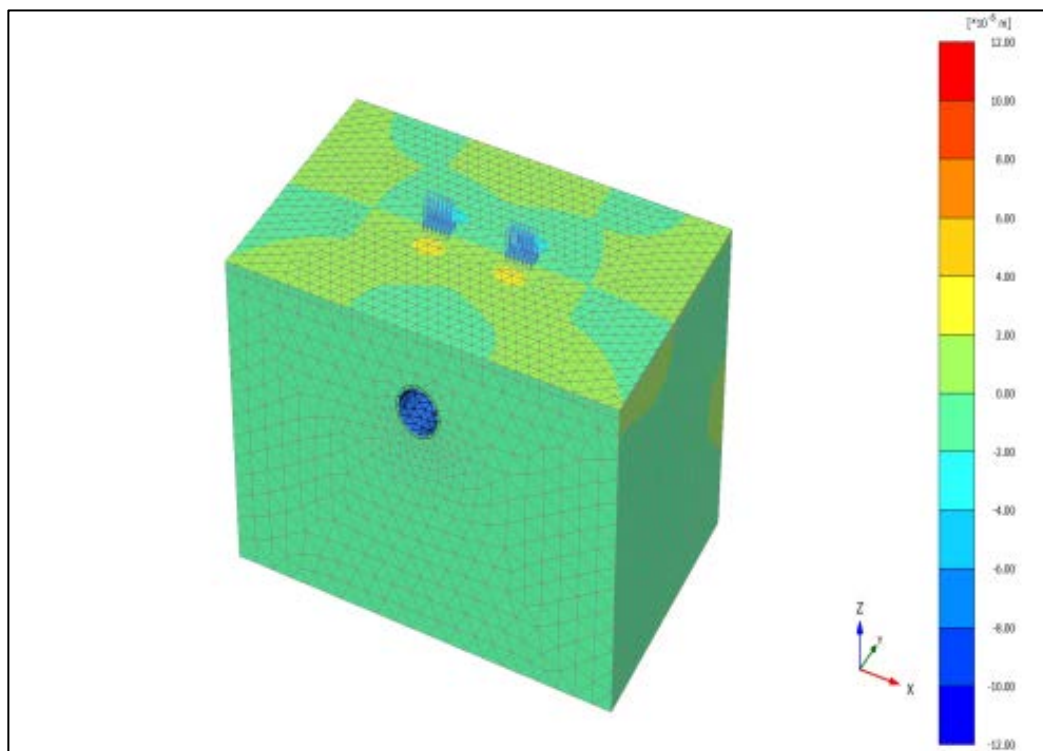
Figure 6.39 Total displacements u_y(m).
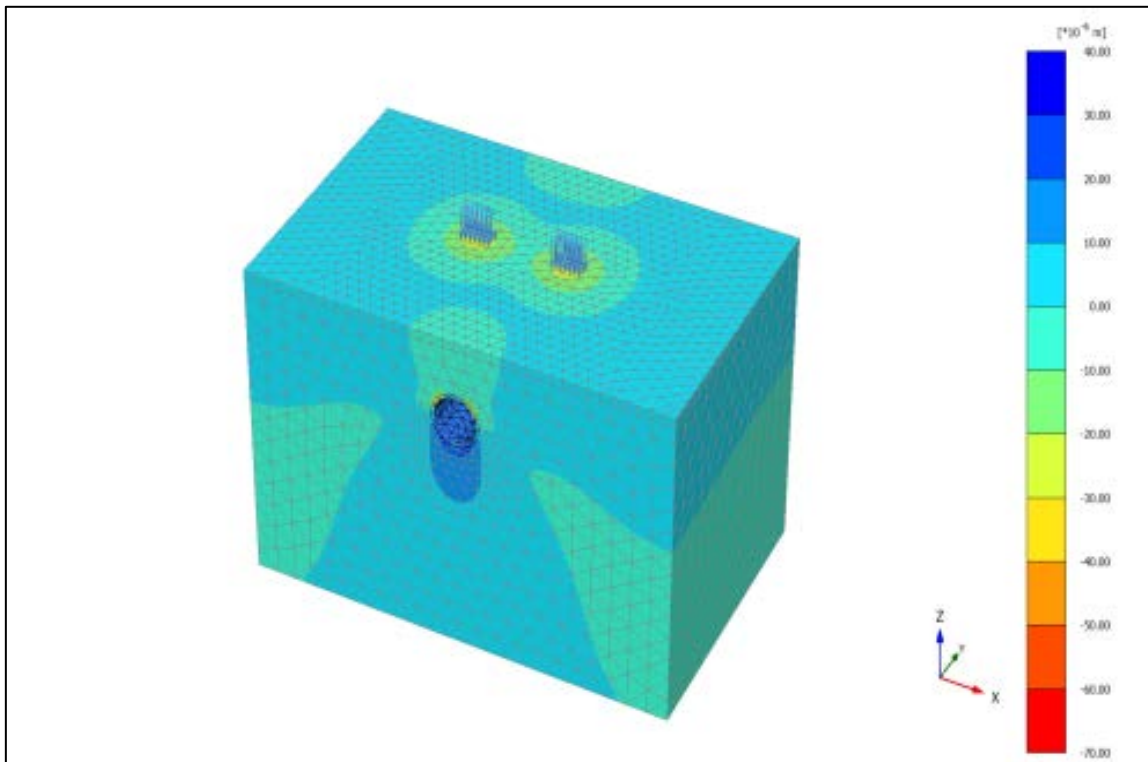
Figure 6.40 Total displacements u_z (m).
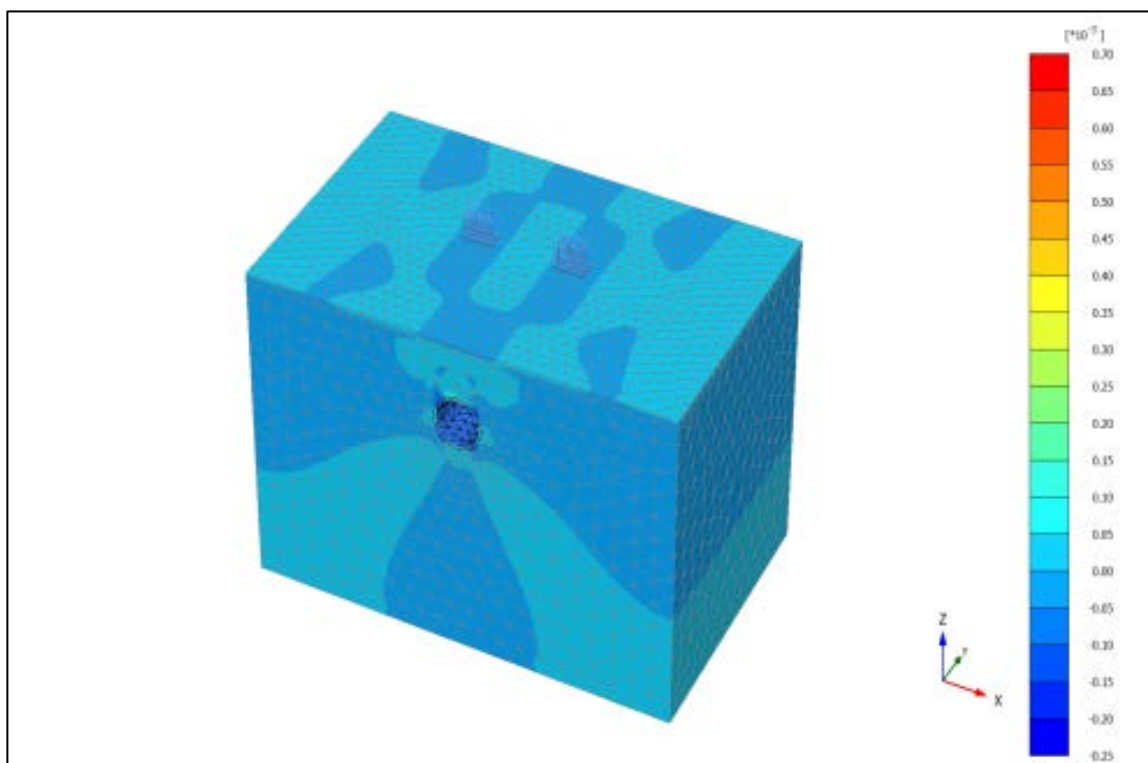
Figure 6.41 Total Cartesian strain ε_{xx}.
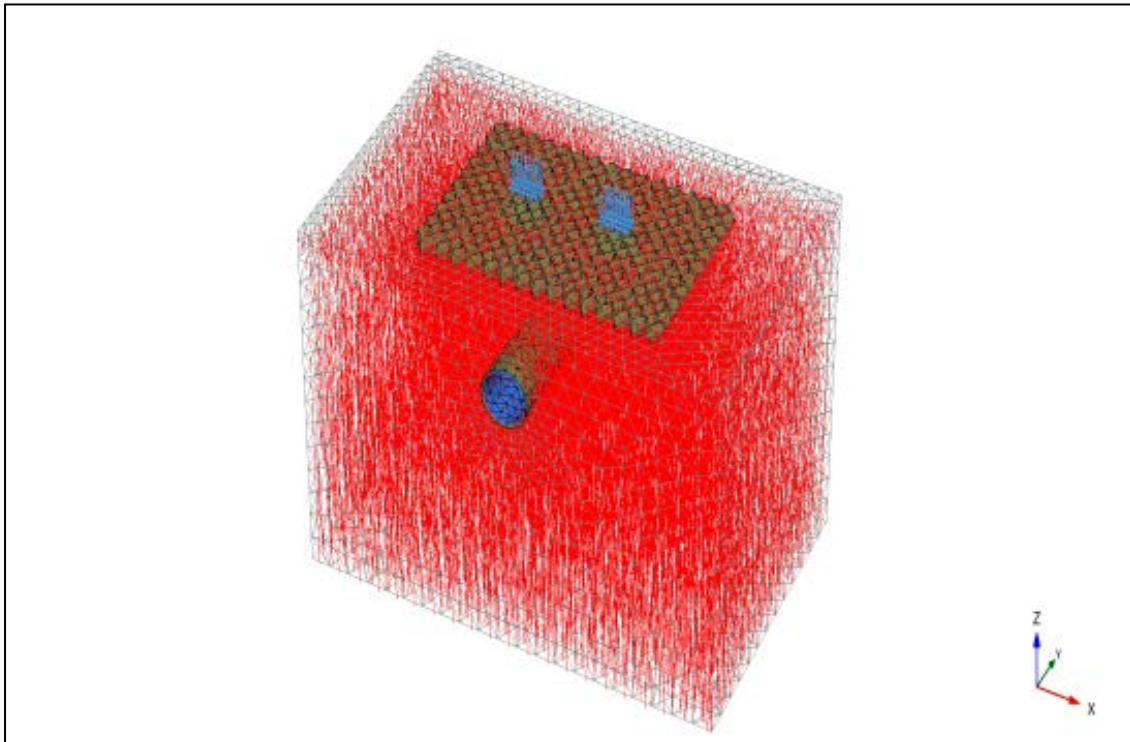
Figure 6.42 Major principal effective stress $\sigma 1$ (kN/m^2).
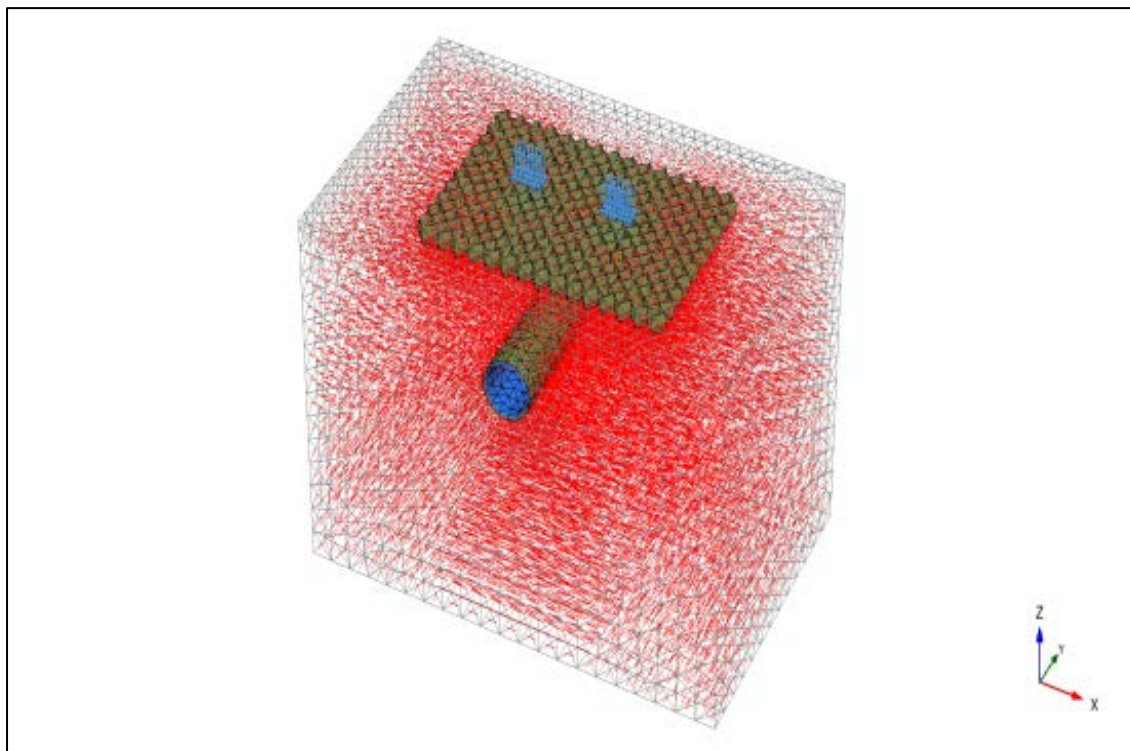
Figure 6.43 Intermediate principal effective stress $\sigma 2$ (kN/m^2).
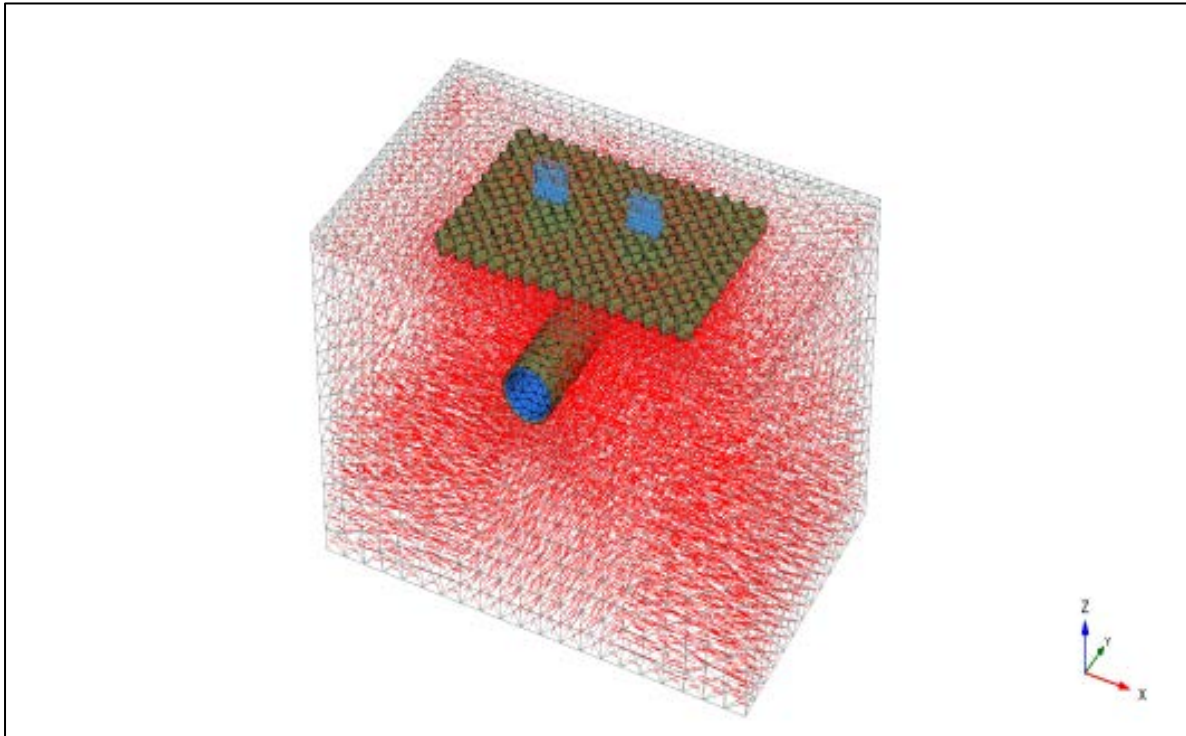
Figure 6.44 Minor principal effective stress σ3 (kN/m^2).
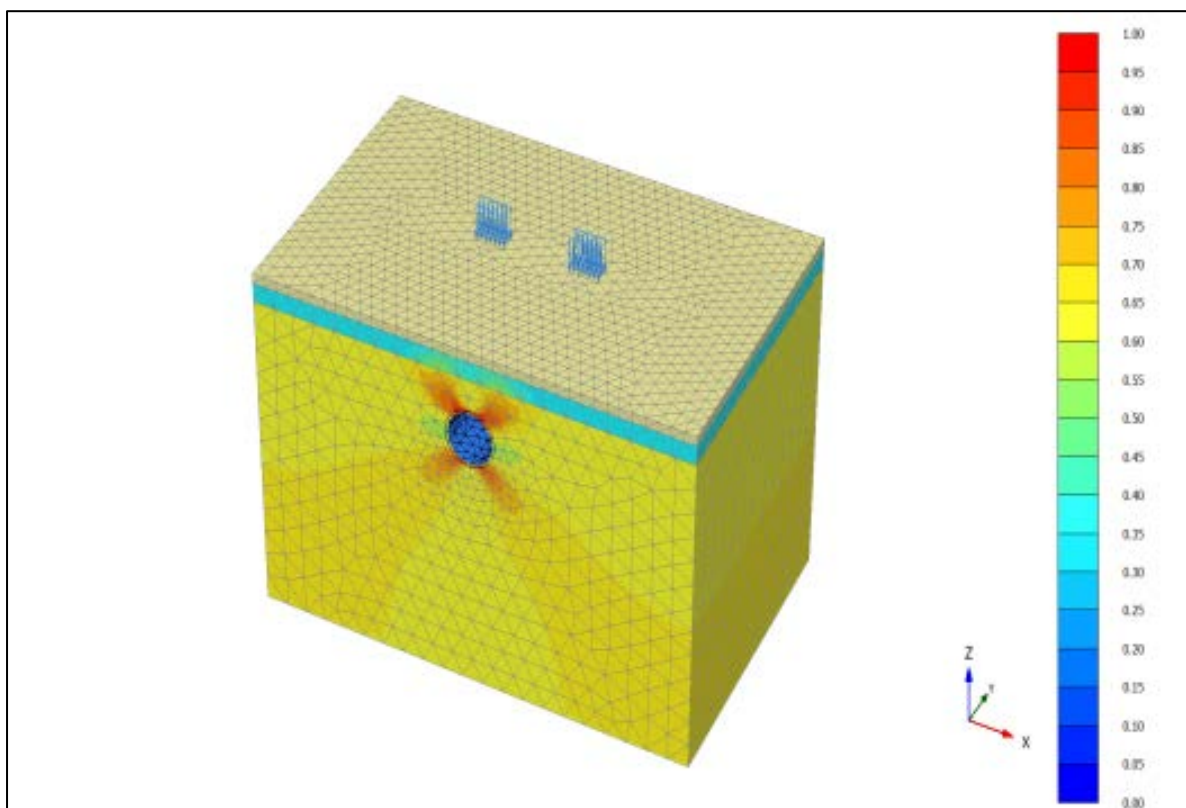
Figure 6.45 Relative shear stress τrel. (kN/m2).
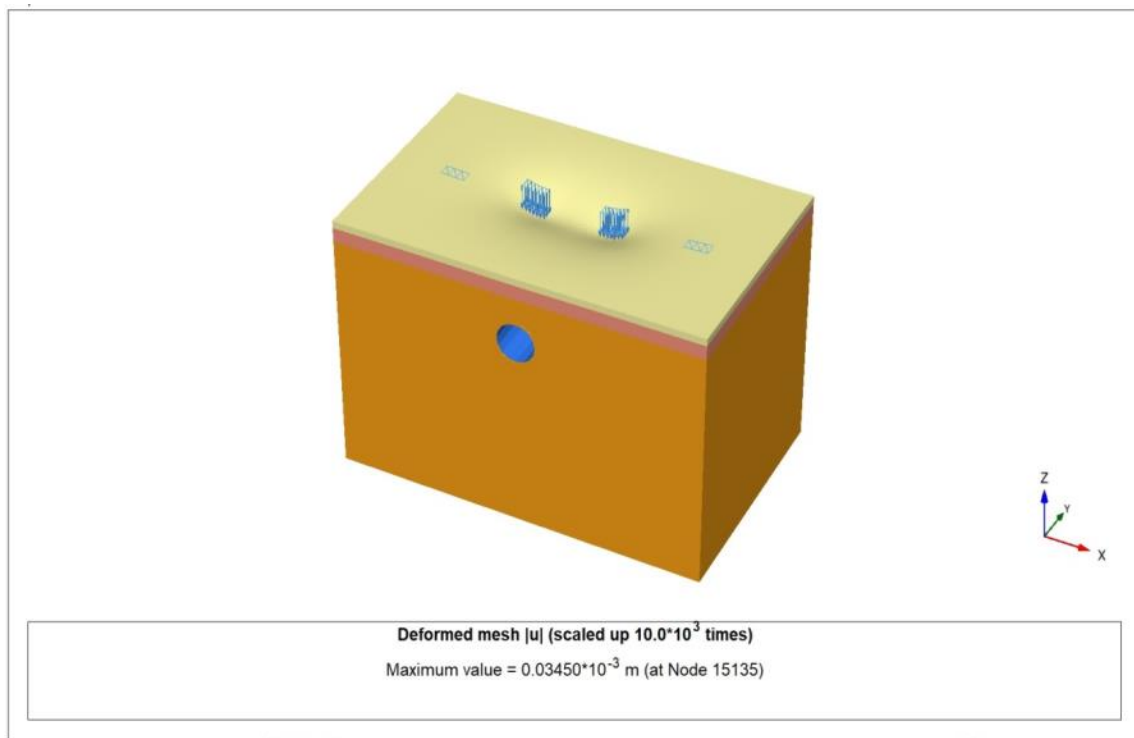
Figure 6.46 Deformed mesh.
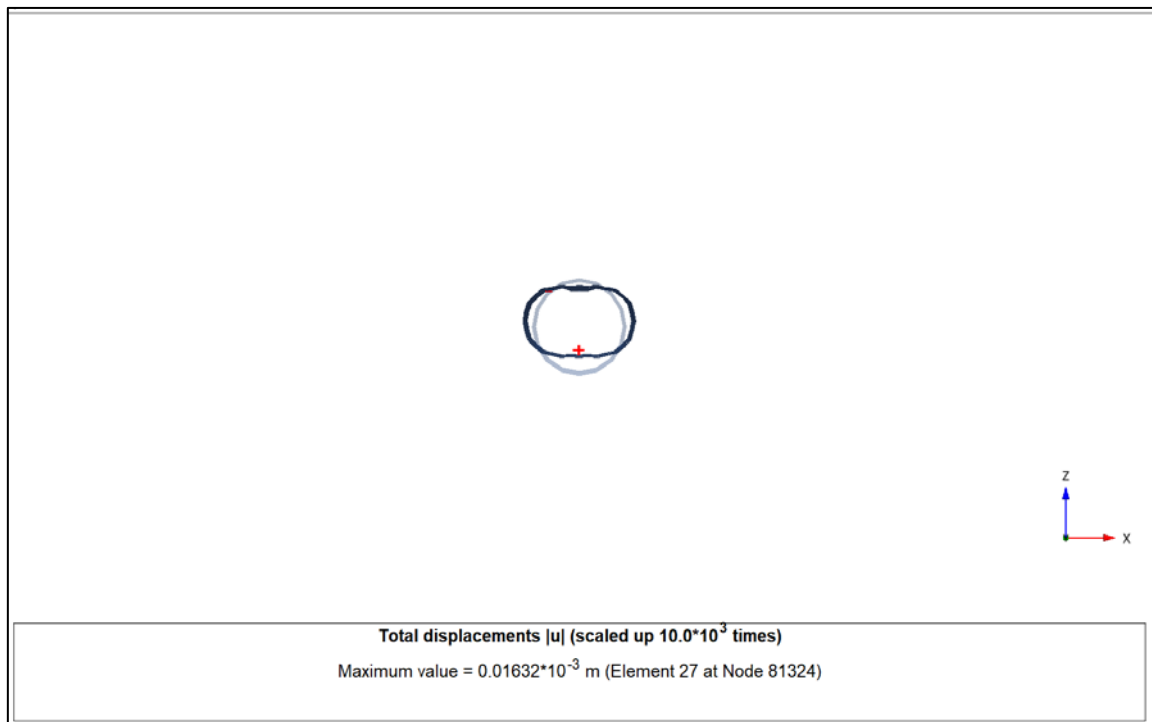
Figure 6.47 Deformed pipe section.

Chapter Seven

Conclusions and Recommendations

7.1 Introduction

The major findings of this study are presented in this chapter, followed by the recommendations for future studies. This study deals with the effect of load frequency, load amplitude and geocell inclusion in subbase layer. A PVC pipe with reasonable dimensions was selected for this study. Two series of tests were conducted with and without the geocell reinforcement, with two different loading amplitudes and three different loading frequencies. The experimental work was then verified by the finite element software PLAXIS 3D.

7.2 Conclusions

7.2.1 Experimental and numerical study

1. Geocell reinforcement greatly improves the performance of buried pipes by reducing the surface settlement, crown displacement and vertical stress above the pipe.

2. The reduction in surface settlement due to geocell reinforcement was about (29 to 43) % when the amplitude of load is (0.5) ton, and this value became (32 to 41) % when the amplitude of load is up to (1) ton.

3. When using geocell reinforcement, the amplitude of crown displacement is reduced by about (25-35) % when the amplitude of load is (0.5) ton and (13-18) % when the amplitude of load is (1) ton.

4. The value of vertical pressure is decreased by about (13-41) % when the load amplitude is 0.5 ton and by about (25-32) % when the load amplitude is 1 ton.

5. The results of numerical modeling were in good agreement with the experimental work, proving that geocell reinforcement can effectively decrease vertical stresses above the pipe crown and the vertical displacement of the pipe crown. This increases the safety of pipes exposed to dynamic loads from vehicles.

6. Viscous boundaries are not applicable in buried pipes problems since they move the boundary horizontally and thus, produce false results.

7. The results of numerical simulation showed that the maximum percentage of error between experimental work and numerical simulation in terms of surface settlement is about 10%.

8. The results of numerical simulation showed that the maximum percentage of error between experimental work and numerical simulation in terms of crown displacement is about 11%.

9. The results of numerical simulation showed that the maximum percentage of error between experimental work and numerical simulation in terms vertical pressure above the crown is about 6%.

7.2.2 Parametric study

1. The value of vertical stress is decreased when the diameter increases due to the stress being distributed on a wider area.

2. Vehicle speed has no significant effect on buried pipes

3. Using the geocell reinforcement decreases the surface settlement by 51% to 54%.

4. Using the geocell reinforcement decreases the pipe crown displacement by 42% to 56%

5. Using the geocell reinforcement decreases the vertical pressure above the pipe by 72% to 75%.

7.3 Recommendations for Future Work

1. It is recommended to consider different pipe materials.

2. Using multiple geocells layers instead of only one.

3. Taking into consideration the effect of water table, and study the generation of pore water pressure and effective stresses in saturated soils.

References

- AASHTO, L. 1998. "Bridge design specifications" *, American Association of State Highway and Transportation Officials*, Washington, DC.

- Abd Al-Kaream, K. W. 2013, "The Dynamic Behavior of Machine Foundation on Saturated Sand", M.Sc. Thesis, *Building and Construction Engineering Department, University of Technology*, Iraq.

- Al-Ameri, A. F. I. 2014, "Transient and Steady State Response Analysis of Soil Foundation System Acted Upon by Vibration", Ph.D. Thesis, *College of Engineering, Civil Engineering Department, University of Baghdad*, Iraq.

- Andreasen, M.M.,1991. Design methodology. *Journal of Engineering Design*, 2(4), pp.321-335.

- American Society of Testing and Materials (ASTM) 2006. "Standard Test Method for Specific Gravity of Soil Solids by Water Pycnometer" *ASTM D854*, West Conshohocken, Pennsylvania, USA.

- American Society of Testing and Materials (ASTM) (2006). "Standard Test Method for Particle Size-Analysis of Soils" *ASTM D422-63*, West Conshohocken, Pennsylvania, USA.

- American Society of Testing and Materials (ASTM) (2006). "Standard Test Method for Maximum Index Density and Unit Weight of Soils Using a Vibratory Table" *ASTM D4253-00*, West Conshohocken, Pennsylvania, USA.

- American Society of Testing and Materials (ASTM) (2006). "Standard Test Method for Minimum Index Density and Unit Weight of Soils and Calculation of Relative Density" *ASTM D4254-00*, West Conshohocken, Pennsylvania, USA.

- American Society of Testing and Materials (ASTM) (2006). "Standard Test Method for Direct Shear Test of Soils under Consolidated Drained Conditions" *ASTM D3080*, West Conshohocken, Pennsylvania, USA.

- American Society of Testing and Materials (ASTM) (2006). "Standard Test Method for Permeability of Granular Soils (Constant Head)" *ASTM D2434-68*, West Conshohocken, Pennsylvania, USA.

- American Society of Testing and Materials (ASTM) (2006). "Standard Test Method for Classification of Soils for Engineering Purposes (Unified Soil

Classification System)" *ASTM D2487-06*, West Conshohocken, Pennsylvania, USA.

- American Society of Testing and Materials (ASTM) (2008). "Standard Practice for Underground Installation of Thermoplastic Pipe for Sewers and Other Gravity-Flow Applications" *ASTM D2321-08*, West Conshohocken, Pennsylvania, USA.

- American Society of Testing and Materials (ASTM) (2008). "Standard Test Method for Determining Tensile Properties of Geogrids by the Single or Multi-Rib Tensile Method" *ASTM D6637*, West Conshohocken, Pennsylvania, USA.

- Berg, R. and Anderson, R.2009. "Silver anniversary: the Tanque Verde retaining walls". In *Geosynthetics* (Vol. 27, No. 5, p. 32).

- Berg, R.R., Christopher, B.R. and Perkins, S., 2000. Geosynthetic reinforcement of the aggregate base/subbase courses of pavement structures (No. *GMA White Paper* II).

- Boushehrian, A.H., Hataf, N. and Ghahramani, A., 2011. Modeling of the cyclic behavior of shallow foundations resting on geomesh and grid-anchor reinforced sand. *Geotextiles and Geomembranes*, 29(3), pp.242-248.

- Brinkgreve, Ronald B. J.; Bürg, Markus; Andreykiv, A.; Lim, Liang J. 2015 "Beyond the Finite Element Method in Geotechnical Analysis". In: *BAWMitteilungen 98. Karlsruhe: Bundesanstalt für Wasserbau (BAW)*. S. 91-102.

- British Standard Institute Plastics pipework (thermoplastics materials): Code of practice for the installation of unplasticized PVC pipework for gravity drains and sewers, BS 5955, 1980.Consoli, N.C., Vendruscolo, M.A., Fonini, A. and Dalla Rosa, F., 2009. "Fiber reinforcement effects on sand considering a wide cementation range". *Geotextiles and Geomembranes*, 27(3), pp.196-203.

- Crofts, J.E., Menzies, B.K. and Tarzi, A.I., 1977. "Lateral displacement of shallow buried pipelines due to adjacent deep trench excavations". *Geotechnique*, 27(2), pp.161-179.

- Das, B.M. and Ramana, G.V., 2011. "Principles of soil dynamics", 2nd edn. *Cengage Learning*.

- Dash, S.K., Sireesh, S. and Sitharam, T.G., 2003. "Behaviour of geocell-reinforced sand beds under circular footing". *Proceedings of the Institution of Civil Engineers-Ground Improvement*, 7(3), pp.111-115.

- Davis, P., Burn, S., Moglia, M. and Gould, S.,2007. "A physical probabilistic model to predict failure rates in buried PVC pipelines". *Reliability Engineering & System Safety*, 92(9), pp.1258-1266.

- Emersleben, A. and Meyer, M., 2010, May. "The influence of hoop stresses and earth resistance on the reinforcement mechanism of single and multiple geocells". *In Proc. 9th International Conference on Geosynthetics*, Brazil (pp. 713-716).

- Evans, C.H.,1983. "An examination of arching in granular soils"*Doctoral dissertation*, Massachusetts Institute of Technology.

- Fang, Y., Chen, J. and Tee, K.F., 2013. Analysis of structural dynamic reliability based on the probability density evolution method. Structural Engineering and Mechanics, 45(2), pp.201-209.

- Fattah, M. Y. and Ridha, W. B. M. 2016. "Effect of Geocell Reinforcement in the Migitation of Traffic Global Journal of Engineering Science and Research Management". 3, pp.118-128.

- FHWA 2001. "HMA Pavement Mix Type Selection Guide". 1-24.

- General Specification for Roads and Bridges, Section R6, 2003, "Selected Granular Material-Subbase Course ", *Department of Planning and Studies, Iraq Minnesota Asphalt Pavement Association.*

- Getzler, Z., Gellert, M., and Eitan R. (1970). "Analysis of arching pressures in ideal elastic soil." *Journal of Soil mechanics and Foundations Division*, ASCE, Vol. 94, No. SM5, pp. 1123–1141.

- Goodman, R.E., Taylor, R.L. and Brekke, T.L., 1968. "A model for the mechanics of jointed rocks". *Journal of Soil Mechanics & Foundations Div.*

- Haas, R., Walls, J. and Carroll, R.G., 1988. "Geogrid reinforcement of granular bases in flexible pavements" (No. 1188).

- Handy, R. and Spangler, M., 2007. "Geotechnical engineering: soil and foundation principles and practice". *McGraw Hill Professional.*

- Haque, M., 1998. "Comparison of behaviour of 1520 mm (60 in.) concrete pipe with sided design under deep cover", *Doctoral dissertation*, Ohio University, USA.

- Harris, G.W., 1974. "A sandbox model used to examine the stress distribution around a simulated longwall coal-face". *In International Journal of Rock Mechanics and Mining Sciences & Geomechanics Abstracts* (Vol. 11, No. 8, pp. 325-335). Pergamon.

- Hegde, A., Kadabinakatti, S. and Sitharam, T.G., 2014. "Protection of buried pipelines using a combination of geocell and geogrid reinforcement: experimental studies". *In Ground Improvement and Geosynthetics*, pp. 289-298.

- Heger, F.J., Liepens, A.A. and Selig, E.T., 1985, August. "SPIDA: An analysis and design system for buried concrete pipe". *In Advances in underground pipeline engineering*, ASCE pp. 143-154.

- Huang, J., Bhandari, A. and Yang, X., 2011. "Numerical modeling of geosynthetic-reinforced earth structures and geosynthetic-soil interactions". *Geotechnical Engineering*, 42(1), pp.43.

- Iglesia, G. R., Einstein, H. H., Whitman, R. V., Jessberger, H. L., Güttler, U. 1991: "Trapdoor experiments with simulated jointed rock". *Centrifuge 91, Balkema, Rotterdam*, 561–567.

- Jaky, J., 1948. "Pressure in silos". *In Proc. 2nd International. Conference. Soil Mechanics and Foundation Engineering*, Vol. 1, pp. 103-107.

- Katona, M.G., Smith, J.M., Odello, R.S. and Allgood, J.R., 1976. "CANDE--A Modern Approach for the Structural Design and Analysis of Buried Culverts "(No. FHWA-RD-77-5 Final Rpt.).

- K.G., Bhatia, 2008. "Foundations for industrial machines and earthquake effects". *ISET Journal of Earthquake Technology*, 45(1-2), pp.13-29.

- Kim, H.K. and Santamarina, J.C., 2008. "Sand–rubber mixtures (large rubber chips). *Canadian Geotechnical Journal*, 45(10), pp.1457-1466.

- Kinney, T., Abbott, J. and Schuler, J., 1998. "Benefits of using geogrids for base reinforcement with regard to rutting. Transportation Research Record": *Journal of the Transportation Research Board,* (1611), pp.86-96.

- Kramer, S.L., 1996. "Geotechnical Earthquake Engineering Prentice Hall". New York.

- Lambert, S., Nicot, F. and Gotteland, P., 2011. "Uniaxial compressive behavior of scrapped tire and sand-filled wire netted geocell with a geotextile envelope". *Geotextiles and geomembranes*, 29(5), pp.483-490.

- Lee, M.S., Choi, Y.S. and Prezzi, M., 2012. "Quality Assessment of Geogrids Used for Subgrade Treatment".

- Marto, A., Oghabi, M. and Eisazadeh, A., 2013. "Effect of Geocell Reinforcement in sand and its effect on the bearing capacity with experimental test; A review". *Electronic Journal of Geotechnical Engineering*, 18, pp.3501-3016.

- McNulty, J.W., 1965. "An Experimental Study of Arching in Sand, Rep. No. I-674. US Army Engineer Waterways Experiment Station", *Corps of Engineers*, Vicksburg, Miss, 170.
- Mooney, C. Z. 1997. "Monte Carlo simulation. Thousand Oaks", Calif.: Sage.
- Moser, A.P. and Folkman, S.L., 2001. "Buried pipe design" . New York: *McGraw-Hill*.
- Murthy, V.N.S., 2002. "Geotechnical engineering: principles and practices of soil mechanics and foundation engineering". *CRC press*.
- Ng, P.C.F., 1994. "Behaviour of buried pipelines subjected to external loading", Doctoral dissertation, University of Sheffield, UK.
- Paikowsky, S.G., 1989. "A static evaluation of soil plug behavior with application to the pile plugging problem", Doctoral dissertation, Massachusetts Institute of Technology, USA.
- Paikowsky, S. and Hajduk, E., "Calibration and Use of Grid-Based Tactile Pressure Sensors in Granular Material," *Geotechnical Testing Journal*, Vol. 20, No. 2, 1997, pp. 218-241.
- Paikowsky, S. G., Player, C. M., and Connors, P. J.,(1995), "A DualInterface Apparatusfor Testing Unrestricted Friction of Soil along Solid Surfaces," *Geotechnical Testing Journal*, Vol. 18,No. 2, pp. 168–193.
- PLASTICS PIPE, I. 1950. " Design of PE Piping Systems. PPI Handbook of Polyethylene Pipe", 155-264.
- Poulos, H.G. and Davis, E.H., 1974. "Elastic solutions for soil and rock mechanics". John Wiley.
- Terzaghi, K., Proctor, R.V. and White, T.L., 1946. "Rock tunneling with steel supports". Commercial Shearing and Stamping Co.
- Rajagopal, K., Krishnaswamy, N.R. and Latha, G.M., 1999. "Behaviour of sand confined with single and multiple geocells". *Geotextiles and Geomembranes*, 17(3), pp.171-184.
- Rea, C. and Mitchell, J.K., 1978, April. "Sand reinforcement using paper grid cells". *In Symposium on Earth Reinforcement*, ASCE (pp. 644-663).
- REDDY, D.V. and ATAOĞLU, Ş., 2002. "Experimental Analysis of Buried High Density Polyethylene Pipes". *Turkish Journal of Engineering and Environmental Sciences*, 26(3), pp.293-300.
- Reddy, D.V., Gazagnaire, C., Ataoglu, S. and Powers, R., 2001. "Analysis of HDPE Pipe-Compacted Soil Interaction". *In International Sample Technical Conference*, Vol. 33, pp. 494-505.

- Richard, P. F. & P, E. 2013. "Method for Prediction of Flexible Pipe Deflection". *Technical Service Genter*, Denver, Colorado Water Conveyance Group, M-25 Second Edition.
- Ridha, W. Protection of Flexible Pipes from Dynamic Traffic Load by Geocell-Reinforced Sand with Different Conditions 2016. M.Sc. thesis, *Building and Construction Engineering Department*. University of Technology, Baghdad, Iraq.
- Rowe, P.W., 1952. "Anchored Sheet-Pile Walls". *Proceedings of the Institution of civil engineers*, 1(1), pp.27-70.
- Rude, Lawrence C. (1983), "Computer Modeling of the Cross Canyon Culvert", Transportation Research Record 903, *Transportation Research Board*, 1983, pp. 109¬ 114.
- Sakaguchi, H., Ozaki, E. and Igarashi, T., 1993. "Plugging of the flow of granular materials during the discharge from a silo". *International Journal of Modern Physics B*, 7(10), pp.1949-1963.
- Sellmeijer, J.B., 1990. "Design of geotextile reinforced paved roads and parking areas". *In Proceedings of the Fourth International Conference on Geotextiles, Geomembranes and Related Products*, pp. 177-182.
- Sivakumar Babu, G.L., Srinivasa Murthy, B.R. and Seshagiri Rao, R., 2006. "Reliability analysis of deflection of buried flexible pipes". *Journal of Transportation Engineering*, ASCE 132(10), pp.829-836.
- Spangler, M.G., Hennessy, R.L. and Barber, E.S., 1947. "A method of computing live loads transmitted to underground conduits". *In Highway Research Board Proceedings* (Vol. 26).
- Srivastava, A., Goyal, C.R. and Raghuvanshi, A., 2012. "Load settlement response of footing placed over buried flexible pipe through a model plate load test", *International Journal of Geomechanics*, ASCE 13(4), pp.477-481.
- Suleiman M.T., "Structural Performance of Flexible Pipes", MS. Thesis, *School of Civil Engineering*, Iowa State University, Iowa, USA (2002).
- Szechy K (1973). "The art of tunneling". *Akademiai Kiado*. Budapest, 2nd English edition, (SW/37), 1097.
- Tafreshi, S.M. and Dawson, A.R., 2010. "Behaviour of footings on reinforced sand subjected to repeated loading–Comparing use of 3D and planar geotextile". *Geotextiles and Geomembranes*, 28(5), pp.434-447.

- Tafreshi, S.M. and Dawson, A.R., 2012. "A comparison of static and cyclic loading responses of foundations on geocell-reinforced sand". *Geotextiles and Geomembranes*, 32, pp.55-68.
- Tafreshi, S.M. and Khalaj, O., 2008. "Laboratory tests of small-diameter HDPE pipes buried in reinforced sand under repeated-load". *Geotextiles and Geomembranes*, 26(2), pp.145-163.
- Tafreshi, S.M. and Mehrjardi, G.T., 2008. "The use of neural network to predict the behavior of small plastic pipes embedded in reinforced sand and surface settlement under repeated load". *Engineering Applications of Artificial Intelligence*, 21(6), pp.883-894.
- Tan, Z. and Moore, I.D., 2007. "Effect of backfill erosion on moments in buried rigid pipes", *In Transportation Research Board 86th Annual Meeting*, No. 07-2674.
- Mehrjardi, G.T., Tafreshi, S.M. and Dawson, A.R., 2012. "Combined use of geocell reinforcement and rubber–soil mixtures to improve performance of buried pipes". *Geotextiles and Geomembranes*, 34, pp.116-130.
- Terzaghi, K.V., 1936, June. "The shearing resistance of saturated soils and the angle between the planes of shear". *In Proceedings of the 1st International Conference on Soil Mechanics and Foundation Engineering*, Harvard University Press Cambridge, MA ,Vol. 1, pp. 54-56..
- Terzaghi, K., 1943. "Theoretical soil mechanics", New York, John Wiley and Sons.
- Trickey, S.A. and Moore, I.D., 2007. "Three-dimensional response of buried pipes under circular surface loading", *Journal of Geotechnical and Geoenvironmental Engineering*, ASCE 133(2), pp. 219-223.
- Van Langen, H. and Vermeer, P.A., 1991. "Interface elements for singular plasticity points", *International Journal For Numerical and Analytical Methods in Geomechanics*, 15(5), pp.301-315.
- Vardoulakis, I., Graf, B. and Gudehus, G., 1981. "Trap-door problem with dry sand: A statical approach based upon model test kinematics", *International Journal for Numerical and Analytical Methods in Geomechanics*, 5(1), pp. 57-78.
- Whitman, R.V., Z. Getzler, and K. H6eg (1962) "Static Tests Upon Thin Domes Buried in Sand", MIT Research Project Report No. R62-41, December, 1962.

- Wilson, E.L., 1971. "Solid SAP–A static analysis program for three-dimensional solid structures". *SESM Report 71–19*, Dept. Civil Engng. Univ California, Berkeley.

- Zhang, L., Zhao, M., Shi, C. and Zhao, H., 2010. "Bearing capacity of geocell reinforcement in embankment engineering". *Geotextiles and Geomembranes*, 28(5), pp.475-482.

- Zhang, M.X., Zhou, H., Javadi, A.A. and Wang, Z.W., 2008. "Experimental and theoretical investigation of strength of soil reinforced with multi-layer horizontal–vertical orthogonal elements", *Geotextiles and Geomembranes*, 26(1), pp.1-13.

- Zienkiewicz, O.C. and Taylor, R.L.,1991 , "The Finite Element Method," Vol. II: *Solid and Fluid Mechanics, Dynamics and Non-Linearity*, McGraw-Hill, Maidenhead.

الخلاصة

تطوير إنموذج مختبري هي الطريقة الشائعة للحصول على المعلومات المتعلقة بالتماس بين التربة والانبوب والتي تستطيع توفير ظروف مختلفة. الدراسة الحالية تتعلق بالتحريات المختبرية الخاصة بالأنابيب البلاستيكية المدفونة. تم اجراء عدد من التجارب المختبرية حول انابيب PVC مدفونة في طبقية رملية ذات كثافة نسبية متوسطة تحت طبقة سبيس مسلحة بشبكة Geocell تحت تأثير احمال ديناميكية تتراوح قيمها بين (0.5 الى 1) طن وقيم هيرتزية (0.5, 1, 2) هيرتز لدراسة تأثير وجود شبكة Geocell في السبيس على كمية الاجهادات التي تصل الى الانبوب, اهتزازات الانبوب ونزول التربة. أظهرت النتائج المختبرية ان نزول التربة يقل بمقدار يتراوح من 29 الى 43 % عندما يكون مقدار الحمل 0.5 طن بينما تكون نسبة التقليل من 32 الى 41 % عندما يكون مقدار الحمل 1 طن. عند استخدام شبكة Geocell, تقل أهتزازات الانبوب التربة بمقدار يتراوح بين 25 الى 35 % و13 الى 18 % عندما تكون الاحمال 0.5 و 1 طن على التوالي. استخدام شبكة Geocell يؤدي الى تقليل الاجهادات التي تصل الى الانبوب بنسبة 13 الى 41 % عندما يكون الحمل 0.5 طن وبنسبة 25 الى 32 % عندما يكون الحمل 1 طن.

تم تأكيد النتائج المختبرية بأستخدام برنامج PLAXIS 3D الذي يعمل بطريقة العناصر المحددة. تم تمثيل Geocell بواسطة عنصر Geogrid ثلاثي الابعاد والذي له القدرة على تحمل الاجهادات المحورية ولا يستطيع تحمل اجهادات اللي. بمعنى ان Geogrid يتحمل اجهادات الشد ولا يتحمل اجهادات الضغط. اظهرت نتائج البرنامج ان اكثر نسبة خطأ بين التجارب المختبرية والإنموذج العددي بالنسبة لنزول التربة هي 10%. بالنسبة لأهتزازات الانبوب فأن اكثر قيمة للفرق هي 6%. بالنسبة للاجهادات التي تصل للانبوب فأن اكثر نسبة خطأ للفرق 11%. تم اثبات نجاح هذا الإنموذج عند مقارنته بالإنموذج المختبري وأظهرت النتائج نجاح استخدام تسليح Geocell بتقليل نزول التربة, الاجهادات الواصلة للأنبوب واهتزازات الانبوب. تم تطوير دراسة محددة ايضا اعتمادا على المراجعة الادبية, النتائج المختبرية والموديلات العددية لدراسة تأثير عوامل مختلفة على إنموذج بمقياس كامل.

الأداء المختبري للانابيب البلاستيكية المدفونة بعمق قليل تحت طبقة سبيس مسلحة بالجيوسيل تحت تأثير احمال دايناميكية متكررة

أطروحة

مقدمة الى قسم الهندسة المدنية في كلية الهندسة في جامعة كربلاء وهي جزء من متطلبات نيل شهادة الماجستير في العلوم لهندسة البنى التحتية

من قبل

سجاد عماد رشيد

بكلوريوس هندسة مدنية (2014)

بأشراف

الاستاذ الدكتور محمد يوسف فتاح

الاستاذ المساعد الدكتور واقد حميد حسن

ذي الحجة (1438)   **أيلول (2017)**